

QUARTERLY JOURNAL  
OF THE  
ROYAL METEOROLOGICAL SOCIETY

Vol. 111

OCTOBER 1985

No. 470

*Quart. J. R. Met. Soc.* (1985), **111**, pp. 877–946

551.509.3:551.511.2:551.511.32

On the use and significance of isentropic potential vorticity maps

By B. J. HOSKINS<sup>1</sup>, M. E. McINTYRE<sup>2</sup> and A. W. ROBERTSON<sup>3</sup>

<sup>1</sup> *Department of Meteorology, University of Reading*

<sup>2</sup> *Department of Applied Mathematics and Theoretical Physics, University of Cambridge*

<sup>3</sup> *Laboratoire de Physique et Chimie Marines, Université Pierre et Marie Curie, 75230 Paris Cédex 05*

(Received 12 February 1985; revised 2 July 1985)

SUMMARY

The two main principles underlying the use of isentropic maps of potential vorticity to represent dynamical processes in the atmosphere are reviewed, including the extension of those principles to take the lower boundary condition into account. The first is the familiar Lagrangian conservation principle, for potential vorticity (PV) and potential temperature, which holds approximately when advective processes dominate frictional and diabatic ones. The second is the principle of 'invertibility' of the PV distribution, which holds whether or not diabatic and frictional processes are important. The invertibility principle states that if the total mass under each isentropic surface is specified, then a knowledge of the global distribution of PV on each isentropic surface and of potential temperature at the lower boundary (which within certain limitations can be considered to be part of the PV distribution) is sufficient to deduce, diagnostically, all the other dynamical fields, such as winds, temperatures, geopotential heights, static stabilities, and vertical velocities, under a suitable balance condition. The statement that vertical velocities can be deduced is related to the well-known omega equation principle, and depends on having sufficient information about diabatic and frictional processes. Quasi-geostrophic, semi-geostrophic, and 'nonlinear normal mode initialization' realizations of the balance condition are discussed. An important constraint on the mass-weighted integral of PV over a material volume and on its possible diabatic and frictional change is noted.

Some basic examples are given, both from operational weather analyses and from idealized theoretical models, to illustrate the insights that can be gained from this approach and to indicate its relation to classical synoptic and air-mass concepts. Included are discussions of (a) the structure, origin and persistence of cutoff cyclones and blocking anticyclones, (b) the physical mechanisms of Rossby wave propagation, baroclinic instability, and barotropic instability, and (c) the spatially and temporally nonuniform way in which such waves and instabilities may become strongly nonlinear, as in an occluding cyclone or in the formation of an upper air shear line. Connections with principles derived from synoptic experience are indicated, such as the 'PVA rule' concerning positive vorticity advection on upper air charts, and the role of disturbances of upper air origin, in combination with low-level warm advection, in triggering latent heat release to produce explosive cyclonic development. In all cases it is found that time sequences of isentropic potential vorticity and surface potential temperature charts—which succinctly summarize the combined effects of vorticity advection, thermal advection, and vertical motion without requiring explicit knowledge of the vertical motion field—lead to a very clear and complete picture of the dynamics. This picture is remarkably simple in many cases of real meteorological interest. It involves, in principle, no sacrifices in quantitative accuracy beyond what is inherent in the *concept* of balance, as used for instance in the initialization of numerical weather forecasts.

CONTENTS

1. INTRODUCTION AND HISTORICAL REVIEW
  - 1(a) Early ideas
  - 1(b) Rossby and Ertel
  - 1(c) Subsequent developments
  - 1(d) The invertibility principle for potential vorticity
2. ISENTROPIC POTENTIAL VORTICITY MAPS FROM ROUTINE ANALYSES
  - 2(a) Preliminaries

- 2(b) Vertical structure and time-variability
- 2(c) Development of a North Atlantic cutoff cyclone
- 2(d) A minor blocking episode
- 2(e) The conceptual duality between cutoff cyclones and blocking anticyclones
- 3. SOME SIMPLE EXAMPLES, FOLLOWING KLEINSCHMIDT
- 4. ON THE CANCELLATION OF HORIZONTAL ADVECTION BY VERTICAL MOTION
- 5. ANOMALIES AT THE LOWER BOUNDARY, AND THE INVERTIBILITY PRINCIPLE FOR GENERAL, TIME-DEPENDENT FLOW
  - 5(a) Surface and near-surface anomalies
  - 5(b) Quasi-geostrophic theory
  - 5(c) Semi-geostrophic theory and Salmon's generalization
  - 5(d) Inversion by nonlinear normal-mode initialization
- 6. ROSSBY WAVES AND SHEAR INSTABILITIES
  - 6(a) Rossby wave propagation and the scale effect
  - 6(b) Baroclinic and barotropic shear instabilities
  - 6(c) Lateral and vertical Rossby wave propagation
  - 6(d) The nonlinear saturation of baroclinic instabilities
  - 6(e) Further remarks about cyclogenesis in the real atmosphere
- 7. THE MAINTENANCE AND DISSIPATION OF CUTOFF CYCLONES AND BLOCKING ANTICYCLONES
- 8. FURTHER REMARKS ABOUT CUTOFF SYSTEMS AND AIR MASSES
- 9. CONCLUDING REMARKS

## ACKNOWLEDGEMENTS

## APPENDIX: THE COMPUTATION OF VERTICAL MOTION

## 1. INTRODUCTION AND HISTORICAL REVIEW

(a) *Early ideas*

Circulation and vorticity have been recognized as fundamental concepts in meteorology and oceanography for many years, dating back to the pioneering work of V. Bjerknes (1898a, b, 1901, 1902); see also, e.g., Eliassen (1982). The three-dimensional vorticity equation, as it appears in textbooks on general fluid dynamics, may be written for frictionless motion relative to a coordinate system rotating with angular velocity  $\boldsymbol{\Omega}$  as

$$\frac{D}{Dt}(\boldsymbol{\zeta}_a/\rho) = (\boldsymbol{\zeta}_a/\rho) \cdot \nabla \mathbf{u} - (1/\rho)\nabla(1/\rho) \times \nabla p \quad (1)$$

where the absolute vorticity

$$\boldsymbol{\zeta}_a = 2\boldsymbol{\Omega} + \boldsymbol{\zeta} \quad (2)$$

and

$$\boldsymbol{\zeta} = \nabla \times \mathbf{u}, \quad (3)$$

the relative vorticity.  $D/Dt$  is the material rate of change, and  $\nabla$  is the three-dimensional gradient operator. We denote the three-dimensional velocity by  $\mathbf{u} = (u, v, w)$  to distinguish it from the horizontal wind velocity  $\mathbf{v} = (u, v, 0)$ . The first term on the right-hand side of (1) is the stretching-twisting term, and the second the so-called solenoid term.

The absolute circulation around a material circuit  $\Gamma$  moving with the fluid is

$$C_a = C + 2\boldsymbol{\Omega}A, \quad (4)$$

where

$$C = \oint_{\Gamma} \mathbf{u} \cdot d\mathbf{l} \quad (5)$$

is the relative circulation and  $A$  is the area bounded by a projection of the circuit onto a plane normal to  $\boldsymbol{\Omega}$ . Circulation is another measure of the rotational character of the air motion (which is the aspect of the air motion usually of interest in dynamical meteorology) and is equal to the integral of the vorticity over a surface bounded by the circuit. Following Bjerknes, we may write the circulation theorem for frictionless motion as

$$dC_a/dt = - \oint_{\Gamma} (1/\rho) dp. \quad (6)$$

The stretching–twisting term, the first term on the right of (1), has been absorbed into the behaviour of the material circuit and does not appear explicitly in (6).

When the usual meteorological approximations are made, i.e. neglecting vertical accelerations and the horizontal component of the rotation  $\boldsymbol{\Omega}$ , taking the geoid to be spherical, and replacing the distance of an air parcel from the centre of the earth by a constant representative value of the earth's radius, the equations are unaltered except that

- (i) where  $\mathbf{u}$  appears explicitly in (3) and (5) it is replaced by the horizontal wind vector  $\mathbf{v}$ ;
- (ii) only the vertical component  $f$  of  $2\boldsymbol{\Omega}$  is used in (2) and (4); and
- (iii) the plane involved in the definition of the projected area  $A$  in (4) is horizontal, rather than perpendicular to  $\boldsymbol{\Omega}$ .

#### (b) Rossby and Ertel

In general, the complexity of the foregoing equations means that detailed argument from them is difficult. Rossby (1939) took a key step by realizing that in practice the vertical component of absolute vorticity  $\zeta_a = f + \mathbf{k} \cdot (\nabla \times \mathbf{v})$ ,  $\mathbf{k}$  being a unit vertical vector, is the most important for the large-scale atmospheric flow. He realized furthermore that many features of the flow could be surprisingly well modelled by assuming conservation of  $\zeta_a$  in two-dimensional horizontal motion—the familiar barotropic model of large-scale atmospheric dynamics. The streamfunction for this flow is obtainable at any time by inversion of the Laplacian operator linking it and the vorticity; we shall refer to this as the ‘invertibility principle’ for vorticity in the barotropic model. Rossby’s insight, which clarified and simplified some earlier insights from what Rossby referred to as “a remarkable paper by J. Bjerknes” (1937), led to a number of important developments, for instance the theory of Rossby wave motion, the use of constant absolute vorticity trajectories, and, a decade later, the conception and execution of the first practicable numerical forecasting models.

Rossby (1940) took a further key step by noticing that if  $h$  is the depth of a material fluid column in the barotropic model, then

$$\zeta_a/h = \text{constant} \quad (7)$$

following the fluid column. This describes, in an ingeniously simple way, the two processes that often dominate the vorticity budget, namely the creation of vorticity by vertical stretching of vortex tubes, and the horizontal advection of absolute vorticity. This is the simplest version of the modern concept of ‘potential vorticity’.

In the late 1930s, Rossby and his co-workers (e.g. Rossby 1937a, b; Namias

1940; for some more history see Namias 1983) had made systematic use of isentropic charts for displaying the motion of the atmosphere and had recognized their power in elucidating the Lagrangian, air-mass structure of the large-scale flow given that diabatic processes were of secondary importance. The use of isentropic charts had previously been advocated by Shaw (1930). It was therefore natural for Rossby to move straight from Eq. (7), the conservation of  $\zeta_a/h$ , to the proof of a similar result for an adiabatic, frictionless atmosphere consisting of a finite number of layers of constant potential temperature,  $\theta$ . Making the hydrostatic approximation, and expressing the layer thickness  $\Delta = -\delta p/g$  as the mass per horizontally projected area, he showed (in the same paper, 1940) that, for each such layer,

$$P_R = (f + \zeta_\theta)/\Delta = \text{constant} \quad (8)$$

following an air parcel. Here  $\zeta_\theta$  is the relative 'isentropic vorticity'

$$\zeta_\theta = \mathbf{k} \cdot \nabla_\theta \times \mathbf{v} = (\partial v/\partial x)_\theta - (\partial u/\partial y)_\theta \quad (9)$$

where, as before,  $(u, v)$  are the horizontal wind components and  $dx, dy$  are horizontal increments of distance, but differentiations are carried out on the isentropic surface  $\theta = \text{constant}$  (*op. cit.*, p. 72). This is another ingenious mathematical device of great simplifying power. Rossby pointed out that "it is possible to derive corresponding results also for an atmosphere in which the potential temperature varies continuously with elevation", and introduced the term 'potential vorticity' for the value of  $\zeta_\theta$  which the isentropic fluid layer would have if it were moved to a standard latitude and its mass per unit area,  $\Delta$ , brought to a standard value. The term 'potential vorticity' is today used for quantities like (7) and (8) instead, but the underlying concept is the same, namely the idea that there is a potential for creating vorticity by changing latitude and by adiabatically changing the separation of isentropic layers.

The Bjerknes circulation theorem (6) gives a simple alternative derivation of the result (8) obtained by Rossby. When (6) is applied to any material circuit  $\Gamma$  in an isentropic surface,  $\rho$  is a function of  $p$  only so that  $C_a$  must be constant for frictionless, adiabatic motion. However, integration of  $P_R$  over the mass of an isentropic layer bounded by any material circuit  $\Gamma$  gives

$$\iint P_R \Delta dA = \iint (f + \zeta_\theta) dA = C_a = \text{constant}, \quad (10)$$

where  $dA$  is the horizontal projection of the area element of integration, so that  $\Delta dA$  is the mass element. The third step applies Stokes' theorem in two dimensions to the horizontal projection of the circuit  $\Gamma$ , giving the appropriate versions of (4) and (5) under the modifications (i)–(iii). Since (10) is true for any material circuit  $\Gamma$ , and the mass  $\iint \Delta dA$  is constant,  $P_R$  must itself be conserved following the fluid.

Rossby's result (8) was given full hydrodynamical generality by the independent work of Ertel (1942). If  $\theta$  is a function of the state variables  $p$  and  $\rho$  alone, then the three-dimensional scalar product of  $\nabla\theta$  with the solenoid term in the vorticity equation (1) is zero. If, moreover,

$$\theta = \text{constant} \quad (11)$$

for an air parcel, signifying adiabatic motion, then, expressing this as  $D\theta/Dt = 0$  and taking its three-dimensional gradient, and then taking the scalar product of  $\nabla\theta$  with the frictionless vorticity equation (1), we obtain after some manipulation the celebrated result

$$P = \rho^{-1} \zeta_a \cdot \nabla\theta = \text{constant} \quad (12)$$

following an air parcel. This is Ertel's theorem for adiabatic, frictionless motion. Remarkably, no approximations are involved;  $P$  is conserved even for fully three-dimensional, nonhydrostatic motion. The generalization to include diabatic and frictional effects is straightforward; it is noted in section 7 below, together with an important integral constraint on those effects, arising from the fact that quantities like  $\zeta_a \cdot \nabla\theta$  can always be expressed as exact divergences  $\nabla \cdot (\zeta_a\theta)$ .

Normally in meteorology,  $\theta$  is taken to be the potential temperature, although it can equally well be taken to be the specific entropy or any other function of potential temperature. If the meteorological approximations are made, including the hydrostatic approximation, the isobaric and isentropic coordinate versions of the expression in (12) become

$$P = -g(f\mathbf{k} + \nabla_p \times \mathbf{v}) \cdot \nabla_p \theta \quad (13)$$

and

$$P = -g(f + \mathbf{k} \cdot \nabla_\theta \times \mathbf{v})/(\partial p/\partial \theta), \quad (14)$$

respectively, where  $\mathbf{k}$  is again a unit vertical vector and  $\nabla_p$  and  $\nabla_\theta$  are the three-dimensional gradient operators in  $xyp$  and  $xy\theta$  space respectively. Note that the second expression, involving once more the 'isentropic vorticity'  $\zeta_\theta = \mathbf{k} \cdot \nabla_\theta \times \mathbf{v}$  defined in (9), is much simpler than the first, where there is a scalar product which expands to three terms. From comparison of (14) and (8) it is apparent that what is now known as 'Ertel's potential vorticity',  $P$ , as it is used in meteorology, is merely the continuous-atmosphere extension of (8) to which Rossby referred. We shall simply call  $P$  'the potential vorticity', or PV for short.

### (c) *Subsequent developments*

Rossby's co-workers quickly seized on the importance of the PV as an air-mass tracer. Starr and Neiburger (1940) noted that, for adiabatic, frictionless flow, it provided the third Lagrangian marker necessary to identify an air parcel, the other two being potential temperature and specific humidity. They constructed isentropic potential vorticity maps ('IPV maps') for the 299 K–303 K isentropic layer over North America for 21 and 22 November 1939, and checked for three fluid elements that the conservation of PV was approximately satisfied in the free atmosphere. They contemplated possible future investigations in which the PV might be used for studying non-adiabatic processes, mixing, and even "prediction of the upper air winds" using the fact that "the transport of potential vorticity affects the wind-field". The correlation between specific humidity and potential vorticity was given further study by Spar (1943).

The further application of this new tool to elucidate the Lagrangian behaviour of the atmosphere appears to have proceeded at a slower rate. Platzman (1949) used data which Palmén and Newton (1948) had composited relative to the polar front at 80°W, to demonstrate a salient feature of the isentropic PV distribution for the 310 K–350 K layer. He found relatively uniform high PV values on the polar, stratospheric side of the jet stream, and uniform low values on the equatorward side, with a near discontinuity at the jet stream. He then proposed this as a suitable basic state to consider in a barotropic model.

Kleinschmidt (1950a, b; 1951, 1955, 1957) used the notion of PV anomalies in the upper troposphere to explain observed cyclogenesis events, noting among other things the likely importance of quasi-horizontal advection along isentropes from the stratospheric 'reservoir' of high-PV polar air found by Platzman (1949). Seen in the light of more recent developments, Kleinschmidt's work must be classed as an extremely important piece of pioneering, if only because for the first time he placed full emphasis on what we

shall call the 'invertibility principle' for potential vorticity, namely the idea that not only can one use the PV as a Lagrangian tracer but that one can also deduce, diagnostically, the complete flow structure *from* the spatial distribution of PV. His ideas were, however, too far ahead of theoretical developments and were largely displaced, at the time, by the ideas associated with the new baroclinic instability theory with its emphasis on lower tropospheric baroclinicity. Ironically, we shall see that a more complete picture of what goes on in the atmosphere actually involves *both* ideas, and in particular that the invertibility principle gives the key to one of the simplest ways of thinking physically about the baroclinic instability process itself.

The next significant line of development was initiated in the important papers by Reed and Sanders (1953) and Reed (1955), which began the process of mapping out in detail the upper air PV structures whose gross features Platzman and Kleinschmidt had seen earlier. Useful historical reviews are given by Shapiro (1976) and by Keyser and Shapiro (1985). Reed and Sanders used PV values to determine which air was of stratospheric origin in a detailed cross-section of an upper tropospheric front. In a further study of upper tropospheric frontogenesis Reed (1955) produced IPV maps like those of Starr and Neiburger, but locally with far better resolution, for the 300 K isentropic surface over North America daily from 13 to 15 December 1953. Both papers strongly suggested a remarkable fact, to be amply confirmed by later studies, namely that stratospheric air could be advected down sloping isentropic surfaces to altitudes usually considered to be well within the troposphere. The suggested picture was confirmed in greater detail by Reed and Danielsen (1959), who gave the first convincing local picture of the associated 'tropopause folding' process in vertical cross-sections. Further confirmation, including exquisitely detailed pictures using special aircraft data, has been recorded in papers by, for instance, Mahlman (1965), Reiter and Mahlman (1965), Danielsen (1968), Danielsen *et al.* (1970) and Shapiro (1974, 1976, 1978), to name only a few. Staley (1960) sounded a note of caution by finding examples in which PV was apparently not well enough conserved to use as a tracer. However, Danielsen (1968), using simultaneous measurements of ozone and nuclear test radioactivity as well as calculations of potential vorticity, was able to make a strong case that the PV, even in cases where it was changed by sub-synoptic-scale mixing or convection, generally provided an extremely good indication of air of recent stratospheric origin, and that a definition of the 'tropopause' in terms of PV is more useful than a lapse-rate definition. Implicit in this and other practical uses of the PV is a presumption that a certain amount of fine-grain structure in its horizontal and vertical distribution can be ignored for practical purposes. As we shall indicate shortly, some theoretical justification can be found for this. Observational evidence for such structure, especially that due to fine structure in static stability profiles, and for its local generation by, for instance, clear air turbulence, is plentiful (e.g. Danielsen 1959; Shapiro 1976, 1978; Vaughan and Tuck 1985).

Another historical landmark was the first publication of computer-generated IPV maps giving a global-scale, coarse-grain view, by Obukhov (1964) and Danielsen (1967, 1968) for the 300, 305 and 310 K surfaces. In subsequent years, IPV maps have been increasingly used in the diagnosis of observed atmospheric behaviour (e.g. Danielsen *et al.* 1970; Bleck 1973; Holopainen and Rontu 1981; McIntyre and Palmer 1983, 1984; Bleck and Mattocks 1984; Uccellini *et al.* 1985; Al-Ajmi *et al.* 1985; Clough *et al.* 1985; Shutts 1985; Young *et al.* 1985), in the diagnosis of atmospheric model simulations (e.g. Hsu 1980; Dunkerton *et al.* 1981), and in studies of oceanic circulations (McDowell *et al.* 1982; Sarmiento *et al.* 1982; Holland *et al.* 1984; Woods *et al.* 1985). For a recent review of related developments in the Soviet Union, the reader may consult Obukhov (1984).

*(d) The invertibility principle for potential vorticity*

As Rossby, Starr and Neiburger, and Kleinschmidt had evidently appreciated, the significance of potential vorticity does not end with its importance as an air-mass tracer. It is also the key to a very powerful and succinct view of the *dynamics*. IPV maps, in particular, are a natural diagnostic tool well suited to making dynamical processes directly visible to the human eye and to making meaningful comparisons between atmospheric models and reality. We shall see that IPV maps can play a role in improving our understanding of dynamical processes closely analogous to the role played by maps of the absolute vorticity  $\zeta_a$  in understanding the behaviour of barotropic models.

Two properties of  $P$  and  $\zeta_a$  underlie these statements. First, there are the Lagrangian conservation properties already noted and, where relevant, their frictional, diabatic generalizations. Second, there is the invertibility principle. For the barotropic model, this is the familiar fact that, given the vorticity distribution, one can deduce the stream-function, and thence the wind field, the calculation involving the inversion of a Laplacian operator as mentioned earlier. Thus one can, if one wishes, *think* entirely in terms of the (barotropic) vorticity field, since this contains all the relevant information; and indeed the simplifying power and general usefulness of this particular mode of thinking about rotational fluid motion has long been recognized, and made routine use of, in another field, that of classical aerodynamics (e.g. Prandtl and Tietjens 1931; Goldstein 1938; Lighthill 1963; Batchelor 1967; Saffman 1981).

As Kleinschmidt seems to have realized, at least intuitively, a similar invertibility principle must hold for the potential vorticity field in baroclinic flow: given the PV distribution, one can deduce the wind, pressure and temperature fields. Kleinschmidt's early attempts to express this idea mathematically were successful as far as they went, but they were tied to particular examples and did not establish procedures suitable for general use either computationally or conceptually. Seeing in a general way that such procedures exist was a far less trivial problem than in the barotropic case, and had to await later theoretical developments, one of which was quasi-geostrophic theory in the form developed by Charney and Stern (1962). More refined and powerful versions of the theory are still being developed today; they will be discussed in section 5.

It might be asked (and this may have been part of why Kleinschmidt's ideas were not widely accepted) how knowledge of the potential vorticity, i.e. of the *product* of absolute vorticity and static stability as expressed by (14), can possibly determine the two factors separately—for that is what the invertibility principle asserts. The answer lies in the fact that we must of course specify some more information—a fact so familiar to theoretical specialists today that it is not always spelt out explicitly. Regardless of which particular theoretical device is used for the inversion, one must

- (i) specify some kind of balance condition, the simplest albeit least accurate option being ordinary geostrophic balance;
- (ii) specify some kind of reference state, expressing the mass distribution of  $\theta$ , in essentially the same way as in Lorenz's theory of available potential energy; and
- (iii) solve the inversion problem *globally*, with proper attention to boundary conditions.

The last point comes as no surprise, of course, because it is equally true of the barotropic case. The first and second points imply that if we wish to be precise we must speak of inversion under this or that balance condition, and relative to this or that reference state. It is only when all these constraints operate in the problem that the arbitrariness is removed. In other words, while it is perfectly true that a purely local knowledge of  $P$  cannot determine the local absolute vorticity and static stability separately, there is only one pair of values of them which will fit into a given *global* distribution

of  $P$  in which thermal wind balance (or some more accurate balance) is satisfied everywhere.

There are, of course, two well-known provisos to all this. First, the balance referred to in condition (i) must be a physically realizable and therefore stable balance in the sense that static instability, inertial instability, and the related parcel instabilities usually studied under the heading 'symmetric baroclinic instability', are all assumed to be absent. Second, the space and time scales of the motion must be compatible with the assumed balance; in practice this will often mean that the invertibility principle will apply most accurately to motions of synoptic scale upwards, although it may also apply to certain mesoscale motions.

It might well be asked whether it is possible to talk about any scale separation at all, in this connection, since there are many observational and theoretical reasons for supposing that actual IPV distributions may have significant fine structure on scales even smaller than the mesoscale. Indeed it can be argued that there will be no lower limit to the fineness of the structures that may occur, all the way down to the length scales on which molecular diffusion acts. It is here that integral relations like relation (10) between PV and absolute circulation are of fundamental importance. The relation suggests that, for the purpose of applying the invertibility principle, it should be meaningful to integrate over the fine structure on each isentropic surface and think in terms of 'coarse-grain' IPV distributions expressing the absolute circulation around all isentropic circuits of resolvable size, with reference to a vertically smoothed static stability. Indeed, if some such coarse-grain approximation to actual IPV distributions were *not* dynamically meaningful, "numerical model simulations of the large-scale behaviour of the atmosphere would hardly be practicable" (McIntyre and Palmer 1983). The same could be said of any other attempt at understanding and predicting the evolution of weather patterns on the basis of what can be resolved observationally. The integral constraint noted in section 7 is similarly relevant to devising self-consistent ways of ignoring fine structure in the PV field.

Section 3 below gives some simple examples of the static stability and wind fields associated with—or, as an aerodynamicist would put it, 'induced by' or, as Kleinschmidt originally said, "produced by"—a given potential vorticity distribution. The examples convey an intuitive idea of how the PV partitions itself between static stability and absolute vorticity. As in Kleinschmidt's work, invertibility is expressed, in section 3, in terms of an elliptic operator not unlike that occurring in the familiar omega equation (e.g. Eliassen 1984), and having the qualitative character of a three-dimensional Laplacian. The well-known fact that such operators are *smoothing* operators provides another way of seeing the likely dynamical relevance of coarse-grain approximations to IPV distributions. Even if it were practicable to retain all fine-grain structure, the inversion operation itself would generally speaking tend to be insensitive to the details of that structure.

Once one has an idea of the typical wind, temperature and pressure fields associated with a given IPV distribution, one can begin to use IPV maps not only as a means of studying tracer-transport processes, but also as a means of gaining a very direct insight into the concomitant dynamical processes, in much the same way as aerodynamicists have long used 'vorticity thinking', as already mentioned, to study the dynamical processes with which they are concerned. One such process, which is of meteorological as well as aerodynamical interest, is that of barotropic shear instability. The analogous use of 'IPV thinking' to gain insight into *baroclinic* shear instability will be noted in section 6. Another aerodynamical phenomenon in whose baroclinic counterpart we shall be interested, for reasons to emerge in section 8, is that of 'vortex rollup'.

The quantitative precision of IPV maps as a complete representation of the dynamics

is limited, in principle, by one thing only, namely the limits of accuracy inherent in condition (i) above. Related questions arise in the context of initialization procedures for numerical weather forecasting; for some interesting discussion bearing on these questions, the reader may consult, for instance, the paper by Leith (1980) and the comprehensive review by Daley (1981). As far as large-scale motions are concerned, the main limitation of IPV maps is their inability to represent equatorial Kelvin modes in the tropics. On smaller scales, other limitations are likely to be encountered in fast processes like the 'collapse' stage of surface frontogenesis, in which the motion may develop a spontaneous imbalance leading to a strong local coupling to gravity modes (Ley and Peltier 1978; Blumen 1980; Ogura and Portis 1982; Cullen and Purser 1984), and similarly in other highly transient situations especially if very rapid advection is involved (e.g. Uccellini *et al.* 1984). It is to be hoped that current research may soon lead to a better understanding of these limitations.

## 2. ISENTROPIC POTENTIAL VORTICITY MAPS FROM ROUTINE ANALYSES

### (a) Preliminaries

Daily northern hemispheric IPV maps have been constructed for numerous isentropic surfaces for the 42 days from 20 September to 31 October 1982. The data source is the routine analysed and initialized product available four times a day from the European Centre for Medium Range Weather Forecasts (ECMWF). The actual data set employed in this study comprises the 12 z analyses on a  $3.75^\circ$  horizontal grid and at 11 pressure levels (1000, 850, 700, 500, 400, 300, 250, 200, 150, 100, 50 mb). Simple centred finite differences were used to construct  $P$  objectively on isobaric surfaces from Eq. (13) and then linear interpolation to give  $\mathbf{v}$  and  $P$  on  $\theta$  surfaces. Some results will be presented for the first 18 days analysed. It should be kept in mind that the maps can at best be coarse-grain approximations to the real IPV distributions and indeed may well fall short of the best possible such coarse-grain estimates because of the fact that the raw data were analysed isobarically rather than isentropically. Superadiabatic lapse rates were encountered in the data in small regions in the subtropics where the boundary layer was extremely warm, but these boundary layer values were ignored and the PV set to zero in what was presumed (for large-scale dynamical purposes) to be effectively an adiabatic layer.

To get a feel for the numerical values, it is useful to consider first the standard potential vorticity

$$P_s = -fg \partial \theta / \partial p = \rho^{-1} f \partial \theta / \partial z \quad (15)$$

associated with idealized, standard-atmosphere profiles at various latitudes, for a fictitious atmosphere at rest. Figure 1 shows  $P_s$  for standard-atmosphere profiles at  $15^\circ\text{N}$ ,  $45^\circ\text{N}$  and  $75^\circ\text{N}$ . Apart from the polar boundary layer and the top of the trade wind layer, the tropospheric values on the left show a latitudinal variation which is essentially that of  $f$ , and a vertical variation attributable mainly to the factor  $\rho^{-1}$  on the right of (15). Note that for  $f = 10^{-4} \text{ s}^{-1}$ , a unit of  $10^{-6} \text{ m}^2 \text{ s}^{-1} \text{ K kg}^{-1}$  corresponds approximately to a 10 K change in  $\theta$  per 100 mb. The unit of  $10^{-6} \text{ m}^2 \text{ s}^{-1} \text{ K kg}^{-1}$  is convenient in practice and we shall call it a 'potential vorticity unit', 'PV unit', or simply 'unit' for short. We see from Fig. 1 that tropospheric values are generally below about 1.5 units. At the tropopause  $P_s$  jumps to stratospheric values typically in excess of four units, and then rises steeply with height. The crosses in Fig. 1 mark points at which  $\theta = 350 \text{ K}$ , and show how the 350 K isentropic surface, though varying little in height, generally samples stratospheric PV values in middle and high latitudes but tropospheric values in the subtropics.

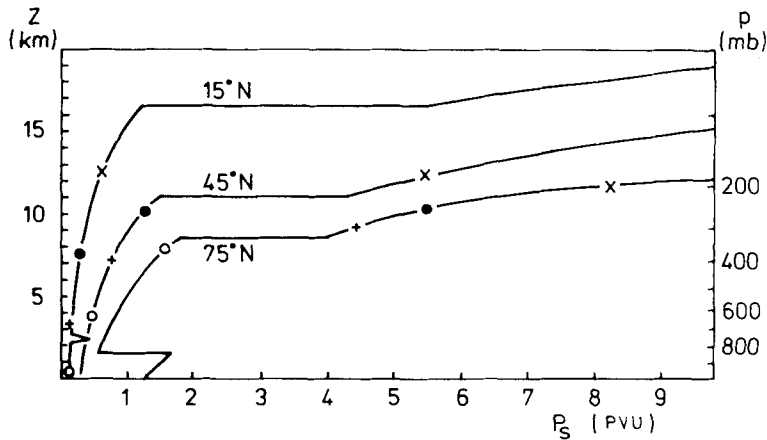


Figure 1. The potential vorticity  $P_s$  associated with standard atmospheric temperature profiles and zero relative vorticity as defined in (15). The profiles are the U.S. Standard Atmosphere 15°N annual, mid-latitude spring/autumn (labelled 45°N) and 75°N January (cold). The unit of the abscissa (1 PVU) is  $10^{-6} \text{m}^2 \text{s}^{-1} \text{K kg}^{-1}$ . At each latitude,  $P_s$  is discontinuous at the tropopause. The positions of various isentropic surfaces are indicated by  $\times$  (350 K),  $\bullet$  (330 K),  $+$  (315 K) and  $\circ$  (300 K).

The 330 K isentropic surface (dots) and the 315 K surface (pluses) also sample both stratospheric and tropospheric PV values, intersecting the tropopause at different latitudes but in a manner broadly consistent with the overall picture for the 310–350 K layer originally found by Platzman (1949). The 300 K surface (open circles) is generally in the upper troposphere even in polar regions, descending to sea level in the tropics.

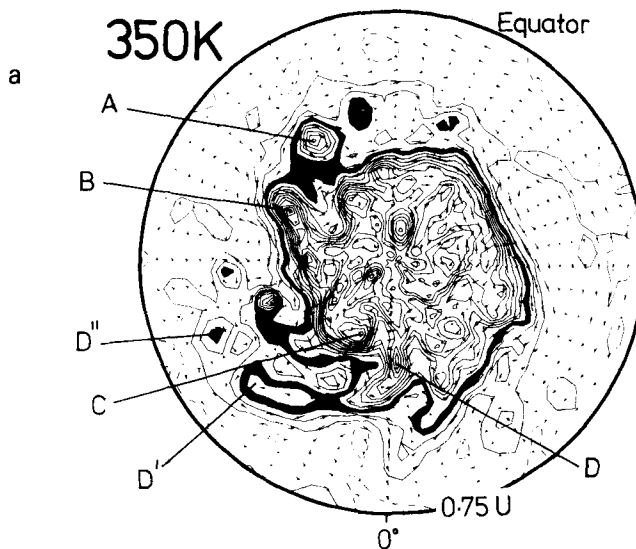
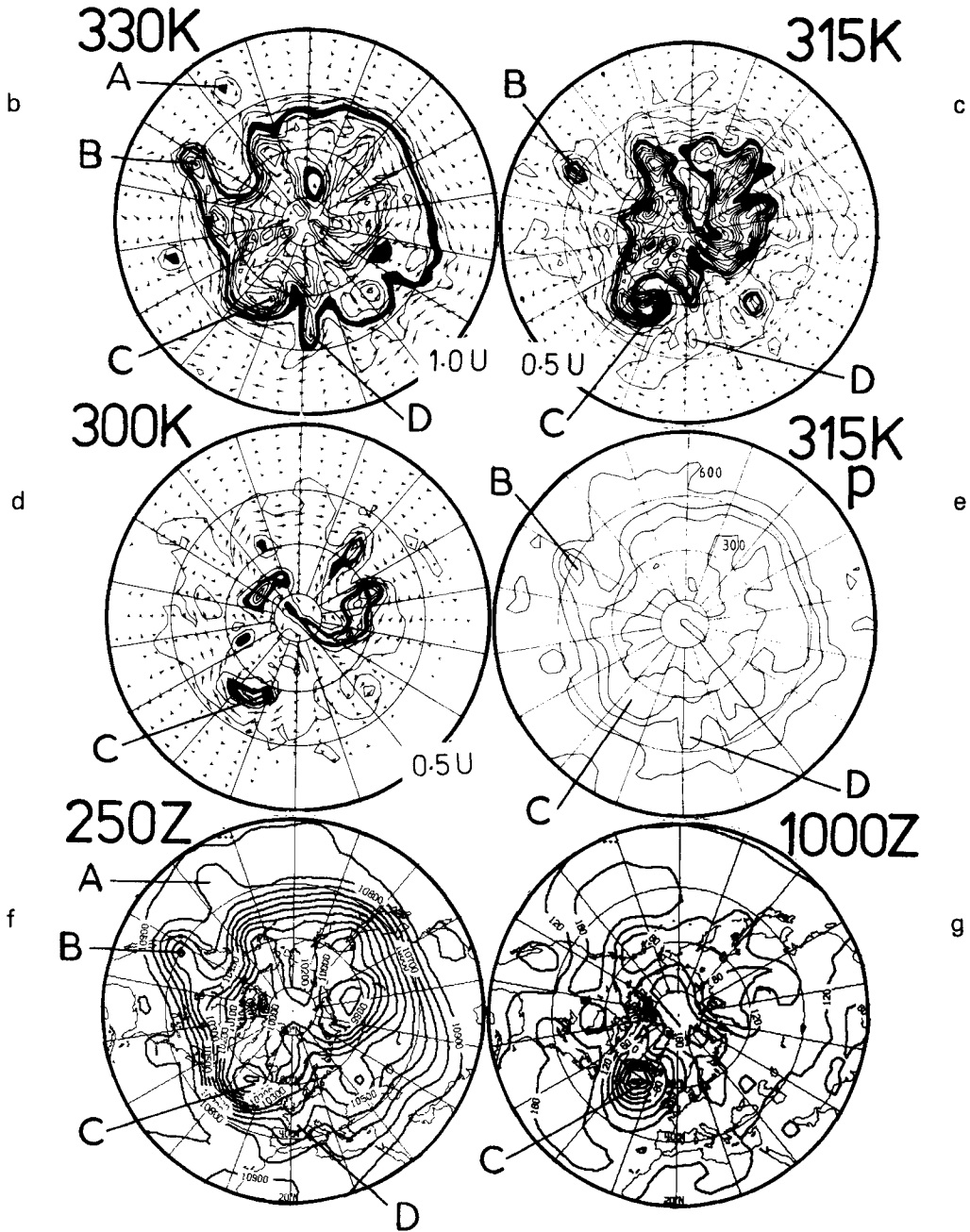


Figure 2. Northern hemispheric synoptic fields for the 30 September 1982. Shown in (a) above, (b) opposite top left, (c) opposite top right and (d) are the IPV maps for the 350 K, 330 K, 315 K and 300 K isentropic surfaces, respectively. As indicated, the contour intervals are 0.75, 1.0, 0.5 and 0.5 PV units ('U') respectively. The regions with values 2.25–3 units in (a), 2–3 units in (b) and 1.5–2 units in (c) and (d) have been blacked in. Also shown in these figures are arrows indicating the horizontal component of the velocity vector on these isentropic surfaces. The points of the arrowheads are plotted at the mid-points of the arrows which also mark the grid-points to which the vectors refer. An arrow length from the 40°–60° latitudinal circles would indicate a speed of  $100 \text{ m s}^{-1}$ . The boundary circle in (a) is the equator, but it is 20°N in all the other maps. The contours in (e) are of the pressure  $p$  on the 315 K surface, the contour interval being 100 mb. The 250 mb and 1000 mb geopotential height fields are shown in (f) and (g), with contour intervals of 100 m and 60 m respectively. The lettering denotes features referred to in the text.

(b) Vertical structure and time-variability

To give an idea of how coarse-grain IPV distributions vary from one isentropic surface to another in the real atmosphere, IPV maps for the 350 K, 330 K, 315 K and 300 K surfaces for 30 September 1982 are presented in Figs. 2(a)–(d). Also shown are the 315 K pressure contours (Fig. 2(e)) and the 250 mb and 1000 mb geopotential height fields (Figs. 2(f), (g)). It should be noted that for compactness of presentation all the fields *except* the 350 K IPV maps are restricted to the domain north of 20°N. In the PV units used above, the contour intervals for Figs. 2(a), (b), (c), (d) are respectively 0.75,



1.0, 0.5 and 0.5 units. The contours representing values from 1.5 to 4 units tend to bunch together conspicuously at the edge of the stratospheric air, indicating that the data analysis, while not capturing the almost discontinuous change at the tropopause seen in

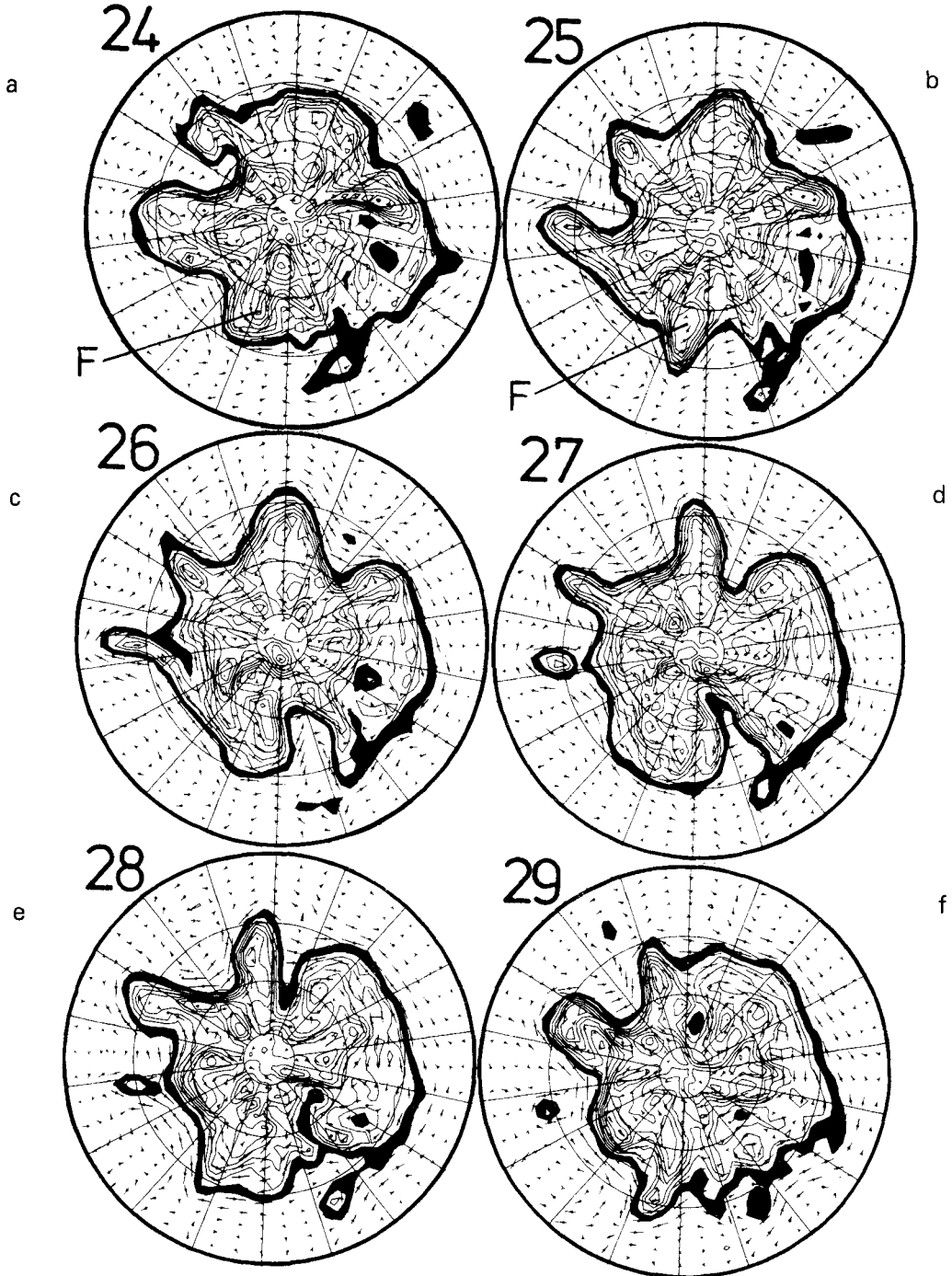


Figure 3. 330 K IPV maps for the region north of  $20^{\circ}\text{N}$  for the period 24–29 September 1982. The contour interval is 1.0 PV units and the regions with values 1–2 units are blacked in. Also shown are the horizontal velocity vectors on this surface, scaled as in Fig. 2.

higher resolution analyses using special data, such as those of Danielsen (1968) and Shapiro (1976), is representing the transition from tropospheric to stratospheric air in a reasonable manner, in much the same way as the objective 300–310 K maps of Obukhov

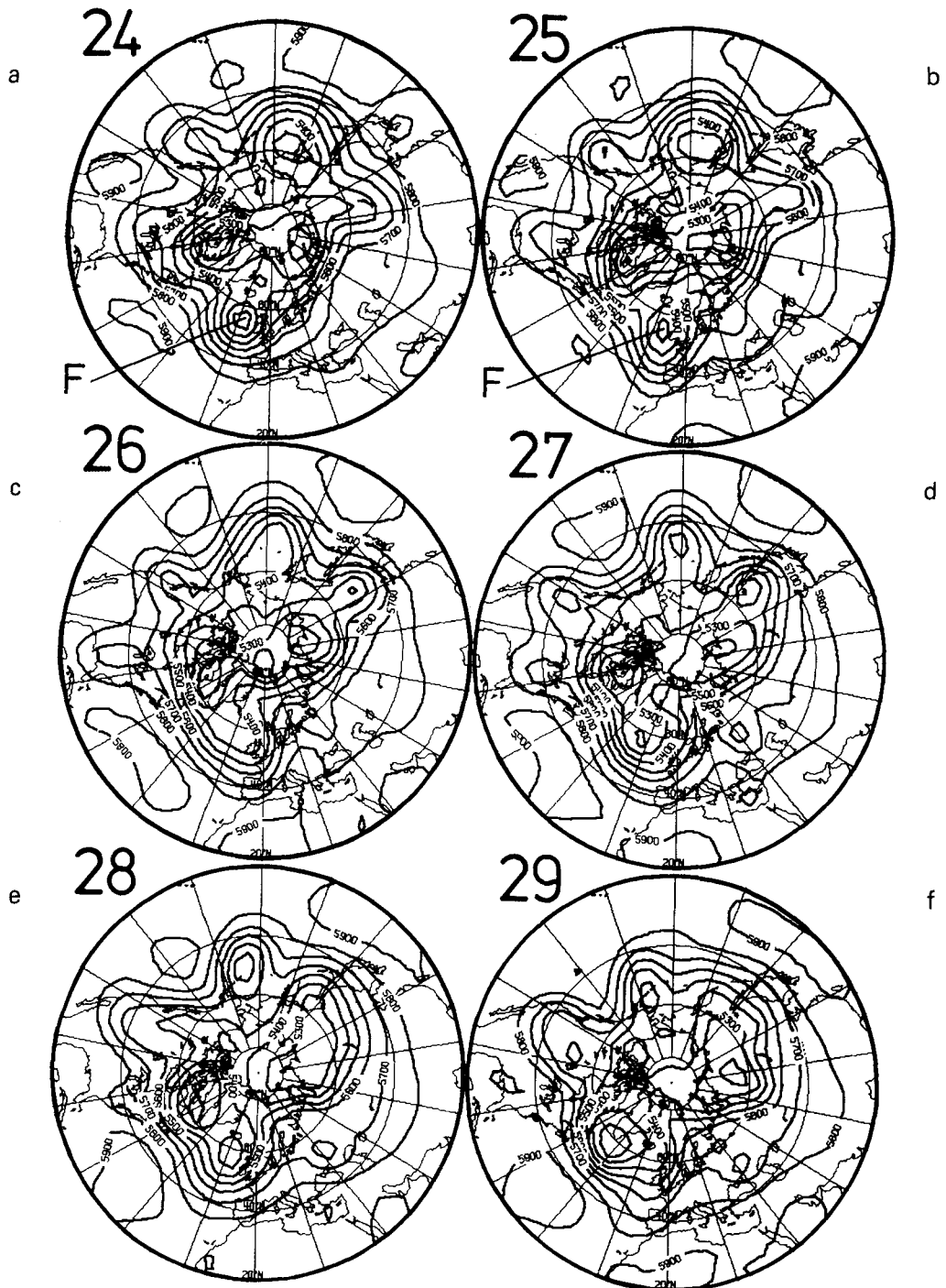


Figure 4. The 500 mb geopotential heights corresponding to the IPV maps shown in Fig. 3. They are for the period 24–29 September 1982 and cover the region north of 20°N. The contour interval is 100 m.

(1964), Danielsen (1967, 1968), and others. To aid visibility in Figs. 2(a)–(d), the region from 2.25 to 3 PV units is darkened in (a), and similarly 2 to 3 units in (b) and 1.5 to 2 units in (c) and (d).

On inspection of Figs. 2(a)–(d), vertical continuity is clear although different features tend to be more apparent at different levels. For example the cutoff high-PV region A near 30°N 145°W with its cyclonic circulation is predominantly an upper air feature. It is conspicuous at 350 K, present at 330 K but absent below. It is also just noticeable in the 250 mb height field, though its separation from the trough\* to the north is less apparent. The trough B near 40°N 115°W changes character with depth, becoming cut off at 315 K. It should be noted from Fig. 2(e) that this isentropic surface rises to just above 400 mb here, the high PV values in Fig. 2(c) indicating that the tropopause dips below 400 mb locally. The upstream ridge near 60°N 120°W is also most marked in the upper isentropic surfaces. The high potential vorticity in the trough C is apparent on all four surfaces. Figure 2(d) shows this to be one of the few regions in which stratospheric air (or so we presume it to be, for reasons to be elaborated in sections 2(c) and 8) is present even at the 300 K level. The associated surface low is by far the most prominent feature of the 1000 mb height field on this day (Fig. 2(g)). Trough D near 5°E 45°N shows to some extent on the 330 K and 315 K surfaces, but its structure, along with that of the neighbouring upstream ridge, is clearest and most interesting on the 350 K surface. There, the trough extends to 15°N (D' in Fig. 2(a)) and both it and the ridge are strongly tilted. A similar structure in a model nonlinear baroclinic wave will be described in section 6(d) and Fig. 20. It is interesting to note that the trough occupies the position of the mean mid-Atlantic tropical upper-level trough. Krishnamurti (1975) has interpreted this mean trough as due to the frequent appearance in this region of transient upper tropospheric cold cyclonic vortices; cf. feature D'' in Fig. 2(a). It is well known that similar phenomena are associated with the corresponding mid-Pacific trough (e.g. Shimamura 1981; Sugi and Kanamitsu 1982), although they may not always show clearly in the operational data. This point will be returned to in section 9.

It should be noted for later reference that the isobaric height field charts (Figs. 2(f), (g)) appear very much as highly smoothed versions of the IPV maps, particularly away from the earth's surface (Figs. 2(b), (f)).

The temporal development seen in the IPV maps is illustrated in Fig. 3, by the 330 K maps for the period 24–29 September 1982. The corresponding 500 mb geopotential height maps are given in Fig. 4; note again that the latter look like highly smoothed versions of the former. A considerable degree of continuity in the time development is immediately apparent, despite the presence of data or analysis errors which might be expected to distort or erase smaller-scale features such as thin, trailing troughs or shear lines (E. F. Danielsen, personal communication). For instance the trough initially near 90°W 40°N sharpens, cuts off and then decays while moving slowly eastwards. The trough near 140°W 40°N appears to shrink, then sharpen, then grow again as it too moves eastwards. The ridge near 140°E 50°N develops, sharpens, moves eastwards and cuts off, as does also the one near 10°E 50°N. However, that at 120°W 60°N weakens and disappears. Recall that Fig. 2 provides a large amount of information about the subsequent day, 30 September.

### (c) *Development of a North Atlantic cutoff cyclone*

Two specific developments during the period investigated will now be discussed in

\* The word 'trough' is used for an equatorward extension of high PV values since this corresponds to a trough in the associated height field structure. Similarly, 'ridge' is used for the poleward extension of low PV values.

more detail. The first is the formation of a cutoff cyclone in middle and high latitudes, as opposed to the lower-latitude cyclones already mentioned. The associated surface development is rapid and substantial, and the whole process closely resembles one of the scenarios envisaged by Kleinschmidt. Recently, Bleck and Mattocks (1984) have shown how related ideas can illuminate the phenomenon of Alpine lee cyclogenesis.

The development is especially well illustrated by the portion of the 300 K IPV map shown in Fig. 5 for 20–25 September 1982. Note carefully that the Greenwich meridian is at the right-hand edge of the 120° section: these maps are rotated 60° anticlockwise relative to those of Fig. 3. On 20 September the 300 K isentropic surface intersects the stratosphere in the vortex over the Davis Straits region, on the left of the map. (We shall see that this acts as Kleinschmidt's stratospheric 'reservoir' of high-PV air.) On 21–23 September, a large piece of high-PV air moves rapidly eastwards from the region, in a manner highly suggestive of a quasi-conservative process involving advection by strong upper air winds. By 23 September this high-PV region is greatly elongated. By 24 September, it appears to have cut off, by which time it has its own, very conspicuous, cyclonic circulation. On 25 September the feature is still present, though it has weakened. Note that its position corresponds to that of the trough F indicated for 24 and 25 September in Figs. 3(a) and (b) at altitudes further up in the stratosphere.

The corresponding 500 mb height fields (Fig. 6) show what looks like a smoothed, out-of-focus view of the same process. On 24 September a prominent cutoff cyclone has formed at 500 mb. Figure 7(a) gives the 1000 mb height maps for the middle period of Fig. 5, i.e. 22–24 September, showing the correspondingly rapid development of a large and conspicuous surface cyclone. It is particularly to be noted that the low-level circulation develops from 22 to 24 September without the low-level temperature field showing much structure until late in the period, when a cold pool of air sits over the surface low pressure (Fig. 7(b)). This is in marked contrast with developments in which surface baroclinicity is crucial.

Sections have been made across the cutoff cyclone in order to illustrate its vertical structure, which conforms well to the typical cutoff cyclone structures found in many earlier investigations, e.g. that of Peltonen (1963; see also Palmén and Newton 1969, Fig. 10.8). These sections will not be shown here; they can be found in Robertson (1984). However, a similar and more detailed section from Peltonen's paper is reproduced as Fig. 8, which according to Palmén and Newton "illustrates in beautiful form the characteristic thermal structure of a high-level cyclone". We also present, in Fig. 9, two sections across an Icelandic low at 12 z, 12 April 1983. These are of special interest since we can compare the portrayal of this cyclonic system by the present operational analyses (Fig. 9(a)) with a corresponding cross-section at far higher resolution (Fig. 9(b)) obtained by M. A. Shapiro (personal communication), using special aircraft measurements and drop-windsondes. The routine data analysis and the centred differences on a 3.75° grid, Fig. 9(a), while not showing the finest details of the local tropopause-folding process, does capture the essential nature of the situation to a remarkable degree. The tropopause dips down to at least 500 mb in this case, the isentropes bow up in the troposphere and down in the stratosphere, and the 0.75 PV contour even suggests, crudely, the shallow tongues of stratospheric air seen at high resolution in Fig. 9(b).

It is noteworthy that vertical cross-sections through *subtropical* upper tropospheric cold cyclones, for instance those given by Erickson (1971), Krishnamurti (1975), Shimamura (1981), Bengtsson *et al.* (1982), Kelley and Mock (1982) and Sugi and Kanamitsu (1982), all show the same gross features as in Figs. 8 and 9, namely a cold troposphere, a low tropopause and a warm stratosphere. Figure 10 shows a well-documented example taken from Erickson (1971). The same structure was also seen in

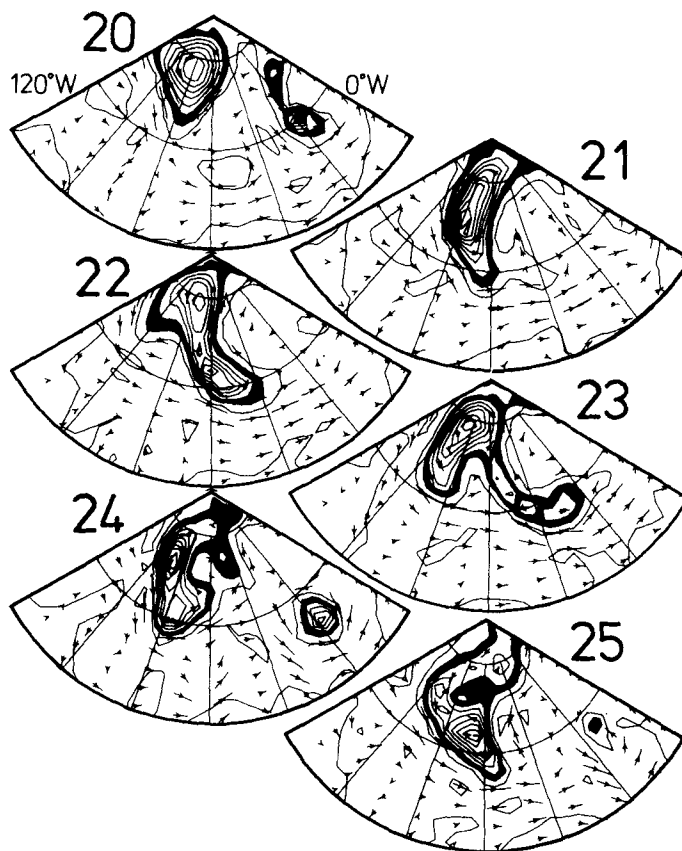


Figure 5. Sectors of the 300 K IPV maps for the period 20–25 September 1982. The region covered is from 40°N to the north pole and from 120°W to 0°W with the 60°W meridian central. The contour interval is 0.5 PV units and the region 1.5–2 units is blacked in. Also shown are the horizontal velocity vectors on this surface, scaled as in Fig. 2.

the present data in association with the feature D'' in Fig. 2(a). We shall see in section 3 that such a structure, which all the above-mentioned cases share qualitatively, is precisely that expected theoretically for the flow structure associated with an upper air high-PV anomaly like that originally postulated by Kleinschmidt. Moreover such gross differences as there are between tropical and high latitude cases are qualitatively consistent with those predicted theoretically from the different values of the Coriolis parameter (Eqs. (33) below).

Finer details such as the shallow tongues seen in Fig. 9(b), whose presence or absence may be difficult to determine observationally, are probably explicable, when they occur, in terms of the detailed spatial structure of the PV anomaly and its formation by competing processes such as different amounts of advection along different isentropic surfaces, and non-conservative effects such as clear air turbulence (e.g. Staley 1960; Shapiro 1978, 1980; Holopainen and Rontu 1981), which may tend to modify such tongues locally (see section 7).

(d) *A minor blocking episode*

The other development to be singled out for discussion is that of a blocking anticyclone, again in the North Atlantic. A portion of each 330 K IPV map for the period 30 September–7 October is shown in Fig. 11. Note that this period follows on from that

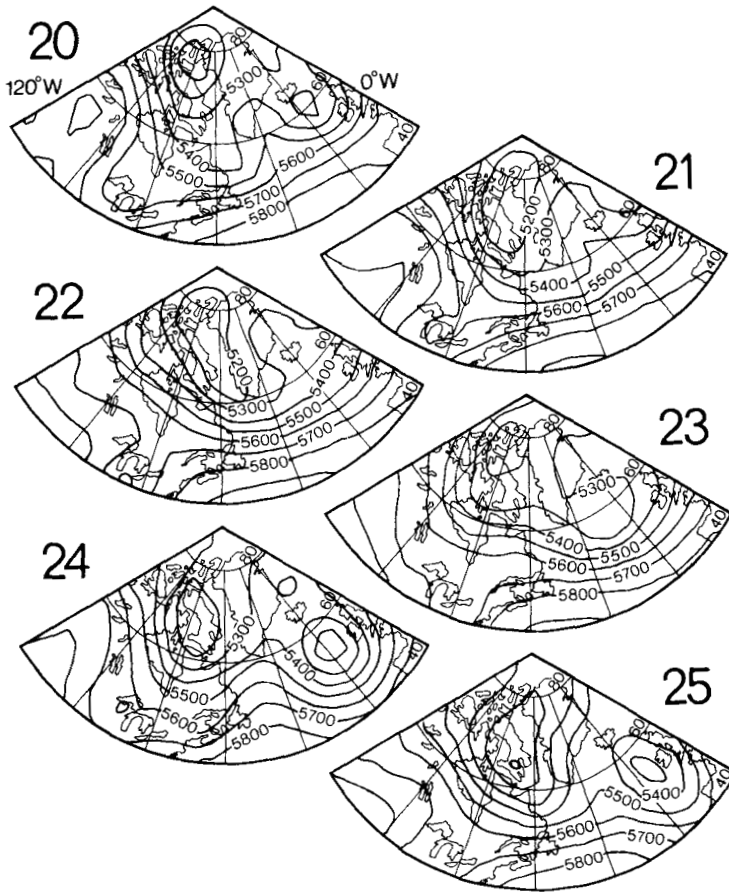


Figure 6. The 500 mb geopotential heights corresponding to the IPV maps shown in Fig. 5. They are for the period 20–25 September 1982 and the region  $40^{\circ}\text{N}$ – $90^{\circ}\text{N}$  and  $120^{\circ}\text{W}$ – $0^{\circ}\text{W}$ . The contour interval is 100 m.

illustrated in Figs. 2 and 3 with an overlap of one day (Figs. 2(b) and 11(a)), and that unlike Figs. 5–7 these maps have the *same* orientation as Figs. 2 and 3, with the Greenwich meridian central. The trough near  $30^{\circ}\text{W}$  in Fig. 11(a) corresponds to the broad trough C of Fig. 2(b).

Figures 2(a)–(d) and 2(g) indicate that the trough C represents an IPV anomaly of great strength, depth and breadth with which is associated a strong cyclonic circulation at all levels. Note in particular the suggestion of a cyclonic spiral pattern in Fig. 2(c). Figures 11(a) to (c) indicate that the strong south-westerly winds ahead of this system are very effective in advecting low-PV air polewards, the more so once they are reinforced by the anticyclonic circulation developing around the encroaching low-PV air. By 2 October, this low-PV air has reached  $70^{\circ}\text{N}$  and is starting to cut off. On 3 October the cutting-off process is complete with a large pool of low-PV air of subtropical origin stranded at  $60^{\circ}\text{N}$  with its own strong anticyclonic circulation. Over the next few days this low-PV air moves eastward and southward, spinning as it goes, with little change in magnitude and, on 7 October, appears to have linked back with the subtropical air. Upstream, starting on 4 and 5 October, the same sequence of events recurs so that by 8 October (not shown) a new cutoff has formed to the west of the previous one. Again the 250 mb height field sequence in Fig. 12 shows what looks like a smoothed version of these maps, with a blocking anticyclone forming and moving south-eastwards and a new

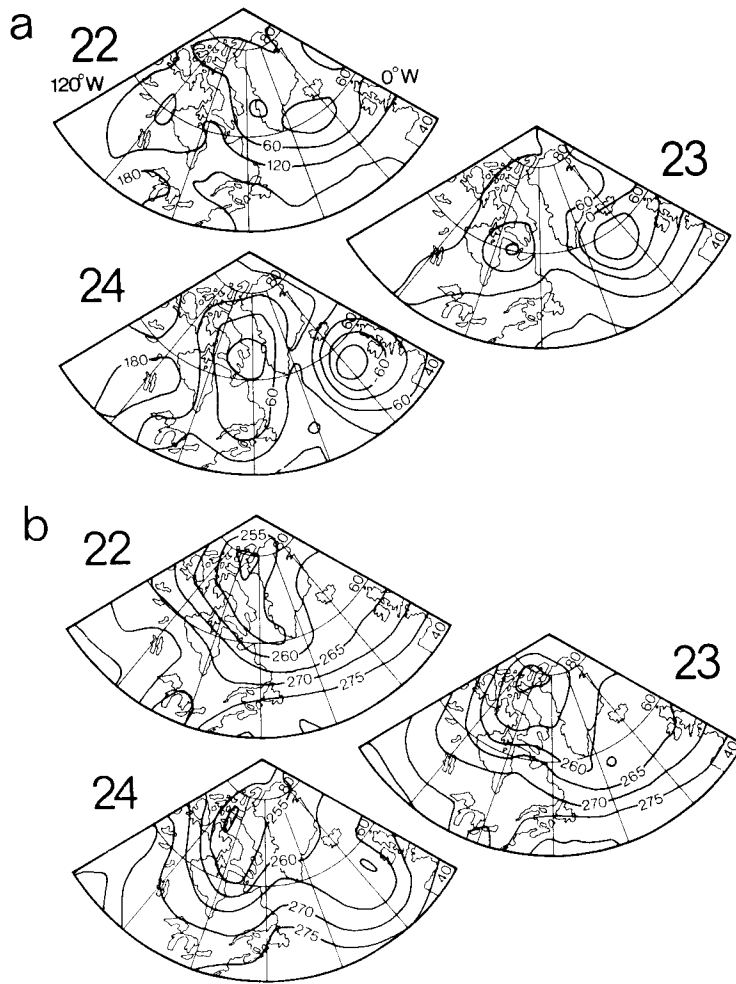


Figure 7. The 1000 mb geopotential (a) and 700 mb temperature (b) for the period 22–24 September 1982 and the region  $40^{\circ}\text{N}$ – $90^{\circ}\text{N}$  and  $120^{\circ}\text{W}$ – $0^{\circ}\text{W}$  corresponding to that shown in Figs. 5 and 6. The contour intervals are 60 m and 5 K, respectively.

one beginning to appear upstream. The 1000 mb height and 700 mb temperature for 2 October (Fig. 13) emphasize the deep vertical scale of the poleward flow of subtropical air. The low-level temperature reflects the invasion of the subtropical air mass seen so clearly in Fig. 11(c).

Having studied this one event we should note that Fig. 3 shows a very similar incipient blocking sequence occurring from 25 to 29 September (although less high-PV air is finally cut off) so that near  $20^{\circ}\text{E}$  the entire two-week period, 25 September to 8 October, is dominated by blocking associated with two separate poleward incursion episodes and the subsequent cutting off of low-PV subtropical air. As already mentioned, a third incursion occurred after 8 October, albeit further west. Such repeated incursions seem typical (e.g. Berggren *et al.* 1949; Palmén and Newton 1969, § 10.1), and as Mahlman (1979) points out they may be the physical reality behind the recently developed ‘eddy-mean’ view of the maintenance of time-averaged or low-pass-filtered blocking events (Green 1977; Mahlman 1979; Shutts 1983, 1985; Hoskins *et al.* 1983; Illari and Marshall 1983; Illari 1984).

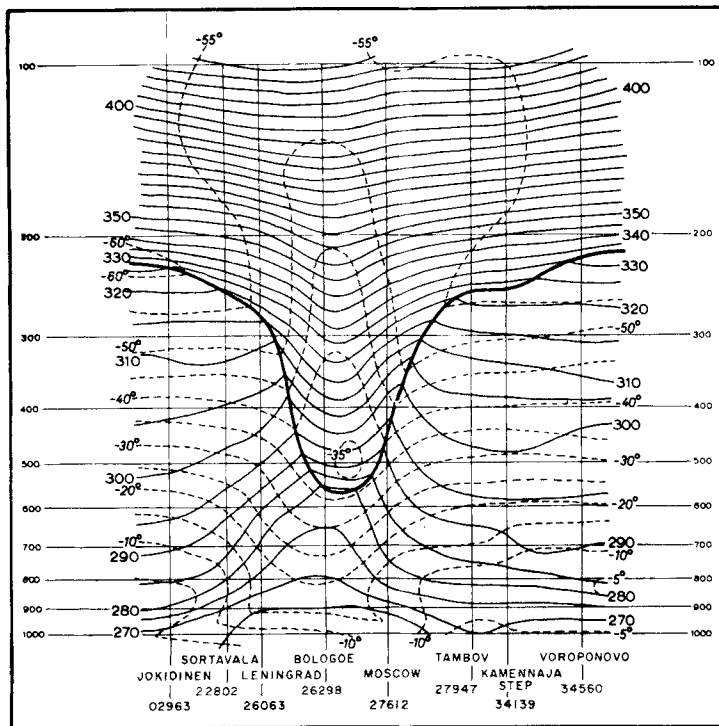


Figure 8. A vertical section through a cutoff cyclone at 12 GCT November 16 1959 produced by Peltonen (1963). The heavy line represents the tropopause; dashed lines are isotherms at 5°C intervals and solid lines isentropes every 5 K. The centre of the cyclone was at about 35°E, 58°N.

The advective nature of the process, i.e. approximate satisfaction of Eqs. (11) and (12), was directly checked in the case of Fig. 11 by performing numerical experiments in which a passive tracer was advected starting with the initial conditions of the 330 K IPV map of 2 October, and using the 330 K horizontal velocity field interpolated between 2 and 3 October (Robertson 1984). The advection equation was integrated using simple centred finite differences in space and time with a half-hour timestep. With no dissipation included, the essential nature of the cutoff at 3 October is reproduced, but there is a large amount of small-scale structure. The inclusion of a nonlinear scale-selective dissipation, acting on a time scale of order one day for features of length scale  $L \sim 200$  km, reduces the noise and produces a picture which resembles the observed picture very well in the features to which attention has been drawn including, again, the cutoff at 3 October.

Similar phenomena are observed in ocean currents. The best-documented cases are probably those of 'Gulf Stream rings' (e.g. Rhines 1979, Fig. 1; Robinson 1983; Kennelly *et al.* 1985).

(e) *The conceptual duality between cutoff cyclones and blocking anticyclones*

The individual cutoff cyclones and blocking anticyclones which we have studied appear to be formed in a basically similar manner, by advection leading to the cutting-off of upper IPV anomalies of the appropriate sign. Indeed the cutoff cyclone and blocking anticyclone appear from this viewpoint to be fundamentally the same phenomenon, the only difference (apart from differences of spatial scale) being the sign of the IPV anomaly. Confidence in this conceptual duality is further strengthened by a comparison of vertical cross-sections. Figure 14 shows a cross-section through the blocking anticyclone of 4 October along the line of longitude indicated in Fig. 11(e), from the operational data.

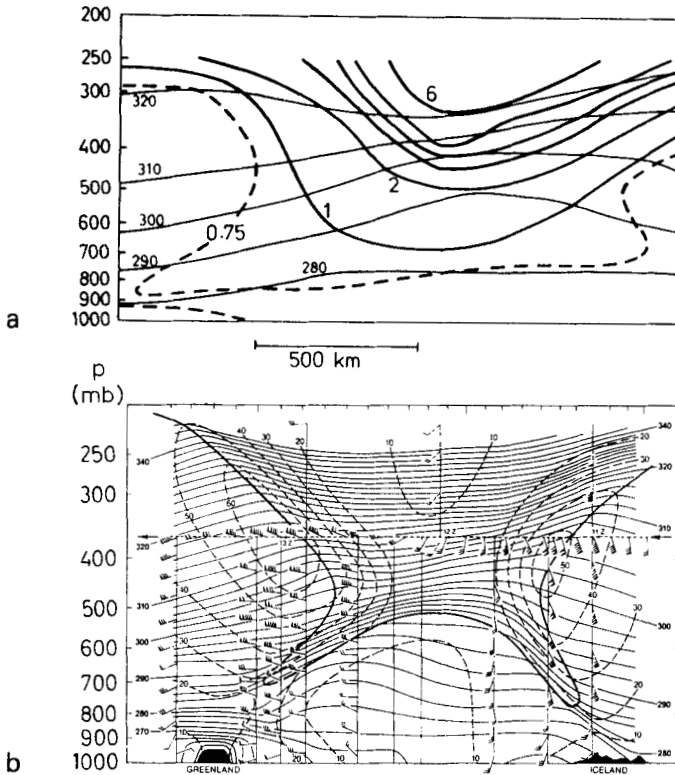


Figure 9. Vertical cross-sections along a SW-NE line through the Icelandic low on 12 April 1983. The first section (a) shows the results obtained by simple finite differences applied to the routine ECMWF analysis at 12z on that day. The thin lines indicate isentropes at 10 K intervals and the thick lines PV at 1 unit intervals. The 0.75 PV unit contour is shown by a heavy dashed line. The second section (b), from M. A. Shapiro (personal communication), is the result of detailed measurements using aircraft and dropwindsondes. Isentropes every 2 K are indicated by light solid lines, isotachs every  $10 \text{ m s}^{-1}$  by dashed lines and the estimated tropopause position by a heavy continuous line. The scales and orientation of the two sections are approximately the same.

As far as gross features are concerned, everything is the opposite way round from Figs. 8–10. The tropopause is high, the isentropes in the troposphere bow downwards, and those in the stratosphere bow upwards. The very low potential vorticity just under the tropopause, less than 0.5 PV units, is particularly striking. Once again we shall see that this structure is just that expected theoretically for the fields induced by an isolated, upper air IPV anomaly of the appropriate sign.

The question of diabatic and frictional effects will be postponed until sections 6(e) and 7. As we shall argue in section 7, the duality ends there: diabatic effects, in particular, are likely to be quite different for the two signs of anomaly.

### 3. SOME SIMPLE EXAMPLES, FOLLOWING KLEINSCHMIDT

We next present and discuss some theoretical examples which will illustrate, in idealized form, the typical flow structures induced by isolated IPV anomalies of either sign in a given, statically stable reference state. These examples will prove useful as basic building blocks for IPV thinking.

The examples assume a horizontally uniform reference state, with a constant Coriolis parameter  $f$ . The mass distribution of potential temperature  $\theta$  is specified by prescribing the associated hydrostatic pressure field  $p$  as a function of  $\theta$ :

$$p = p_{\text{ref}}(\theta). \tag{16}$$

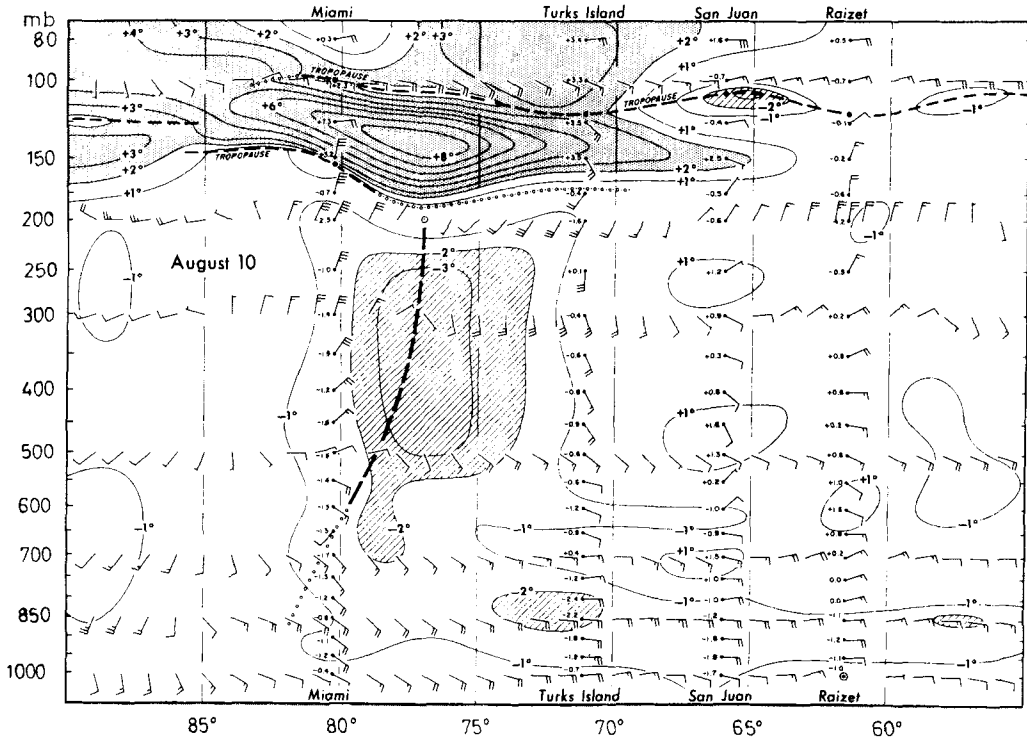


Figure 10. A vertical section along a NW-SE line just north of Cuba through a subtropical oceanic upper-level cold vortex at 1200 GMT 10 August 1966, produced by Erickson (1971). Isolines are temperature deviations ( $^{\circ}\text{C}$ ) from a mean Caribbean atmosphere for August. Deviations exceeding  $2^{\circ}\text{C}$  are shaded. Data are also plotted for four individual stations; interpolated winds (full barb =  $10\text{ kt} \approx 5\text{ m s}^{-1}$ ) are from streamline-isotach analysis. The heavy dashed line is the axis of the upper-level cyclonic curvature.

The function  $p_{\text{ref}}(\theta)$  is assumed to be monotonically decreasing, so that the reference state is statically stable. Being horizontally uniform, the reference state has constant PV on each isentropic surface,  $P_{\text{ref}}(\theta)$  say.

We express condition (ii) of section 1(d) by requiring that the actual state have the same mass distribution as the reference state (16), i.e. that the actual state can be obtained from the reference state by an adiabatic rearrangement of mass. Thus the actual hydrostatic pressure field  $p(x, y, \theta)$ , expressed in isentropic coordinates, will be required to satisfy, for each value of  $\theta$ , the relation

$$\iint \frac{\partial p(x, y, \theta)}{\partial \theta} dx dy = \frac{dp_{\text{ref}}(\theta)}{d\theta} \iint dx dy \tag{17a}$$

where the derivative  $\partial/\partial\theta$  is taken at constant horizontal position  $(x, y)$ . The area integral is understood to be taken over a horizontal domain much larger than the size of the IPV anomaly. The condition (17a) is equivalent to requiring that the mass lying between the isentropic surfaces  $\theta$  and  $\theta + d\theta$  be the same as in the reference state. It should be noted that together with (14) this implies, in the same way as in (10), a relationship between the distribution of IPV anomalies  $P' = P(x, y, \theta) - P_{\text{ref}}(\theta)$  on each isentropic surface, and the relative circulation  $C_b(\theta)$  around the intersection of that surface with the domain boundary, assuming smooth stratification. The relationship may be written

$$-\iint g^{-1}(\partial p/\partial\theta)P' dx dy = C_b(\theta). \tag{17b}$$

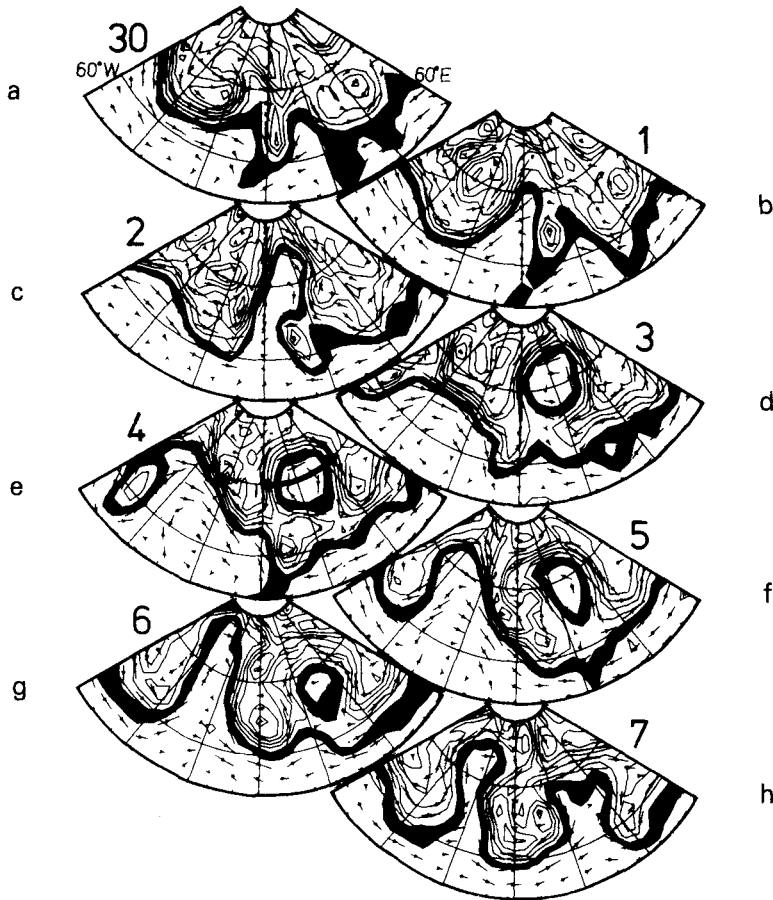


Figure 11. Sectors of the 330 K IPV maps for the period 30 September–7 October 1982. The region covered is from 30°N to 80°N and from 60°W to 60°E, with the Greenwich meridian central. The contour interval is 1 PV unit with the regions 1–2 units blacked in. The line at 60°N on 4 October indicates the location of the section shown below in Fig. 14. Also shown are the horizontal velocity vectors on this surface, scaled as in Fig. 2. Again, the points of the arrow heads are plotted at the mid-points of the arrows which also mark the grid-points to which the vectors refer.

For horizontally large domains it may be useful to restrict attention to cases in which  $C_b(\theta)$  is, say, zero or constant, and the restrictions then imposed by (17b) on possible configurations of IPV anomalies should be noted. In particular, an ‘isolated’ anomaly must then be considered to be embedded in a surround of weak  $P'$  values inversely proportional to the area of the domain. This is to be understood, where necessary, in what follows.

Suppose now that the actual state has a given, circularly symmetric PV anomaly on some of the isentropic surfaces. Considerations of symmetry imply that the associated wind, pressure and temperature fields will also be circularly symmetric. If friction and diabatic heating are neglected, the flow must also be steady, nondivergent and purely azimuthal. This will now be assumed to be the case, and the azimuthal wind speed written as a function  $v(r, \theta)$  of  $\theta$  and the horizontal distance  $r$  from the centre of the anomaly. The *balance condition*, condition (i) of section 1(d), is here expressed by the gradient wind and hydrostatic relations, which are exact under the present assumptions. In terms of the Montgomery potential  $M(r, \theta) = \phi + c_p T$ ,  $\phi$  being the geopotential, the gradient

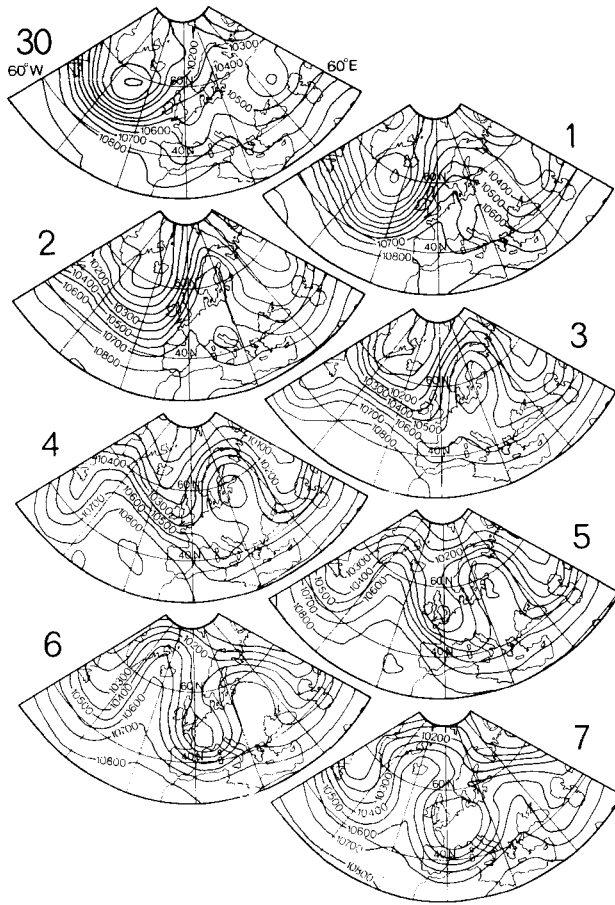


Figure 12. The 250 mb geopotential heights corresponding to the IPV maps shown in Fig. 11. They are for the period 30 September–7 October 1982 and the region 30°N–80°N and 60°W–60°E. The contour interval is 100 m.

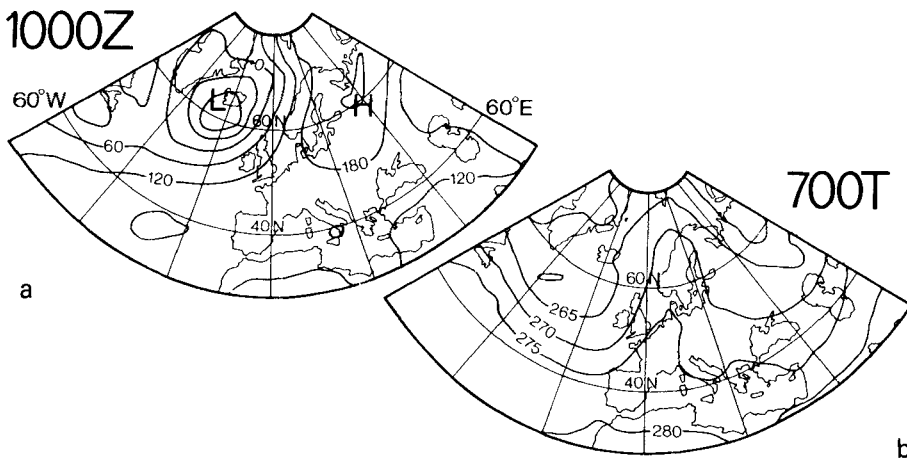


Figure 13. The 1000 mb geopotential height (a), and 700 mb temperature (b), for 2 October 1982 and the region 30°N–80°N and 60°W–60°E corresponding to that shown in Figs. 11 and 12. The contour intervals are 60 m and 5 K respectively.

wind and hydrostatic relations may be written

$$\partial M(r, \theta)/\partial r = (f + v/r)v \quad \text{and} \quad \partial M(r, \theta)/\partial \theta = \Pi(p) \quad (18a, b)$$

where

$$\Pi(p) = c_p(p/p_0)^\kappa, \quad (19a)$$

the Exner function, with  $\kappa = (\gamma - 1)/\gamma \approx 2/7$  and  $p_0 = 1000$  mb. (To verify (18a, b) from their isobaric forms, recall that the specific enthalpy

$$c_p T = \Pi(p)\theta, \quad (19b)$$

so that the first derivative of the function  $\Pi(p)$ , which we denote by  $R(p)$ , satisfies

$$R(p) = d\Pi(p)/dp = \kappa\Pi(p)/p = \kappa c_p T/(p\theta) = 1/(\rho\theta), \quad (20)$$

the last step using the perfect gas equation  $p = \kappa c_p \rho T$ , where  $\rho$  is density. Recall also, in applying (19b), that the differentiation in (18a) is to be carried out at constant  $\theta$ .) Elimination of  $M$  by cross-differentiation of (18a) and (18b) gives the isentropic form of the thermal wind equation, which after making use of (20) can be written

$$f_{\text{loc}} \partial v / \partial \theta = R(p) \partial p / \partial r \quad (21)$$

where  $f_{\text{loc}} = f + 2v/r$ , twice the local absolute angular velocity. From (14), the potential vorticity is

$$P = P(r, \theta) = \sigma^{-1} \zeta_{a\theta}, \quad (22)$$

where

$$\sigma = -g^{-1} \partial p / \partial \theta > 0, \quad (23)$$

the mass density in  $xy\theta$  space, and where

$$\zeta_{a\theta} = f + \zeta_\theta, \quad (24)$$

the absolute isentropic vorticity. The relative isentropic vorticity  $\zeta_\theta$  is given by (9), which under the assumption of circular symmetry is equivalent to

$$\zeta_\theta = r^{-1} \partial(rv) / \partial r, \quad (25)$$

the horizontal derivative again being taken at constant  $\theta$ .

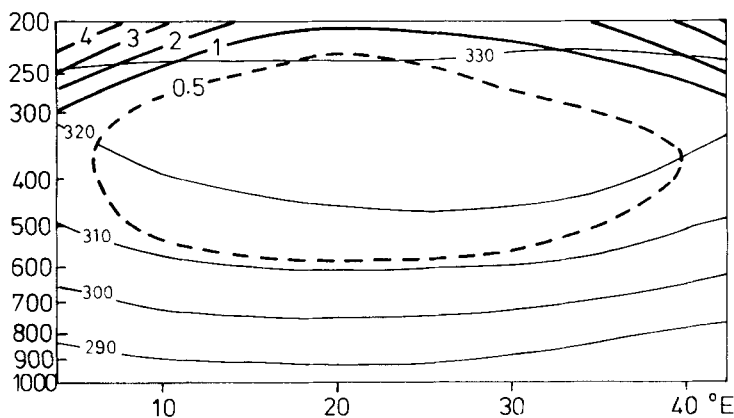


Figure 14. A vertical section on 4 October 1982 along the line at  $60^\circ\text{N}$  shown in the corresponding panel of Fig. 11. As in Fig. 9(a), the light continuous lines are isentropes drawn every 10 K and the heavy continuous lines are PV contours every 1 unit. The heavy dashed contour indicates a PV value of 0.5 units.

Under these assumptions, the invertibility principle can be expressed in the following way. If (22) is differentiated with respect to  $r$ , using (24), (25) and the assumption of constant  $f$ , the result after multiplication by  $\sigma$  can be written as

$$\frac{\partial}{\partial r} \left[ \frac{1}{r} \frac{\partial(rv)}{\partial r} \right] - \frac{\zeta_{a\theta}}{\sigma} \frac{\partial \sigma}{\partial r} = \sigma \frac{\partial P}{\partial r}. \tag{26}$$

Differentiating (23) with respect to  $r$  and making use of the thermal wind equation (21), we get

$$-g \frac{\partial \sigma}{\partial r} = \frac{\partial^2 p}{\partial r \partial \theta} = \frac{\partial}{\partial \theta} \left[ \frac{f_{loc}}{R} \frac{\partial v}{\partial \theta} \right]. \tag{27}$$

(For later reference, the relation between  $R$ ,  $\sigma$  and the static stability can be shown to be

$$R = g/(\sigma N^2 \theta^2) > 0, \tag{28}$$

$N^2$  being the static stability expressed as the square of the Brunt–Väisälä or buoyancy frequency.) Using (22) and (27), we can write (26) finally as

$$\frac{\partial}{\partial r} \left[ \frac{1}{r} \frac{\partial(rv)}{\partial r} \right] + g^{-1} P \frac{\partial}{\partial \theta} \left( \frac{f_{loc}}{R} \frac{\partial v}{\partial \theta} \right) = \sigma \frac{\partial P}{\partial r} \tag{29}$$

a nonlinear equation which can be solved, for instance by relaxation methods, as described below, for the wind profile  $v(r, \theta)$  given the PV distribution  $P(r, \theta)$ . Note that the *isentropic gradient* of  $P$  appears on the right-hand side as a prescribed forcing function.

Together with suitable boundary conditions, and the condition (17a), Eq. (29) expresses the invertibility principle in much the same way as was done in Kleinschmidt's original work. Note that if

$$f_{loc} P > 0, \tag{30}$$

as we shall assume, then Eq. (29) is an elliptic equation, so that the problem is well posed. As is well known, (30), together with (23), also expresses the assumption of static, inertial, and 'symmetric' baroclinic stability previously made in section 1(d) (e.g. Hoskins 1974, with  $f$  replaced by  $f_{loc}$ ). Equation (29) is exact; its simple form is due to the assumption of circular symmetry and the use of isentropic coordinates.

Note further that if we were to make the approximations

$$f_{loc} \approx \zeta_{a\theta} \approx f, \quad R \approx R_{ref}(\theta), \quad \sigma \approx \sigma_{ref}(\theta) \tag{31}$$

everywhere except when calculating the forcing function  $\partial P/\partial r$  from (22), where  $R_{ref}(\theta)$  and  $\sigma_{ref}(\theta)$  are the reference-state profiles of  $R$  and  $\sigma$ , then (29) would simplify to

$$\frac{\partial}{\partial r} \left( \frac{1}{r} \frac{\partial(rv)}{\partial r} \right) + \frac{f^2}{g \sigma_{ref}} \frac{\partial}{\partial \theta} \left( R_{ref}^{-1} \frac{\partial v}{\partial \theta} \right) = \sigma_{ref} \frac{\partial P}{\partial r}, \tag{32}$$

which is the isentropic coordinate version of the usual quasi-geostrophic approximation to (29). The elliptic operator on the left-hand side of (32) is now linear and if, further,  $\sigma_{ref}$  and  $R_{ref}$  were constants, then apart from its slightly different  $r$ -dependence the operator would be a three-dimensional Laplacian, after suitably rescaling the vertical coordinate according to the Prandtl–Rossby–Burger relation

$$\Delta \theta \sim fL/(Rg\sigma)^{1/2} \quad (\text{cf. } H \sim fL/N) \tag{33a}$$

(e.g. Rossby 1938), where  $L$  is the horizontal scale of the flow. For a more accurate scale relation corresponding to (29) we may replace  $f$  by  $(f_{loc}P\sigma)^{1/2}$ , giving

$$\Delta\theta \sim (f_{loc}P/Rg)^{1/2}L \quad (\text{cf. } H \sim (f_{loc}P\sigma)^{1/2}L/N), \tag{33b}$$

which would be relevant near the equator.  $H$  and  $\Delta\theta$  are respectively the scales in physical,  $xyz$  space and in  $xy\theta$  space, measuring the vertical penetration of the induced flow structure above or below the location of the IPV anomaly. The relevance of  $\Delta\theta$  rather than  $H$  in the isentropic coordinate description explains why the square of the Brunt–Väisälä frequency appears in the denominator, rather than the numerator of (28).

We shall call the expressions on the right of (33a) the Rossby heights (in  $xy\theta$  and  $xyz$  space respectively), and denote them by  $\Delta\theta_{Rossby}$  and  $H_{Rossby}$ . As is well known, the concept is complementary to that of the Rossby radius of deformation, which is the horizontal scale  $L$  obtained from (33a) when  $\Delta\theta$  or  $H$  is given. If  $\Delta\theta_{Rossby}$  and  $H_{Rossby}$  greatly exceed the corresponding reference-density scale heights  $\Delta\theta_{density}$ ,  $H_{density}$  (the scale heights for variation of  $\sigma$  and  $\rho$  respectively), then non-Boussinesq effects are important. Order-of-magnitude relations which cover the whole range of  $\Delta\theta$  or  $H$  are

$$\Delta\theta \sim \min\{\Delta\theta_{Rossby}, \Delta\theta_{density}\} \quad \text{and} \quad H \sim \min\{H_{Rossby}, H_{density}\} \tag{33c}$$

for the vertical scales for downward penetration of the induced wind field, and

$$\Delta\theta \sim \max\left\{\Delta\theta_{Rossby}, \frac{(\Delta\theta_{Rossby})^2}{\Delta\theta_{density}}\right\} \quad \text{and} \quad H \sim \max\left\{H_{Rossby}, \frac{(H_{Rossby})^2}{H_{density}}\right\} \tag{33d}$$

for its upward penetration (Rossby, *op. cit.*). These more general scaling rules are related to well-known results in tidal theory.\*

The fact that the inverse Laplacian is a smoothing operator should be kept in mind; for instance it is the essential reason why Figs. 4, 6 and 12 look like smoothed versions of Figs. 3, 5 and 11 (see also (44) below). There is an associated *scale effect*, whereby small-scale features of given strength in the IPV field have a relatively weak effect on the velocity field whereas large-scale features have a relatively strong effect. As already mentioned, this is one of the reasons for supposing that coarse-grain IPV distributions are dynamically meaningful. Note that the smoothing takes place in the vertical as well as in the horizontal.

The exact operator appearing in (29) is nonlinear because of the presence of the unknown functions  $f_{loc}$ ,  $R$  and  $\sigma$  (appearing on the right-hand side). As Figs. 3, 4, 5, 6, 11 and 12 suggest, this operator very often has the same qualitative character as its approximate counterpart in (32), although it should be remembered that differences near fronts and shear lines can be important (e.g. Hoskins and Bretherton 1972). In many circumstances of interest, (29) may be expected to be soluble iteratively, for given  $P(r, \theta)$ , having regard to any constraint imposed via (17b). The conceptually simplest albeit not

\* The alternatives within braces are the asymptotic forms for large and small  $H_{density}/H_{Rossby}$ , as the case may be, of the more precise expression

$$H = |(2H_{density})^{-1} \pm \sqrt{(H_{Rossby})^{-2} + (2H_{density})^{-2}}|^{-1},$$

the + and – signs corresponding to downward and upward penetration respectively, which arises in the theory of very-low-frequency tidal oscillations of negative equivalent depth (Kato 1966; Lindzen 1966). The problem solved by Rossby (1938) is an approximate version of the same problem; both concern the linear response to a forcing effect of a given horizontal scale  $L$  at a given level. A convenient reference is Holton (1975), in which it should be noted that the expression (2.85) corresponds apart from sign convention to minus the square of the expression

$$\sqrt{(H_{Rossby})^{-2} + (2H_{density})^{-2}}$$

above,  $H_{Rossby}$  being equal to  $\sqrt{-gh/N^2}$  in Holton's notation, where  $h$  is the equivalent depth.

the most powerful method starts from a solution to (32) as first guess, and then refines the initial approximations (31) by straightforward iteration. Notice carefully how the condition (17a) invoking the reference state has to enter into this process. As soon as a guess for  $v(r, \theta)$  has been computed from (29), using the previous guesses for  $R(p) = R(r, \theta)$ , and  $\sigma(r, \theta)$ , improved approximations to  $R(r, \theta)$  and  $\sigma(r, \theta)$  must be derived

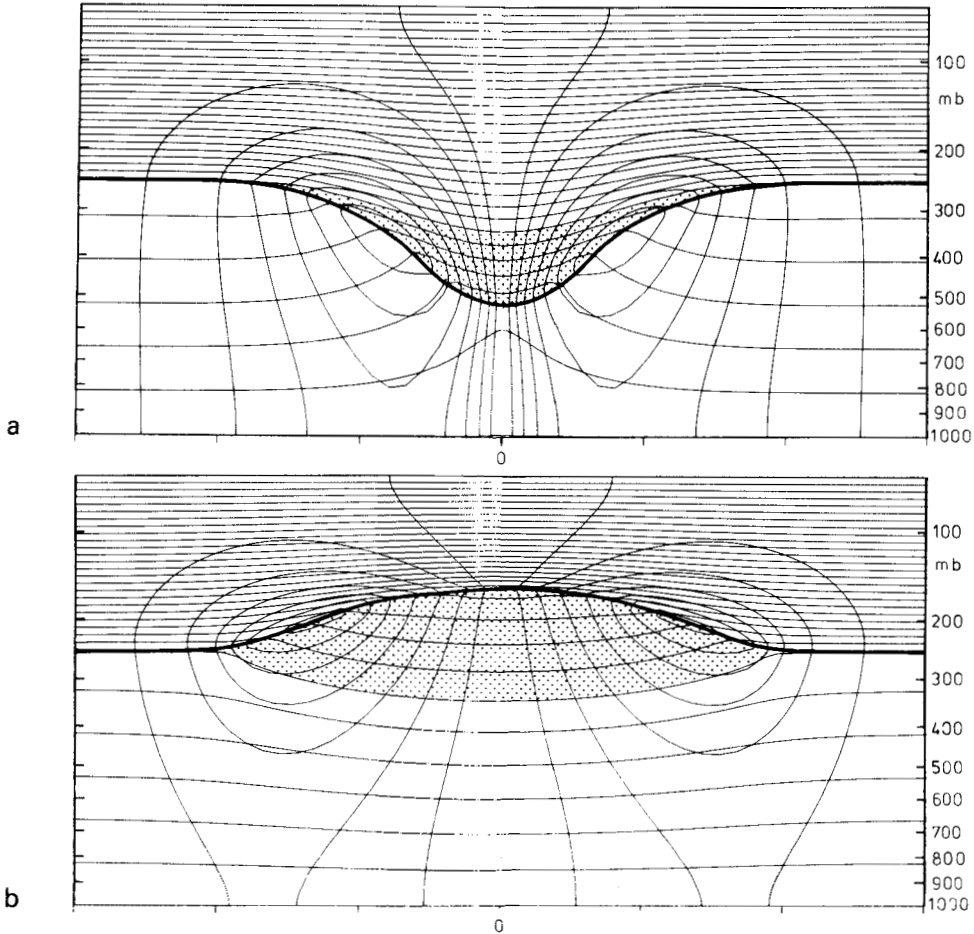


Figure 15. Circularly symmetric flows induced by simple, isolated, IPV anomalies (whose locations are shown stippled) as described in the text. The basic static stability  $\bar{N}$  and therefore  $\bar{P}$  (defined in (34)) was uniform in the tropospheric region and six times larger in the stratospheric region. The vertical coordinate  $z$  is nearly the same as physical height but is defined exactly in (35),  $g/\theta_0$  being taken to be  $(1/30) \text{ m s}^{-2} \text{ K}^{-1}$ . The reference tropospheric 'height'  $z$  was 10 km and the total domain 'height' 16.67 km:  $f$  was taken to be  $10^{-4} \text{ s}^{-1}$ . The IPV anomaly was defined by taking the tropopause potential temperature to vary in the manner  $\frac{1}{2}A\{\cos(\pi\bar{r}/r_0) + 1\}$  for  $\bar{r} < r_0$ , where  $\bar{r} = r(f_{\text{loc}}/f)^{1/2}$ . Here the amplitude  $A$  was taken to be  $-24 \text{ K}$  in (a) and  $+24 \text{ K}$  in (b) which may be compared with a potential temperature increase of 30 K over the depth of the reference troposphere. The parameter  $r_0$  was taken to be 1667 km. The undisturbed  $\theta$  distribution was imposed as a boundary condition at  $\bar{r} = 5000 \text{ km}$ , and the solutions obtained had only a weak dependence of  $C_b(\theta)$  upon  $\theta$  as well as a far-field stratification approximating the reference stratification (16). (In terms of our definitions, the IPV anomaly in the stippled regions must therefore strictly speaking be considered to be embedded in a suitable 'surround' of much weaker anomalies, as noted below (17b).) Only the region  $r < 2500 \text{ km}$  is shown here, and the tick marks below the axes are drawn every 833 km. The thick line represents the tropopause and the two sets of thin lines the isentropes every 5 K and the transverse velocity every  $3 \text{ m s}^{-1}$ . The zero isotach on the axis of symmetry is omitted. In (a) the sense of the azimuthal wind is cyclonic and in (b) it is anticyclonic, in both cases the maximum contour value being  $21 \text{ m s}^{-1}$ . The surface pressure anomaly is  $-41 \text{ mb}$  in (a) and  $+13 \text{ mb}$  in (b) and the relative vorticity extrema (located at the tropopause) are  $1.7f$  in (a) and  $-0.6f$  in (b). The maximum surface winds are  $15 \text{ m s}^{-1}$  and  $6 \text{ m s}^{-1}$  respectively. For more details of the method of computation, see Thorpe (1985).

Courtesy of A. J. Thorpe.

for use in the next iteration. This requires (18a) to be integrated with respect to  $r$ , after which (18b) and (19a) are used to get  $p(r, \theta)$  followed by (20) and (23) to get  $R$  and  $\sigma$ . When (18a) is integrated with respect to  $r$ , an arbitrary function of  $\theta$  arises as a function of integration, and the reference-state condition (17a), along with the boundary conditions, is needed to determine this function of integration.

Figure 15 presents a pair of exact solutions of (29), under the boundary conditions  $v \rightarrow 0$  as  $r \rightarrow \infty$  and  $\theta = \text{constant}$  at 60 and 1000 mb, showing the flow structures induced by isolated, upper air PV anomalies of either sign. The calculations were done by Dr A. J. Thorpe, using a more sophisticated method (Thorpe 1985) which, among other things, is more easily capable of dealing with boundary temperature distributions. The reference state (16) consists of two layers with differing static stabilities representing the troposphere and the stratosphere. Figure 15(a) is the flow structure induced by a positive (cyclonic) IPV anomaly of simple shape, and Fig. 15(b) is that induced by a similar but negative (anticyclonic) anomaly which, like its typical real-atmospheric counterpart, has a somewhat larger radial extent. The location of the anomaly on each isentropic surface is shown stippled. The qualitative resemblance to the observed structures illustrated in Figs. 8–10 and 14 is at once apparent, both for the cyclonic and the anticyclonic anomalies.

The calculations assumed IPV anomalies of simpler shapes than that in Fig. 9(b). The shapes were more like those suggested by Figs. 8 and 14. More precisely, for computational convenience the anomalies and the reference state were defined in terms of the quantities

$$\tilde{P} = g^{-1}P/R = g^{-1}\theta_0\zeta_\theta \partial\theta/\partial z \quad \text{and} \quad \tilde{N}_{\text{ref}}^2 = \frac{g}{\theta_0} \frac{d\theta_{\text{ref}}(z)}{dz} \quad (34)$$

where

$$z = g^{-1}\theta_0\{\Pi(p_0) - \Pi(p)\} \quad (35)$$

is the height-like pressure coordinate used by Hoskins and Bretherton (1972),  $\theta_0$  is a standard potential temperature at 1000 mb, and the suffix 'ref' denotes the reference state as before.  $\tilde{P}$  and  $\tilde{N}^2$  were each given one uniform value throughout the model troposphere, and another value, six times as large, in the model stratosphere, producing strong and qualitatively realistic anomalies on each isentropic surface which intersects the tropopause. The reader is referred to Thorpe (1985) for the detailed method, which uses a transformation to the coordinates  $z$  and  $\tilde{r} = r(f_{\text{loc}}/f)^{1/2}$  introduced by Shutts and Thorpe (1978). The transformed radial coordinate  $\tilde{r}$  is conserved materially in axisymmetric, frictionless, adiabatic motion, and resembles a 'geostrophic coordinate' (Hoskins 1975, Blumen 1981) except that gradient-wind rather than geostrophic balance is used. Some quantitative details of the calculations are given in the caption to Fig. 15; note for instance that the values of  $f_{\text{loc}}$  and the absolute isentropic vorticity  $\zeta_{a\theta}$  greatly exceed  $f$  near the centre of the cyclonic vortex; for this and other reasons both quasi-geostrophic and semi-geostrophic theory (sections 5(b), (c) below) would be poor approximations.

Qualitative features to be especially noted about Figs. 15(a),(b) include the facts that:

- (i) the circulation in the balanced vortex has the same sense, relative to the earth, as the IPV anomaly which induces it;
- (ii) the induced fields penetrate vertically above and below the IPV anomaly, boundary constraints permitting, by amounts consistent with the scale relations (33), especially when  $f$  is replaced by  $(f_{\text{loc}}P\sigma)^{1/2}$  as in (33b), and
- (iii) the static stability  $N^2$ , as well as the absolute vorticity, is anomalously high within a high PV anomaly, and low within a low PV anomaly, relative to the static stability of the reference state.

Note that for this purpose the ‘anomaly’ in the static stability, being the anomaly relative to the reference state, means *isentropic* anomaly, just as it does for  $P$  itself; one is comparing the static stability in the centre of the IPV anomaly with the static stability on the same isentropic surface at the periphery of the picture, where the actual state approximates the reference state.

As suggested by (i) and (iii), the anomaly in  $P$  appears partly as absolute vorticity and partly as static stability. The proportions in which this partitioning occurs can be shown to depend on the shape of the anomaly, a broad, shallow anomaly tending to realize  $P$  more as static stability and a tall one more as absolute vorticity, where ‘tall’ and ‘shallow’ have to be measured against scale relations of the form (33). A more quantitative statement depends on solving the nonlinear equation (29) in each case, taking boundary constraints into account. But it is easy to see that some such partitioning must occur; for instance if the anomaly appeared entirely as an anomaly in absolute vorticity (the static stability retaining its reference-state value, with horizontal isentropes) then thermal wind balance would plainly be impossible to satisfy, the more so the shallower the anomaly. Equally, thermal wind balance would be impossible to satisfy if the anomaly in  $P$  were realized entirely as static stability, the more so the taller the anomaly. In order for the whole picture to fit together it is necessary, furthermore, that

- (iv) the static stability anomalies have the *opposite* sense to the IPV anomaly in the regions above and below that anomaly.

This is because  $\zeta_{a\theta}$  still has the same sense above and below the IPV anomaly (statements (i) and (ii)), and so the static stability must deviate in the opposite sense in order to compensate. The characteristic upward and downward bowing of the isentropes follows immediately from this consideration.

Kleinschmidt recognized all these characteristic features, both theoretically and observationally. For instance, on p. 115 of Eliassen and Kleinschmidt (1957) he expressed statement (iii) in the words “In general, it is found that in an isolated mass with abnormal potential vorticity the vertical stability as well as the absolute vorticity deviate from the normal in the same sense as the potential vorticity.” He also stated, on the same page, that a cyclone *requires* a positive IPV anomaly—an intuitive statement of the invertibility principle.

All the above-mentioned features (i)–(iv) are ‘robust’ in the sense that they are exhibited by the flow fields induced by any isolated, one-signed IPV anomaly of simple shape. For instance Gill (1981) gives some interesting exact solutions, obtained by an elegant analytical method, for very strong, anticyclonic, two-dimensional IPV anomalies. In each case the PV in the anomaly is *zero*, and the anomaly is concentrated on a single isentropic surface. All the qualitative features (i)–(iv) are reproduced even in that extreme limiting case. They are likewise reproduced by solutions to the approximate equation (32), which are valid for a sufficiently *weak* anomaly. For instance, let  $R_{\text{ref}}$  and  $\sigma_{\text{ref}}$  be taken to be constants in (32) (a Boussinesq, quasi-geostrophic model with a constant-static-stability reference state) and let  $P$  be taken to be constant and to be equal to  $\sigma_{\text{ref}}^{-1}f(1 + \varepsilon)$ , with  $\varepsilon \ll 1$ , within an ellipsoidal region  $r^2 + \Theta^2 = C^2 = \text{constant}$ , and to have its reference value  $\sigma_{\text{ref}}^{-1}f$  outside that region, where  $\Theta$  is the scaled coordinate  $f^{-1}(R_{\text{ref}}g\sigma_{\text{ref}})^{1/2}(\theta - \theta_c)$ , cf. (33a),  $\theta_c$  being the value of  $\theta$  at the centre of the ellipsoidal region. Then it is a straightforward theoretical exercise to construct an analytical solution, again exhibiting the same features (i)–(iv), in which

$$\left. \begin{aligned} v &= \frac{1}{3}\varepsilon fr & (r^2 + \Theta^2 < C^2) \\ v &= \frac{1}{3}\varepsilon fr \left( \frac{C^2}{r^2 + \Theta^2} \right)^{3/2} & (r^2 + \Theta^2 > C^2) \end{aligned} \right\} \quad (36)$$

terms of order  $\varepsilon^2$  being neglected as well as non-Boussinesq effects in the far field. It can also be shown that, of the fractional change comprising the IPV anomaly, one third comes from the static stability and two thirds from the relative vorticity anomaly, in this particular case.\*

Kleinschmidt gave various other examples, computed by the approximate methods available to him in the late 1940s and early 1950s, all exhibiting features (i)–(iv). It is worth remarking that one of these examples (e.g. Eliassen and Kleinschmidt, 1957, Fig. 23) is quite like that of Fig. 15(a) in some respects, except that the IPV anomaly is a little lower down, has a somewhat different shape, and is detached from the model stratosphere. The observed case shown in Fig. 9(b) appears to be intermediate between Kleinschmidt's example and cases like those of Figs. 8 and 15(a).

#### 4. ON THE CANCELLATION OF HORIZONTAL ADVECTION BY VERTICAL MOTION

We are now in a position to appreciate one further, very basic point. It can be brought out most clearly by means of a thought-experiment, to whose wider significance we shall return in sections 6(e) and 8. The experiment could be carried out on a computer, with the aid of a multi-layer numerical model, but its outcome can in any case be predicted with certainty since it is an immediate consequence of the invertibility principle together with the robustness of the qualitative features (i)–(iv) just noted.

Consider what would happen if a broad airstream, itself involving comparatively weak IPV and surface  $\theta$  anomalies, were to flow beneath a stationary, upper air IPV anomaly such as the cyclonic anomaly of Fig. 15(a). To a first approximation (anticipating the theory to be reviewed in the next section), we may superpose the airstream onto the structure shown in Fig. 15(a). The invertibility principle tells us that the cyclonic vortex in the lower troposphere will stay in place beneath the upper air anomaly which is inducing it, despite the 'attempt' by the low-level airstream to advect it downstream.

It is interesting to note what the vorticity budget would look like in this thought-experiment, which in order to highlight the point will be imagined to take place in a completely frictionless, adiabatic atmosphere. The isobaric absolute vorticity  $\zeta_{ap} = f + \mathbf{k} \cdot \nabla_p \times \mathbf{v}$  then satisfies

$$\begin{aligned} \frac{\partial \zeta_{ap}}{\partial t} + \mathbf{v} \cdot \nabla_p \zeta_{ap} &= \zeta_{ap} \frac{\partial \omega}{\partial p} + \\ &+ \mathbf{k} \cdot \frac{\partial \mathbf{v}}{\partial p} \times \nabla_p \omega - \omega \frac{\partial \zeta_{ap}}{\partial p}. \end{aligned} \quad (37)$$

Beneath the stationary IPV anomaly vorticity advection, the second term on the left, would be an important term, possibly suggesting a tendency for the lower part of the vortex to be carried downwind. However, if accurate vertical velocities  $\omega$  could be obtained, it would be found that the advection term would be exactly cancelled by the terms on the right-hand side of the equation, of which the dominant term is the vortex-stretching term  $\zeta_{ap} \partial \omega / \partial p$  appearing on the first line. There would be ascent upstream

\* We note in passing that in the absence of boundary effects this flow field is dynamically stable, by the theorems of Charney and Stern (1962) and Blumen (1968), despite what might be concluded from an incautious application of a 'barotropic instability' criterion. It can easily be verified from the bottom line of (36) that there is a reversal in the sign of the vorticity anomaly on isentropic surfaces near the central, horizontal surface  $\Theta = 0$  outside the boundary  $r^2 + \Theta^2 = C^2$  of the central IPV anomaly, a phenomenon complementary to that noted in statement (iv) above. An absolute vorticity configuration of this sort might be taken as suggesting, incorrectly, that the vortex could be barotropically unstable to asymmetric disturbances. The suggestion would be incorrect because it is actually the IPV gradients and not the absolute vorticity gradients that are relevant, for reasons to be recalled in section 6(b). All the other flow fields described in the present section are likewise dynamically stable.

and descent downstream of the IPV anomaly—just enough to keep the vortex in the same place. Similarly, there would be an exact cancellation in the temperature equation, between temperature advection and adiabatic temperature changes. This complete cancellation of terms in the temperature and vorticity equations occurs if and only if the IPV anomaly, to which the presence of the vortex can be attributed, is stationary overhead. In the case of Fig. 15(a), the situation can be pictured by imagining an air parcel approaching the centre of the vortex on the lowest isentropic surface plotted, not counting the isentrope on the bottom boundary. The trajectory would of course be curved, and its closest approach to the centre of the vortex would depend on the detailed circumstances.

Observational data suggest that the same kind of thing happens in the real atmosphere, and Figs. 8 and 10 appear to provide two examples of it. In the case of Fig. 10 there was a low-level airstream flowing roughly westward relative to the upper air anomaly (Erickson 1971, Figs. 1 and 4). Vertical motion was computed from the omega equation and confirmed by “good agreement between areas of major cloudiness and areas of upward total  $\omega$ ” after an easterly wave in the low-level airstream had supplied enough moisture to the middle troposphere for the cloud to form (*op. cit.*, pp. 74, 76). Vortex stretching was strongly positive to the east of the anomaly, which rapidly became cloudy. It was mostly negative to the west of the anomaly, which remained clearer at first. This is broadly consistent with what one expects from the foregoing reasoning. Of course the effects of neighbouring anomalies, frictional convergence in the planetary boundary layer, and diabatic effects such as latent heat release, would have to be added in order to obtain a completely realistic picture. In the case of Fig. 8, it appeared that air parcels from low levels were approaching the upper air IPV anomaly mostly from the south, the air motion again being viewed relative to the upper air cyclone. There was a corresponding region of precipitation lying mainly to the south (Peltonen 1963; Palmén and Newton 1969, Figs. 10.7a, b), as well as a small region of stronger precipitation just under the centre of the cyclone, which may have been associated with frictional convergence as well as with reduced static stability.

In some cases it may be more natural to think of the upper air IPV anomaly as moving relative to the lower layers; the characteristic pattern of vertical motion may then be described as large-scale ascent and vortex stretching ahead of the anomaly, and descent and vortex shrinking behind it. Such a pattern is conspicuous in, for example, Fig. 11 of Petterssen and Smebye (1971), where vertical motion was estimated for a situation somewhat like that of the present Fig. 5.

One may think of, say, an eastward-moving upper air anomaly like that in Figs. 5(c)–(f) as acting on the underlying layers of the atmosphere somewhat like a broad, very gentle ‘vacuum cleaner’, sucking air upwards towards its leading portion and pushing it downwards over the trailing portion. The vertical motion field arises in response to the need to maintain mass conservation and approximate balance, in the manner assumed in the derivation of theoretical results such as the omega equation, and the Sawyer–Eliassen equation used in discussions of two-dimensional models of frontogenesis. If an IPV anomaly were to arrive overhead without any adjustment taking place underneath it, then the wind, temperature and pressure fields would be out of balance to an improbable extent; cf. the discussion of statements (i)–(iv) of section 3. Note that the strength of the suction effect will increase with the relative speed at which the upper air anomaly is advected.

The sense of the vertical motion, and the associated contribution to surface development, will often be correctly given by the well-known PVA (positive vorticity advection) rule. The foregoing considerations show that, as recently emphasized by Bleck and

Mattocks (1984), the same rule should work when IPV advection is used in place of vorticity advection. Moreover this avoids the dangers (Hoskins *et al.* 1978) inherent in traditional vorticity arguments. The reasons why the two viewpoints agree in many circumstances of interest are, first, the practice of applying the PVA concept only to upper air charts “near the level of maximum wind” (Palmén and Newton 1969, p. 317ff, and refs.), second, the observed fact that the strongest IPV anomalies in the free atmosphere are often upper air anomalies (which is understandable in terms of the proximity of the stratospheric high-PV reservoir), and, third, the theoretical fact that within an IPV anomaly of simple shape the induced vorticity anomaly has the same sign as the IPV anomaly, point (iii) of section 3.

There is a case to be made, perhaps, for permitting the acronym ‘PVA’ to be read alternatively as (positive) ‘*potential* vorticity advection’. Be that as it may, the thought-experiment described above is typical of many telling illustrations of the fact that it is often simplest to think directly in terms of IPV anomalies and their advection, whenever IPV information is available. Equivalent descriptions in terms of vorticity advection and stretching, and temperature advection and adiabatic temperature change, will always be valuable, of course, but the conceptual task of linking all these elements in a mutually consistent way is often quite complicated. ‘Mutual consistency’, in the sense in which it is usually understood (e.g. Palmén and Newton, p. 320) requires explicit consideration of the vertical motion field, simultaneously with the application of some balance condition. The alternative description in terms of IPV advection simplifies the problem, with no loss of accuracy in principle, by allowing for the effects of vertical motion in a way that is implicit but automatically self-consistent. The application of the balance condition, and the extraction of explicit information about the vertical motion field, as well as the other fields, can then be considered as a subsequent, *conceptually separate* problem to be dealt with under the heading of the invertibility principle.

The deduction of the vertical velocity field is discussed further in the appendix, where the direct use of the IPV concept will be compared with other methods. Each method has different advantages, and no single one is best for all practical and conceptual purposes. In connection with the thought-experiment described above, we may also refer to an elegant statement by Kleinschmidt (1957, p. 121) of the essential point about advectively-induced vertical motion. His statement reads “if a cyclone lies in a baroclinic basic flow, ascending motion takes place on that side of the cyclone towards which the thermal wind vector of the basic flow points.” This is applicable to a cyclonic IPV anomaly at any altitude.

We next show how, in order to apply the invertibility principle in its full generality, the concept of the ‘IPV anomaly’ must be enlarged to take account of near-surface temperature anomalies.

## 5. ANOMALIES AT THE LOWER BOUNDARY, AND THE INVERTIBILITY PRINCIPLE FOR GENERAL, TIME-DEPENDENT FLOW

### (a) *Surface and near-surface anomalies*

Figures 16(a), (b) give two more computations illustrating a contrasting idealized situation in which there is no upper air IPV anomaly but in which  $\theta$  has an anomaly at 1000 mb. The model atmosphere is still stably stratified all the way down to the surface. The reference-state condition (17a) is interpreted as if the isentropes which intersect the 1000 mb surface were bunched along that surface (see insets to figures), corresponding, as Bretherton (1966a) pointed out in the context of quasi-geostrophic theory, to static stability and PV values of very large magnitude in a region of very small thickness, like

a surface charge in electrostatics. In particular, a warm surface potential temperature anomaly is equivalent to a cyclonic IPV anomaly concentrated at the surface. As statement (i) of section 3 predicts, it induces a cyclonic vortex (Fig. 16(a)). A cold surface anomaly induces an anticyclonic vortex (Fig. 16(b)).

Note that the magnitudes of the induced wind and pressure fields are very significant. For instance the computation on which Fig. 16(a) is based implies that a 10 K warm surface anomaly, on the scale shown, can induce a surface pressure low of  $-31$  mb relative to its surroundings. The figure caption gives more detail.

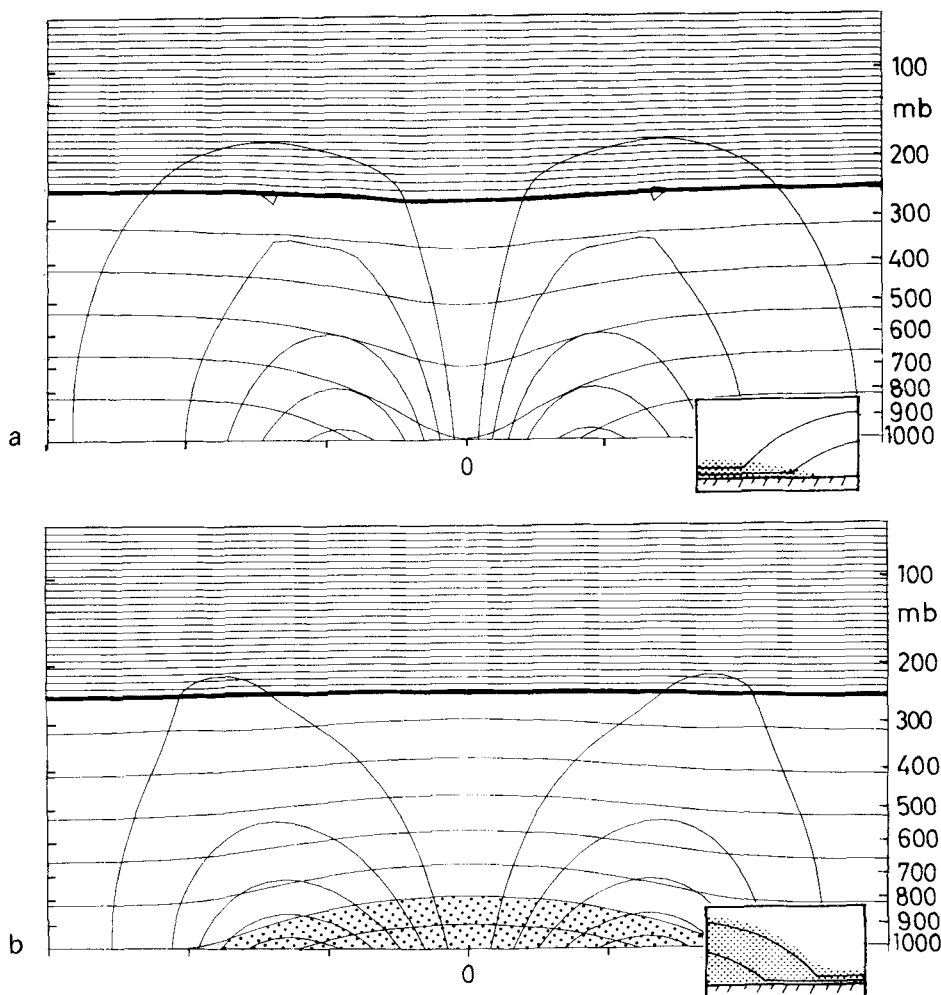


Figure 16. Circularly symmetric flows induced by simple boundary temperature anomalies. The basic situation, and the method of solution, is as in Fig. 15 except that here there is no potential temperature variation along the tropopause, but the boundary potential temperature is taken to vary in the manner  $\frac{1}{2}A\{\cos(\pi r/r_0) + 1\}$  for  $\tilde{r} < r_0 = 1667$  km. The amplitude  $A$  was taken to be  $+10$  K in (a) and  $-10$  K in (b). The thick line again represents the tropopause, and the thin lines the isentropes every 5 K and the transverse velocity every  $3$   $\text{m s}^{-1}$ . The zero isotach on the axis of symmetry is omitted. The warm anomaly induces a cyclonic circulation, and the cold anomaly an anticyclonic circulation. The surface pressure anomalies are  $-31$  mb and  $+18$  mb respectively, and the maximum (surface) winds are about  $16$   $\text{m s}^{-1}$  and  $17$   $\text{m s}^{-1}$  respectively. The relative vorticity extrema are at the surface and have values  $+0.8f$  and  $-0.5f$  respectively. The insets and stippling suggest the interpretation of the warm surface potential temperature anomaly as equivalent to a cyclonic IPV anomaly, and the cold surface potential temperature anomaly as part of an anticyclonic IPV anomaly (see text). For more details of the method of computation, see Thorpe (1985). Courtesy of A. J. Thorpe.

The qualitative statements (i)–(iv) of section 3 all hold for surface temperature anomalies interpreted in this manner. Note that in order to have positive static stability everywhere, within the notional surface layer as well as above it, the cold (anticyclonic) anomaly must be regarded as being embedded in a layer of high static stability and PV in the reference state, as suggested by the inset to Fig. 16(b). However, this is just a conceptual device and it is probably best simply to think in terms of the surface  $\theta$  anomalies and the rule that ‘warm is cyclonic and cold is anticyclonic’.

In the real atmosphere,  $\theta$  ‘at the ground’ is probably best interpreted to mean  $\theta$ , or temperature  $T$ , on some convenient isobaric surface lying just above the planetary boundary layer.

In Fig. 16(b), the anticyclonic case, the low-level IPV anomaly actually resides not only at the surface but also throughout the cold dome, under the highest isentrope that intersects the surface (stippled region in Fig. 16(b)). By contrast, the cyclonic anomaly is strictly confined to the notional surface layer (see stippling in the inset to Fig. 16(a)). The difference arises because, as Eq. (29) illustrated earlier, the concept of IPV ‘anomaly’ refers strictly to the distribution of PV on an isentropic and not on a horizontal surface. That distribution must be compared with the distribution of PV on the same isentropic surface in the reference state; and here, as in section 3, the reference state is horizontally uniform, and practically the same as the actual state far from the anomaly.

In the real atmosphere one generally sees what look like various superpositions of the structures whose idealized forms are exemplified in Figs. 15 and 16. For instance one often sees what looks qualitatively like the vertical superposition of a cyclonic upper air anomaly (Fig. 15(a)) with an anticyclonic (cold) surface anomaly (Fig. 16(b)). Figure 8 is a case in point. One reason is probably the fact that advection in the lower troposphere may often take place in roughly the same sense as upper air advection, as least as far as the meridional component is concerned. For instance the formation of a cutoff cyclone may involve positive upper air IPV advection simultaneously with low-level cold advection. This can account for the formation of structures like that seen in Fig. 8. These structures, and their opposite-signed counterparts exemplified by Fig. 14, are consistent with the traditional view of air masses and their recognition by low-level thermal properties and tropopause height. In the case of Fig. 14 it is clear from Figs. 13(b) and 11(c) that both negative upper air IPV advection and warm low-level advection must have contributed to the formation of the structure. We note that frictional convergence and divergence is another process which may create somewhat similar low-level structures.

In real synoptic situations one will usually need to take account of several IPV and surface  $\theta$  anomalies in neighbouring locations aloft, near the surface, or both, advecting each other via their induced wind fields. We shall see in section 6 that certain kinds of real and idealized cyclogenesis can be usefully thought of in this way.

The approximate superposition principle employed here, and in section 4, is strictly true only within the confines of quasi-geostrophic theory. But it is often a useful qualitative guide in practice. As we shall see shortly, that theory shows that one can indeed think of the interior and surface IPV anomalies as qualitatively like the interior and surface charge distributions of a problem in electrostatics, and the induced flow structures as analogous to the (superposable) induced electric fields, with the Montgomery potential or the geopotential height playing the role of the electrostatic potential. For the purpose of this analogy it must be understood that the vertical coordinate is scaled according to (33a) (and that the Coriolis parameter is being assumed not to vary too much), and that the non-Boussinesq effects indicated by (33c, d) are not overwhelmingly important. In applications where quasi-geostrophic theory is not sufficiently accurate, we can still think of the geopotential height field induced by an IPV or surface  $\theta$  anomaly as somewhat

analogous to an electrostatic potential, but in a nonlinear medium whose dielectric properties are locally altered by the induced field. Such local nonlinear effects are apt to be important in regions of very high baroclinicity such as fronts.

(b) *Quasi-geostrophic theory*

It was quasi-geostrophic theory, in the form developed in the landmark paper of Charney and Stern (1962), a decade after Kleinschmidt's early publications, which provided the first clear way of expressing the invertibility principle which was also sufficiently general to apply directly to time-dependent, non-circular motion with variable  $f$ . Charney and Flierl (1981) and Eliassen (1984) give interesting surveys of the history of the theory, whose development began in the late 1940s. The equations were usually written in terms of height or pressure rather than isentropic coordinates, and consequently led to an approximate conservation principle for a quantity  $q$  which differed from  $P$  in significant aspects. Today  $q$  is usually called the quasi-geostrophic potential vorticity, although Charney and Stern called it, perhaps more appropriately, the pseudopotential vorticity. In the absence of diabatic and frictional effects it is conserved, in an approximate sense, not following an air parcel but, rather, following the horizontal geostrophic flow, ignoring all vertical motion. It can be written in pressure coordinates in the form

$$q = f + \mathbf{k} \cdot \nabla_p \times \mathbf{v} + f_0 \frac{\partial}{\partial p} \left( \frac{\theta'}{d\theta_{\text{ref}}/dp} \right) \tag{38}$$

where  $f_0$  is a constant standard value of  $f$ ,  $\theta_{\text{ref}}(p)$  is the reference potential temperature distribution, and  $\theta'$  the deviation from it. Despite its name  $q$  is not, except in special circumstances, an approximation to the full potential vorticity  $P$ . Charney and Stern elegantly clarified the general relationship between  $q$  and  $P$  by pointing out that  $q$  is a quantity whose variation on a constant altitude or pressure surface is approximately proportional to the variation of  $P$  on an isentropic surface. More precisely, they derived a result (*op. cit.*, Eq. (2.31)), which can be written in pressure coordinate form as

$$\left( \frac{\partial}{\partial t} \right)_\theta P \approx -g \frac{d\theta_{\text{ref}}}{dp} \left( \frac{\partial}{\partial t} \right)_p q \quad \text{and} \quad \nabla_\theta P \approx -g \frac{d\theta_{\text{ref}}}{dp} \nabla_p q. \tag{39a, b}$$

Adding (39a) to  $\mathbf{v} \cdot (39b)$  we see that the rate of change of  $P$  following an air parcel is approximately proportional to the rate of change of  $q$  following an isobaric trajectory.

Charney and Stern furthermore expressed  $q$  in terms of the geostrophic streamfunction

$$\psi' = f_0^{-1} \{ \phi - \phi_{\text{ref}}(p) \} \tag{40}$$

where  $\phi_{\text{ref}}(p)$  is the reference geopotential by linearizing the hydrostatic relation  $\partial\phi/\partial p = -R\theta$ , for small deviations at constant  $p$ , to give

$$f_0 \partial\psi'/\partial p = -R\theta' \tag{41}$$

where  $R = R(p)$  is the quantity defined in (20). Substituting this and the geostrophic approximation  $\mathbf{v} = \mathbf{k} \times \nabla\psi'$  into (38), and introducing the reference-state  $q$  field,

$$q_{\text{ref}} = f, \tag{42}$$

we can write the result in the form (*op. cit.*, Eq. 2.25b),

$$\mathcal{L}_g(\psi') = q - q_{\text{ref}} \tag{43}$$

where the linear operator  $\mathcal{L}_g(\ )$  is defined by

$$\mathcal{L}_g(\psi') = \nabla_h^2 \psi' + f_0^2 \frac{\partial}{\partial p} \left( N^{-2} \frac{\partial \psi'}{\partial p} \right), \tag{44}$$

$\nabla_h^2$  being the usual two-dimensional horizontal Laplacian, and

$$N^2 = -Rd\theta_{\text{ref}}(p)/dp = N_{\text{ref}}^2/g^2\rho_{\text{ref}}^2, \tag{45}$$

another measure of the static stability.

This result of Charney and Stern's made it obvious that, if  $q$  is regarded as known, so that the PV anomaly, defined as the right-hand side of (43), is known, then  $\psi'$  can be deduced by inverting the three-dimensional, Laplacian-like operator  $\mathcal{L}_g$ , just as we can invert the two-dimensional Laplacian of barotropic (two-dimensional aerodynamic) flow. In cases where the lower boundary condition is simply one of constant potential temperature at  $p = p_0 = 1000$  mb, we can take  $\theta' = 0$  there so that, from (41), the boundary conditions for inverting (43) take the homogeneous (unforced) form

$$\boxed{\partial \psi' / \partial p = 0 \quad \text{at } p = 0, p_0.} \tag{46}$$

If, on the other hand, the potential temperature is not uniform on the lower boundary, a well-known mathematical device enables us to express this, whilst retaining the homogeneous boundary condition (46), by adding a contribution

$$-f_0^2 \left( N^{-2} \frac{\partial \psi'}{\partial p} \right)_{p=p_{0-}} \delta(p - p_0) = \left\{ \frac{f_0 \theta'}{-d\theta_{\text{ref}}/dp} \right\}_{p=p_{0-}} \delta(p - p_0), \tag{47}$$

to  $q$  on the right-hand side of (43), where  $\delta(\ )$  is the Dirac delta function and the suffix  $p = p_{0-}$  means evaluation just above the boundary, i.e. just above the implied discontinuity in  $\partial \psi' / \partial p$ . The Dirac delta function  $\delta(x)$  represents a quantity concentrated at the origin  $x = 0$  (a classical example being surface charge density in electrostatics) and is defined such that

$$\int_{-\epsilon}^{\epsilon} \delta(x) dx = 1$$

for any positive number  $\epsilon$ . The device (47), due to Bretherton (1966a), is one way of expressing mathematically the idea suggested by the insets in Fig. 16 but in a form relating more directly to  $q$  than to  $P$ . It allows us to think of the surface temperature distribution as part of the PV distribution. Thus, in an approximate but beautifully simple way, the boundary value problem (43), (46) expresses invertibility under geostrophic balance, relative to the standard reference state assumed in quasi-geostrophic theory, in which the static stability is horizontally uniform, but  $f$  is allowed to vary provided that its change over the horizontal scale  $L$  of the motion is small in comparison with  $f_0$ . There is now no restriction to axisymmetric, steady motion as there was with Eqs. (29) and (32): the theory applies to general, time-dependent flow.

Bretherton further noted that under adiabatic conditions, with  $\omega = Dp/Dt = 0$  at  $p = p_0$ ,

$$\left( \frac{\partial}{\partial t} + \mathbf{v} \cdot \nabla_p \right) \theta' = 0, \quad \text{i.e.} \quad \left( \frac{\partial}{\partial t} + \mathbf{v} \cdot \nabla_p \right) \left( \frac{f_0 \theta'}{d\theta_{\text{ref}}/dp} \right) = 0 \quad \text{at } p = p_0 \tag{48}$$

so that, even in the extended sense implied by (47),  $q$  is, indeed, still conserved on an isobaric trajectory.

Once  $\psi'$  is determined from (43) and (46) the geopotential, potential temperature and horizontal velocity fields may all be calculated directly from (40), (41) and the geostrophic relation  $\mathbf{v} = \mathbf{k} \times \nabla \psi'$ . The vertical velocity field may be found from the adiabatic thermodynamic equation, or alternatively, and strictly diagnostically, from the quasi-geostrophic omega equation (e.g. Eliassen 1984):

$$\mathcal{N}^2 \nabla_h^2 \omega + f_0^2 (\partial^2 \omega / \partial p^2) = g(\psi'), \quad (49)$$

together with the boundary conditions  $\omega = 0$  at  $p = 0, p_0$ . Here  $g(\psi')$  is a nonlinear function which may be written in various ways, some of which are related to the discussion in section 4. Details, including frictional and diabatic contributions, are given in the appendix.

In terms of the height-like coordinate (35) and the static stability  $\tilde{N}^2$  defined by (34), the operator  $\mathcal{L}_g$  can be shown to take a form resembling more closely the height coordinate form originally derived by Charney and Stern:

$$\mathcal{L}_g(\psi') = \nabla_h^2 \psi' + \frac{f_0^2}{\rho_s} \frac{\partial}{\partial z} \left( \frac{\rho_s}{\tilde{N}^2} \frac{\partial \psi'}{\partial z} \right), \quad (50)$$

where

$$\rho_s(z) = \{\theta_0 R(p)\}^{-1} = (p_0 / \kappa c_p \theta_0) (p/p_0)^{1/\gamma}, \quad (51)$$

a standard density distribution (which would be identical to the reference density distribution if the reference atmosphere were neutrally stable). The appropriate form of (47) is then

$$f_0^2 \left( \tilde{N}^{-2} \frac{\partial \psi'}{\partial z} \right)_{z=0_+} \delta(z) = \left\{ \frac{f_0 \theta'}{d\theta_{\text{ref}}/dz} \right\}_{z=0_+} \delta(z), \quad (52)$$

by virtue of (35) and the second of (34). Notice incidentally how quasi-geostrophic theory, which in effect is a 'weak-anomaly' theory, treats both the anticyclonic, cold-dome anomaly exemplified in Fig. 16(b) and the cyclonic surface anomaly exemplified in Fig. 16(a) as if they were concentrated at the surface, even though  $P$  has (isentropically) anomalous values throughout the finite, stippled region in the case of Fig. 16(b).

Bretherton also pointed out that the same mathematical device can be used even in the presence of smoothed, large-scale topography of height  $h$  (a function of horizontal position) provided that the approximation

$$\theta_{\text{ref}}(h) - \theta_{\text{ref}}(0) \approx h(d\theta_{\text{ref}}/dz)_{z=0} \quad (53)$$

is acceptable where  $\theta_{\text{ref}}$  is now expressed for convenience as a function of  $z$  instead of  $p$ , as in the second of (52). The approximation (53) can be shown by standard scaling arguments to be formally consistent with the other approximations used in quasi-geostrophic theory. Then under adiabatic conditions (48) is replaced, again using  $z$  as vertical coordinate in place of  $p$ , by the statement that total potential temperature is conserved for an air parcel following the topography,

$$(\partial/\partial t + \mathbf{v} \cdot \nabla_z)(\theta' + h d\theta_{\text{ref}}/dz) = 0 \quad \text{at } z = 0. \quad (54)$$

Here it is a self-consistent approximation, according to quasi-geostrophic theory, to evaluate all quantities, including  $\mathbf{v}$  and  $\theta'$ , at  $z = 0$  rather than at  $z = h$ . This is another 'weak-anomaly' approximation. With all these approximations it follows that the problem can once again be given the simple form (43), (46) provided that we add to  $q$  a contribution

$$\left\{ \frac{f_0 \theta'}{d\theta_{\text{ref}}/dz} + f_0 h \right\}_{z=0_+} \delta(z) \quad (55)$$

in place of (52), and to the reference distribution  $q_{\text{ref}}$  a contribution

$$f_0 h \delta(z) \quad (56)$$

so that the *anomaly* in  $q$  is still proportional to  $\theta'$ , and therefore to  $\partial\psi'/\partial z$ , just above  $z = 0$ , and  $q$  is still conserved on isobaric trajectories.

The quasi-geostrophic approximations are inaccurate, of course, for quantitative purposes, in many situations of interest. In particular the assumption of small deviations from the reference stratification is very inaccurate indeed near the tropopause, a point well illustrated in Figs. 8–10 and Fig. 15. However, the link with quasi-geostrophic theory makes evident the central role of potential vorticity in many processes such as instability, Rossby wave propagation, quasi-two-dimensional turbulence, critical-layer processes, and so on, all of which are usually studied theoretically by means of quasi-geostrophic theory. The theory has remained important, not on account of quantitative accuracy, but rather because it incorporates the fundamental qualitative insights arising from PV conservation and the invertibility principle, which do appear to carry over to more accurate representations of the real atmosphere. It also correctly suggests, through results like (54) and (55), that it is the potential temperature at the ground which is the dynamically significant quantity there, for the purposes of IPV thinking.

Perhaps the most basic weakness of quasi-geostrophic theory in its standard pressure coordinate form, as just outlined, arises from the fact that, in order to construct the large-scale distribution of  $q$  from that of  $P$  by integrating the Charney–Stern relation (39b), it is necessary to assume that each isentropic surface is close to a given isobaric surface. This may be a good local approximation in some cases, but the approximation is seldom uniformly valid over large horizontal distances. This is the price paid for the theoretical convenience of a simple description based on isobaric surfaces which, among other things, permits the approximate application of the lower boundary condition at a constant value  $p_0$  of the pressure coordinate  $p$ , or equivalently at  $z = 0$ . This simplification of the lower boundary condition is a necessary device in the construction of many standard theoretical solutions representing dynamical processes of interest.

Similar formulations in isentropic coordinates, comprising generalizations of (32), can overcome the problem of horizontal nonuniformity at the inevitable cost of complicating the lower boundary condition. Such formulations have been used as the bases of numerical models in a number of important papers beginning with Danielsen and Diercks (1967), Eliassen and Raustein (1968, 1970), and Bleck (1973, 1974), following a suggestion by Charney and Phillips (1953). For more recent developments in the use of isentropic coordinates in numerical models, see for instance Uccellini *et al.* (1979), Bleck (1984), and references therein.

Many other ways of improving the standard quasi-geostrophic theory have been proposed, some of which attempt to tackle the problem of horizontal nonuniformity whilst retaining isobaric or sigma coordinates to simplify the lower boundary condition, sometimes at the cost of losing the PV-conservation principle, and most of which seek to improve the accuracy of the balance condition in some way or other. Recent theoretical work is reported, for instance, in the papers by Gent and McWilliams (1984, and refs.) and Williams and Yamagata (1984, and refs.). Amongst the many papers on this topic, a particularly important milestone is the recent pair of papers by Salmon (1983, 1985). They show, for the first time as far as we are aware, how improvements on quasi-geostrophic theory may be systematically constructed in such a way that exact analogues of PV as well as energy conservation are retained. The method used appears to have far-reaching implications for refining the balance and invertibility concepts beyond their present state of development. It goes to the heart of the matter by exploiting the fundamental connection between conservation relations and symmetries.

In the next sub-section we review the simplest IPV-conserving improvement to quasi-geostrophic theory, namely semi-geostrophic theory, together with a significant extension to it discovered by Salmon. Then, in section 5(d), we briefly discuss a rather different approach to expressing the invertibility principle, using the concepts of nonlinear normal-mode initialization. This promises an advantage by way of computationally uniform behaviour across the tropics.

(c) *Semi-geostrophic theory and Salmon's generalization*

Semi-geostrophic theory improves on quasi-geostrophic theory while retaining isobaric coordinates, by:

- (i) improving on the geostrophic balance condition in the wind velocities used to advect potential temperature, momentum, and potential vorticity (the so-called geostrophic momentum approximation introduced by Eliassen (1948)); and
- (ii) alleviating the horizontal nonuniformity problem by means of a quasi-Lagrangian coordinate transformation (Hoskins 1975).

This particular choice of improvements may seem arbitrary at first sight, but PV conservation is retained, and the coordinate transformation puts the equations into a simple form which allows insights from quasi-geostrophic theory to be carried over into situations in which the quasi-geostrophic approximations themselves are poor, including cases of extreme horizontal nonuniformity. For example, the theory handles frontogenetic situations far more accurately than quasi-geostrophic theory (e.g. Hoskins and West 1979), and also shows that much of the extra accuracy can be thought of as coming simply from a geometrical distortion of the corresponding quasi-geostrophic solution. The theory can describe large-amplitude distortions of the tropopause such as those exemplified by Figs. 8, 9 and 15 (Hoskins 1982, and refs.). However, the theory as originally conceived does not permit  $f$  to vary. It is this important limitation that has recently been removed by the work of Salmon (1985) already referred to.

Assuming constant  $f$  to begin with, and denoting the geostrophic wind by  $\mathbf{v}_g = (u_g, v_g, 0)$ , we introduce a transformation of the horizontal independent variables,

$$x = X - v_g/f, \quad y = Y + u_g/f \quad (57)$$

and write  $Z$  for  $z$  with the understanding that  $\partial/\partial Z$  means differentiation at constant  $X, Y$  (whereas  $\partial/\partial z$  implies constant  $x, y$ ). It can be shown that the geostrophic flow and potential temperature are all related to a streamfunction  $\Psi(X, Y, Z)$  in the transformed,  $XYZ$  space, which we shall call 'semi-geostrophic space', by

$$(u_g, v_g, \theta) = (-\partial\Psi/\partial Y, \partial\Psi/\partial X, g^{-1}f\theta_0\partial\Psi/\partial Z). \quad (58)$$

Here  $\theta$  is the full potential temperature, not the deviation from the reference state, and  $\theta_0$  is a constant, representative value of  $\theta$ . Following Hoskins' (1975) derivation of the semi-geostrophic equations we can show that the twisting terms disappear in the transformed system, so that the semi-geostrophic approximation to  $P$  is simply

$$P = \rho_s^{-1} \xi_a \partial\theta/\partial Z, \quad (59)$$

where  $\rho_s$  is defined by (51), and the (isobaric) absolute geostrophic vorticity

$$\xi_a = \frac{f}{1 - (1/f)(\partial v_g/\partial X - \partial u_g/\partial Y)}$$

to a good approximation under the conditions for which semi-geostrophic theory is applicable (Hoskins and Draghici 1977). Thus  $\Psi$  is related to  $P$  by the equation

$$N_p^2(\partial^2\Psi/\partial X^2 + \partial^2\Psi/\partial Y^2) + f^2 \partial^2\Psi/\partial Z^2 = g\theta_0^{-1}\rho_s P, \quad (60)$$

where  $N_p^2 = gf^{-1}\theta_0^{-1}\rho_s P$ . Again  $\Psi$  is related to  $P$  by a simple Laplacian-like operator (although the forcing function also appears on the left, in  $N_p$ , just as  $P$  does on the left of (29)). As in quasi-geostrophic theory, it is possible to define a boundary contribution to  $P$  (and  $N_p$ ) associated with the  $\theta$  distribution at the bottom boundary. The contribution to  $P$  can be expressed as

$$f^3 \frac{\theta_0}{g} \left[ \frac{1}{\rho_s} \frac{\partial \Psi}{\partial z} / \left( f - \frac{\partial^2 \Psi}{\partial x^2} - \frac{\partial^2 \Psi}{\partial Y^2} \right) \right]_{Z=0+} \delta(Z) = \left[ \frac{1}{\rho_s} \zeta_a \theta \right]_{Z=0+} \delta(Z). \quad (61)$$

With this convention, invertibility is expressed by solving (60) subject to  $\partial \Psi / \partial Z = 0$  on  $Z = 0$ . It should be noticed that in this formulation the function  $P(X, Y, Z)$  implicitly supplies both the reference-state information and the IPV information.

In the interior, differentiation of (60) with respect to  $Z$ , after division by  $N_p^2$ , gives

$$\partial^2 \theta / \partial X^2 + \partial^2 \theta / \partial Y^2 + \frac{\partial}{\partial Z} \{ (f^2 / N_p^2) (\partial \theta / \partial Z) \} = 0 \quad (Z > 0), \quad (62)$$

from which  $\theta$  may be determined, although it is simpler to note that (58) gives both  $\theta$  and the horizontal geostrophic velocities once  $\Psi$  is found.

For frictionless, adiabatic motion the conservation of  $P$  and  $\theta$  both take the same form

$$\left( \frac{\partial}{\partial t} + u_g \frac{\partial}{\partial X} + v_g \frac{\partial}{\partial Y} + W \frac{\partial}{\partial Z} \right) (P, \theta) = 0, \quad (63)$$

the vertical velocity  $W = DZ/Dt$  now entering both equations. Advection of  $P$  and  $\theta$  is performed by the horizontal geostrophic velocities in *semi-geostrophic*,  $XYZ$  space. This gives a more accurate representation of advection in physical,  $xyz$  space, improvement (i), which is important near jets and fronts. As noted by Hoskins and Draghici (1977), the vertical velocity  $W$  may be obtained from  $\Psi$  (or  $P$ ) by solving an omega equation in semi-geostrophic space.

In order to extend the theory to the case of a variable Coriolis parameter  $f(x, y)$ , while retaining conservation laws analogous to (63), the key step is to replace (57) by

$$x = X - v_g / f(X, Y), \quad y = Y + u_g / f(X, Y) \quad (64)$$

and to use  $f(X, Y)$  as the Coriolis parameter in the definition of the geostrophic wind (Salmon 1985). In other words, one uses the value of the Coriolis parameter at the transformed, and not at the physical, position of an air parcel. The proof that the resulting equations possess the required conservation properties is a straightforward extension of the analysis given by Salmon (1985), to whose penetrating discussion the reader is referred for more detail.

An alternative approach to the geostrophic momentum equations is to use isentropic coordinates. In the case considered here  $f$  may be allowed to vary slightly about a standard value  $f_0$ . Salmon's method would presumably allow the restriction on  $f$  to be relaxed still further. In  $xy\theta$  space, the geostrophic flow and pressure field are given by

$$(f_0 u_g, f_0 v_g, \Pi) = (-\partial M / \partial y, \partial M / \partial x, \partial M / \partial \theta) \quad (65)$$

where  $\Pi(p)$  is the Exner function defined by (19). The potential vorticity is approximated by

$$P = -g \frac{f + \partial v_g / \partial x - \partial u_g / \partial y}{\partial p / \partial \theta}. \quad (66)$$

Substitution from (65) gives, on rearranging,

$$(1/f_0)(\partial^2 M/\partial x^2 + \partial^2 M/\partial y^2) + \tilde{P}\partial^2 M/\partial \theta^2 = -f, \quad (67)$$

where  $\tilde{P}$  is the quantity defined in (34). If the Boussinesq approximation is not made, it should be noted that the definition (34) gives

$$\tilde{P} = (p_0/\kappa g c_p^{1/\kappa})(\partial M/\partial \theta)^{1/(\gamma-1)} P.$$

There is then a weak nonlinearity in the elliptic equation (67), because of the factor involving  $(\partial M/\partial \theta)^{1/(\gamma-1)}$ . Suitable boundary conditions in the horizontal are easily specified but the usual vertical boundary condition of  $\theta$  specified on a given pressure  $(\partial M/\partial \theta)$  or height  $(M - \theta \partial M/\partial \theta)$  surface makes numerical solution awkward except in the case of uniform  $\theta$  on the boundaries. Methods for overcoming this problem have been proposed by Charney and Phillips (1953), Danielsen and Diercks (1967), Eliassen and Raustein (1968, 1970), Bleck (1973, 1974, 1984), Uccellini *et al.* (1979) and others. Once  $M$  has been determined the other variables follow from (19) and (65). The ageostrophic flow which is needed for a more accurate representation of horizontal advection can be determined from an extension of the omega equation analysis described in Hoskins and Draghici (1977).

It can be shown that for the case of a circularly symmetric distribution of PV on an  $f$  plane, differentiation of (67) with respect to  $r$  gives an approximation to the exact equation (29) in which terms like  $v/r$  are neglected in comparison with  $f$ . This is consistent with the present geostrophic approximation to the full gradient wind balance.

The work of Bleck (1973) cited earlier presented results from a quasi-geostrophic, isentropic coordinate forecast model in which  $P$  and boundary  $\theta$  were advected geostrophically and then an equation like (67) solved for  $M$ . In cases of intense development, which were underestimated by the standard forecast models, spectacular success was obtained even though the numerical resolution of the model was modest by today's standards. In a subsequent paper (Bleck 1974) many more forecasts were investigated using an isentropic coordinate model including ageostrophic horizontal advection, hence resembling the semi-geostrophic models just described, as well as a primitive equation model in isentropic coordinates. In those cases it was concluded that a standard operational forecast model showed the best overall performance. However, considering the very great sophistication of the operational model in comparison with the experimental isentropic models developed by an individual investigator, Bleck's results were an important achievement at the time.

Differentiation of (67) with respect to  $\theta$  gives an equation for  $\Pi$ :

$$(1/f_0)(\partial^2 \Pi/\partial x^2 + \partial^2 \Pi/\partial y^2) + \frac{\partial}{\partial \theta}(\tilde{P}\partial \Pi/\partial \theta) = 0. \quad (68)$$

The four simple elliptic equations, (60) and (62) for  $\Psi$  and  $\theta$  in  $XYZ$  space, and (67) and (68) for  $M$  and  $\Pi$  in  $xy\theta$  space, along with those for the static stability variables  $\partial \theta/\partial Z$  and  $\partial \Pi/\partial \theta$  obtained from the vertical derivatives of (62) and (68), may be used for qualitative discussion of the fields induced by any PV (or boundary  $\theta$ ) anomaly except near the equator, and to justify statements (i)–(iv) near the end of section 3. Within an isolated positive PV anomaly, for instance, there is a tendency for the  $\theta$ -surface separation to approach the small value which would be associated with its PV if there were no change in  $\zeta_a$  (statement (iii) near the end of section 3). However, the closer together the  $\theta$  surfaces are in the anomaly region, the more they must be separated in the surrounding region, for a given reference state of finite horizontal extent. The smoothing properties of the inverse elliptic operators make for a monotonic transition between the two regions.

The balance condition now implies a positive  $\zeta_a$  anomaly. The result is a compromise in which, in both regions, the  $\theta$  surfaces are less distorted than their PV would imply if there were no change in  $\zeta_a$ . The sense of the isentropic slopes between the two regions corresponds to a cyclonic circulation everywhere (statement (i) of section 3). The perturbations all decay away from the region, the vertical length scale in semi-geostrophic space being  $fL/N_p$  where  $L$  is the horizontal length scale of the flow structure in semi-geostrophic space, cf. (33a). For a weak anomaly the scale in physical space is practically the same.

Finally, we note that solutions of the two-dimensional semi-geostrophic equations for situations comprising two-dimensional analogues of those shown in Fig. 15 (calculations by E. Caetano Neto, personal communication, reproduced in Figs. 4.24, 4.25 of Robertson 1984) show that two-dimensional troughs and ridges in the tropopause have very similar static stability and circulation characteristics associated with them, as expected from our qualitative arguments and from Gill's two-dimensional solutions cited in section 3.

(d) *Inversion by nonlinear normal-mode initialization*

With the exception of the circular-vortex equation (29), for circularly symmetric IPV anomalies in an idealized, horizontally uniform reference state with constant  $f$ , none of the foregoing theories, even Salmon's, can express the balance condition (i) of section 1(d) in a way that retains any useful accuracy in the tropics. One way of expressing the invertibility principle for time-dependent motions on the full sphere may be to use the concepts of normal-mode initialization pioneered by Dickinson, Williamson, Baer and Machenhauer (see the review by Daley (1981)).

The basic idea is to express the fields of wind, temperature, etc., as a superposition of modes belonging to a complete set of atmospheric linear normal modes, and then to set to zero the coefficients of all modes not belonging to a subset considered representative of balanced motion. The accuracy of the 'linear balance' thus realized is then improved by iteration on the nonlinear, topographic, and forcing terms in the equations and boundary conditions. The choice of the subset of modes retained generally involves some arbitrariness (e.g. Tribbia 1979), reflecting the fact that 'balanced motion' has no self-evidently unique meaning in the tropics. In the case of the IPV inversion problem, however, there is only one natural choice: the relevant subset consists of the Rossby and westward-propagating Rossby-gravity modes, along with the steady zonal flows. The Kelvin and inertio-gravity modes are omitted. There is no possibility of including the Kelvin mode, since (unlike any of the other linear modes) it is invisible on an IPV map.

In specialist language, the resulting inversion computation would be called an 'IPV-constrained nonlinear normal-mode initialization' (Daley, *op. cit.*). The smoothing property of the inversion operator would be expressed by the fact that the normal-mode expansion coefficients would tend to fall off more rapidly for the wind and geopotential height fields than for the PV field. The reference state would enter the computation as the standard atmosphere whose normal modes are used.

In practice it will seldom be necessary, of course, actually to solve the inversion problem, since in practice the wind and height fields are already available. It is conceptually important, however, to know that the inversion can in principle be carried out, and under what circumstances, and to know how serious are the errors made by ignoring oscillations about 'balance', however the latter is defined. These questions pose a formidable challenge to researchers working on the mathematical aspects of the subject. Present indications are that the errors will often turn out to be much less serious than the errors inherent in quasi-geostrophic theory. It should be noted that 'less serious' may

not necessarily mean ‘small’. Oscillations about balance may have amplitudes which are far from negligible in the data, but may still not seriously affect the evolution of the balanced part of the motion, since the nonlinear coupling between balanced and unbalanced motion may still be small.

## 6. ROSSBY WAVES AND SHEAR INSTABILITIES

From now on it will be assumed that we are dealing with balanced dynamical phenomena such that the invertibility principle holds to sufficient accuracy for the purpose at hand. To the same order of accuracy, whatever it may be, the dynamical evolution can then be described solely in terms of the IPV (and surface  $\theta$ ) distributions, their induced wind fields, and their advective, frictional and diabatic rates of change. In the following sections it will be shown how this viewpoint, which we have referred to as ‘IPV thinking’—and which represents nothing more than a logical extension of Rossby’s original arguments about wave propagation—can give useful insights into a number of different time-dependent situations.

We begin with adiabatic, frictionless Rossby waves and shear instabilities, which provide some of the simplest and thoroughly studied illustrations of time-dependent interactions between IPV anomalies. In each case the anomalies arise from air-parcel displacements across a pre-existing IPV gradient or surface  $\theta$  gradient. The air-parcel displacements are themselves caused by the wind fields induced by neighbouring IPV or surface  $\theta$  anomalies. The insights gained are by no means limited to the linear propagation and growth mechanisms characteristic of small amplitude waves (sections 6(a)–(c)). They also illuminate the ways in which nonlinear saturation may take place at large wave amplitude (section 6(d)), and lead to a sharper perception of relationships between the idealized theoretical models and the behaviour of the real atmosphere (sections 6(d), (e)). They remind us, furthermore, that the basic wave and instability phenomena do not depend, in any crucial way, on the restrictive assumptions of the quasi-geostrophic theories often used to model them. Among the published lines of evidence on this last point we may mention the elegant instability study by Eliassen (1983).

### (a) Rossby wave propagation and the scale effect

For the sake of definiteness we consider the usual undisturbed basic state in which the IPV gradient is directed northwards ( $y$  direction) so that the contours on each IPV map are zonal (parallel to the  $x$  axis). If this basic state is slightly disturbed, adiabatically

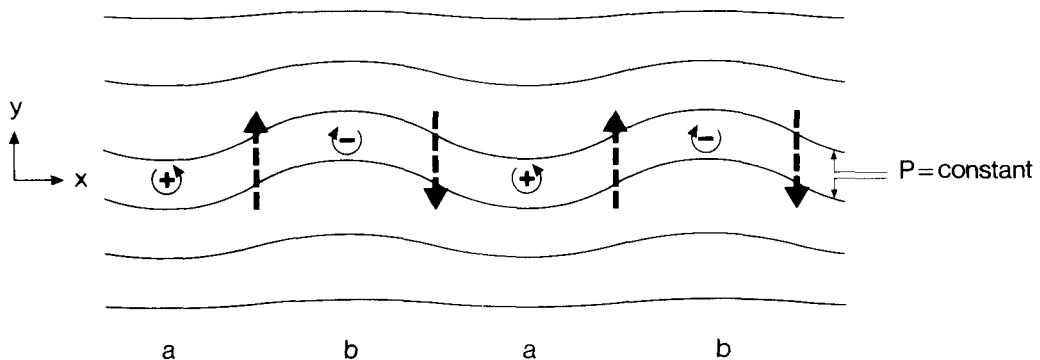


Figure 17. IPV map for a simple,  $x$ -periodic Rossby wave. The + and – signs respectively indicate the centres of the cyclonic and anticyclonic IPV anomalies due to southward and northward air-parcel displacements across a basic northward IPV gradient. The heavy, dashed arrows indicate the sense and relative phase of the induced velocity field (see text) which causes the westward propagation of the phase of the pattern.

and frictionlessly, then the IPV contours, which coincide with material contours, will undulate, following the material motions. The simplest case is that of a periodic, sinusoidal undulation, like that sketched in Fig. 17. If we think of the total flow as consisting of basic state plus disturbance, then the disturbance consists of a row of IPV anomalies of alternating sign, as suggested in Fig. 17 by the + and - signs enclosed by circular arrows, + meaning a cyclonic anomaly and - an anticyclonic anomaly.

To see that this pattern of IPV anomalies will tend to propagate relative to the basic state, one need only picture the qualitative nature of the wind field it induces. For this purpose we take advantage of the approximate superposability of the flow structures induced by isolated IPV anomalies, of which an idea can immediately be gained from the illustrations in Figs. 15 and 16 (although the anomalies should be considered to be weaker, with less distortion of the tropopause, if linear theory is to apply). Consider for example a case in which the anomalies are imagined to be concentrated mainly on those isentropic surfaces which lie in the region of strong basic IPV gradients near the tropopause. Then the induced flow structure, when viewed in a longitude-height cross-section, will look qualitatively like Figs. 15(a) and (b) placed side by side in overlapping positions, the whole pattern being extended periodically in the  $x$  direction as suggested by the labelling a, b, a, b, . . . in Fig. 17. The winds are added vectorially everywhere, and it can be seen, in particular, that the induced wind fields tend to reinforce halfway between each pair of anomalies. The total induced north-south wind field is a quarter wavelength out of phase with the displacement field and has the sense implied by the heavy, dashed arrows in Fig. 17 (statement (i) near the end of section 3). That is, the maximum northward velocity tends to be located a quarter wavelength westward of the maximum northward displacement, and similarly for the maximum southward velocity and displacement. If one now pictures how this velocity field will advect the IPV contours in Fig. 17, one can see that the wave pattern will propagate westward relative to the basic flow.

The well-known fact that the relative westward phase speed increases with the spatial scale of the pattern is a manifestation of the scale effect already mentioned below Eq. (33d). The scale effect is most easily deducible from scaling arguments applied to the approximate form of the inversion operator defined by (44). The larger the spatial scale of an IPV anomaly pattern of given strength, the stronger the induced velocity field. The whole picture can of course be made quantitative, using the standard techniques of linear theory, for any given zonal basic state and for any given mathematical expression of the invertibility principle, from quasi-geostrophic theory onwards, depending on how much computational effort is considered worthwhile for the purpose. Qualitatively speaking it is nothing more than Rossby's original explanation of the wave propagation mechanism, restated in such a way as to highlight (a) the fact that it depends on the concepts of invertibility and induced wind field, and (b) the fact that the propagation mechanism can operate whenever there is an IPV gradient of any sort whatever, including the effective gradient associated with a surface  $\theta$  gradient.

For instance, if we have a surface  $\theta$  gradient instead of an internal IPV gradient, then the same qualitative explanation applies word for word. The only difference is that surface-induced structures like those in Figs. 16(a), (b) are relevant, in place of the upper-air-induced structures of Figs. 15(a), (b). The contours in Fig. 17 then represent the contours of  $\theta$  at the bottom boundary. The resulting wave propagation mechanism gives rise to the topographic Rossby waves noted by Rhines (1970), and also to the short, stable waves arising in the Eady model of baroclinic instability, which are trapped near one or other of the two horizontal boundaries assumed in that model. The causes of the basic-state surface  $\theta$  gradients in the two cases are, respectively, sloping topography, and

thermal wind shear at the boundary (Bretherton 1966a). Various combinations of these effects have been demonstrated in laboratory experiments by, for instance, Hide and Mason (1975, and refs.).

(b) *Barotropic and baroclinic shear instabilities*

An extension of the foregoing picture can now be used, following Lighthill (1963, p. 93) and Bretherton (1966b), to grasp in a direct, intuitive, yet in principle precise, way the physical nature of the simplest linear wave instabilities of a basic zonal shear flow. This in turn will give insights into the circumstances under which certain types of cyclogenesis may or may not be expected to occur, and into the limitations of idealized instability models. The simplest instabilities—by which we mean those with the simplest spatial structures—are also, in many cases, those with the fastest growth rates.

These simplest instabilities are all characterized by a pattern of IPV anomalies of the general sort shown schematically in Fig. 18. The pattern can be thought of as a pair of Rossby waves propagating side by side, or one above the other, depending on whether a barotropic or a baroclinic instability is in question. In the latter, baroclinic case, with the vertical ( $z$ ) axis lying in the plane of the paper, it may be useful to picture the upper Rossby wave as being represented, again schematically, by a copy of Fig. 17 intersecting the paper with the positions of the  $+$  and  $-$  signs brought into correspondence. The angle of intersection is not exactly a right angle, because Fig. 17 represents an isentropic surface. The lower Rossby wave can be visualized in a similar way except that, since the IPV gradient is negative, the  $+$  and  $-$  signs must be exchanged in Fig. 17 and the velocity arrows reversed, as implied by the bottom row of signs in Fig. 18.

Viewed in a reference frame moving with the zonal phase speed  $c$  of the disturbance, each Rossby wave propagates against, and is held stationary by, the local basic flow. From Rossby's argument, this is dynamically possible if the sign of the basic IPV gradient is positively correlated with that of the relative zonal flow ( $\bar{u} - c$ ), i.e. both signs positive, as in the top half of Fig. 18, or both signs negative, as in the bottom half. This is the simplest configuration consistent with the Rayleigh-Kuo and Fjørtoft necessary conditions for instability, and their generalizations (e.g. Charney and Stern 1962; Miles 1964; Pedlosky 1964; Blumen 1968; Eliassen 1983). It will be noticed that if the basic zonal flow  $\bar{u}$  has a continuous profile then a steering level or critical line will be present, where  $\bar{u} - c = 0$ . We shall assume at first that the basic IPV gradient vanishes in some region containing the critical line, and return to the more general case afterwards. Moreover, for expository

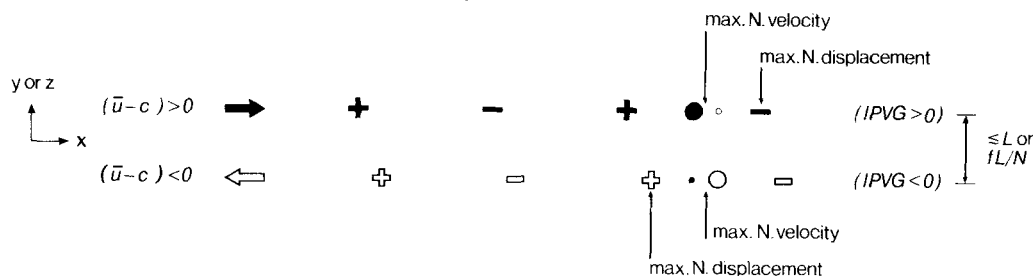


Figure 18. Pattern of IPV anomalies typical of the simplest barotropic and baroclinic instabilities on a zonal shear, the sense of the shear being indicated by the broad arrows at the left. The frame of reference has been chosen to move with the wave pattern. The basic IPV gradients (IPVG) are positive at the top and negative at the bottom of the picture. The solid black dots indicate (for the right-hand-most half wavelength) the  $x$ -location of the maximum northward velocity induced by the upper IPV pattern alone. The open dots indicate the same thing for the lower IPV pattern. The transverse dimension is northward ( $y$ ) in the case of the barotropic instability, and upward ( $z$ ) in the case of the baroclinic instability. Intermediate, 'mixed instability' cases also exist, to which precisely the same kind of pattern is relevant when viewed in tilted coordinates. For the fastest growing instabilities, the phase shift between the two IPV patterns is usually larger than that shown.

purposes we shall restrict attention at first to patterns whose spatial scale is such that, if the induced velocity field associated with each Rossby wave in Fig. 18 did not affect the other, then their phase propagation would be somewhat too weak to hold them stationary against the basic zonal flow.

The essence of the instability mechanism is that the induced velocity fields do, however, overlap significantly. That is why, in order to get a strong baroclinic instability of horizontal scale  $L$ , say, and simple spatial structure, the vertical separation between the two rows of IPV anomalies has to be of the order of one Rossby height  $fL/N$  or less. Similarly, the horizontal separation for a strong barotropic instability of simple spatial structure has to be of order  $L$  or less. The overlapping of the induced velocity fields has the following consequences, under the assumed conditions:

- (i) Inasmuch as the IPV anomaly patterns are less than a quarter wavelength out of phase with each other, the case shown in Fig. 18, each half helps the other to propagate against the basic zonal flow. That is, the contributions to the northward velocity induced by each IPV pattern partially reinforce each other, making the phase of each pattern propagate upstream faster than it would in isolation. This is how the patterns hold themselves stationary against the basic flow, under the assumed conditions.
- (ii) Because of this interdependence between the two counterpropagating Rossby waves, their relative phase tends to lock on to a configuration like that shown. For if the IPV patterns were each to shift slightly downstream, i.e. the upper pattern towards the right and the lower towards the left, so as to be more nearly in phase, then each half would help the other to propagate still more strongly, moving the patterns back upstream towards their original relative positions. Conversely, if the patterns were shifted upstream, so as to be more out of phase, then propagation would be weakened, and advection by the basic zonal flow would tend to restore the original phase relation.
- (iii) Just as in Fig. 17, the northward velocity induced by the upper IPV pattern alone is a quarter wavelength out of phase with that pattern. The large black dot in Fig. 18 marks the position of the northward velocity maximum induced by the upper IPV pattern alone, for the right-hand-most wave period. This is *less than a quarter wavelength* out of phase with the bottom IPV pattern, and therefore with the bottom displacement pattern, as indicated by the position of the small black dot directly below. If we add the velocities induced by the bottom IPV pattern (open dots) to get the total velocity field, we see at once that the total velocity is also less than a quarter wavelength out of phase with the displacement pattern. This is true on the top level as well as on the bottom level.
- (iv) It follows that the total northward velocity field in each half of the disturbance can be regarded as a sum of sinusoidal contributions in phase with, and a quarter-wavelength out of phase with, the northward displacement field. Moreover, the in-phase contribution has the same sign as the displacement. A velocity in phase with the corresponding displacement implies, by simple kinematics, that both must be growing.

The instability mechanism just described can be summarized in one sentence, by saying that

'The induced velocity field of each Rossby wave keeps the other in step, and makes the other grow.'	(69)
---	------

These two effects of the induced velocity field are associated respectively with its in-quadrature and in-phase contributions. The pure, exponentially-growing normal mode

of linear instability theory describes a situation in which the two IPV anomaly patterns have locked on to each other and settled down to a common phase speed  $c$ , such that the rates of growth which each induces in the other are precisely equal, allowing the shape of the pattern as a whole to become precisely fixed, and the growth of all disturbance quantities precisely exponential.

Cases in which the spatial scale is sufficiently large that each wave in isolation would propagate *faster* than the basic zonal flow can be understood in essentially the same way. The main changes needed are in statement (i) of the foregoing, where 'help' is replaced by 'hinder', 'faster' by 'slower', and so on. Whereas in the 'helping' case the phase shift between the two IPV patterns is less than 0.25 of a wavelength, as shown in Fig. 18, in the 'hindering' case the phase shift lies between 0.25 and 0.5 of a wavelength. The relative phase tends to lock on just as before, and the summarizing statement (69) remains true.

In fact this latter case is usually the one which exhibits the largest growth rates, as would generally be expected from the fact that a larger phase shift between the two IPV anomaly patterns enables the total induced velocity to be more nearly in phase with the displacement, tending to give a larger growth rate. This is exemplified by the Eady problem (e.g. Gill 1982, Fig. 13.4c), where the fastest-growing mode has an IPV phase shift of 0.37 of a wavelength. (Note that the IPV anomalies are entirely in the form of surface  $\theta$  anomalies, in the quasi-geostrophic description at least, and that the signs are reversed at the top boundary: there, warm is anticyclonic and cold is cyclonic.) Another example is given in Fig. 13.7 of the same reference, which reproduces Rayleigh's original barotropic instability calculation for the simplest unbounded, unstable shear-layer profile, with three constant-IPV regions side by side, the profile crudely approximating a continuous, tanh-like function by means of three straight-line segments. Such profiles can also be looked on as quasi-geostrophic models of the baroclinic instability of an internal vertical shear layer. In Rayleigh's problem the IPV phase shift for the fastest-growing mode amounts to 0.32 of a wavelength, again greater than 0.25.

The analyses just cited also confirm that the phase shifts in the northward velocity and geopotential height anomaly patterns are substantially less than those in the corresponding IPV anomaly patterns (respectively 0.25 and 0.18 of a wavelength in the two examples), as suggested by Fig. 18. This can be looked upon as another consequence of the smoothing property of the inversion operator.

As Bretherton's (1966b) analysis showed, the picture developed so far applies accurately and without qualification to basic flows of the kind just mentioned, having two separate regions of nonvanishing basic IPV gradients of opposite sign, such that the IPV anomaly patterns have no dynamically significant internal structure, e.g. phase tilts, within each region, and such that there are no significant critical-line or steering-level effects because the IPV gradient vanishes in between the two regions so that no IPV disturbance pattern can develop there. In all such cases the picture suggested by Fig. 18 applies exactly as it stands, apart from the tendency for larger IPV phase shifts already mentioned. It also applies to the Phillips two-layer model of baroclinic instability, for essentially similar reasons, as Bretherton showed in detail.

In cases where the basic IPV gradient does not vanish near the critical line, on the other hand, the foregoing picture needs some modification. How much depends on the circumstances. For a fast-growing instability, the modification will evidently be slight if the IPV gradient is sufficiently weak at the critical line. However, in cases like the Charney baroclinic-instability problem, the results of many published studies show that the IPV gradient at the critical line is not effectively weak. Nevertheless, it turns out, perhaps surprisingly, that the qualitative picture for the fastest-growing instability is still much the same in its essentials, provided we recognize that the 'upper' IPV anomaly

pattern in Fig. 18 is now distributed over a deep layer including the steering level. Its induced fields can still be kept *conceptually* separate from those of the lower anomaly pattern (which, as in the Eady problem, consists of surface  $\theta$  anomalies); and the foregoing arguments then apply almost word for word, even though the upper and lower IPV anomaly patterns are no longer cleanly separated in space, and even though the 'upper' IPV pattern does, now, have its own internal phase structure. It tilts in the opposite sense to, but less strongly than, the main phase shift relative to the lower anomaly pattern. With realistic parameter values, the main IPV phase shift for the fastest-growing mode varies with altitude from half a wavelength at the lower surface to about a third of a wavelength aloft (R. Pierrehumbert, personal communication).\*

For the fastest-growing Charney mode, the 'upper' IPV anomaly pattern is concentrated mainly in the lower half of the troposphere. Its maximum amplitude, as measured by the quantity  $q$  defined by (38), occurs near the steering level between 600 and 700 mb. Above that the disturbance amplitude of  $q$  falls off quite rapidly with height: at 200 mb it is about a third of its maximum value, and at 100 mb, about a fifth; the precise values depend on the precise choice of parameters. The flow fields induced by the 'upper' pattern alone are therefore intermediate in character between those suggested by Figs. 15 and 16, being centred neither at the tropopause nor at the ground but, rather, somewhat below mid-troposphere. When the fields induced by the surface pattern are added, the large main phase shift leads to considerable cancellation in the lower troposphere.

Instabilities on more realistic, jet-like zonal flows are very like the Charney mode in all these respects (Edmon *et al.* 1980; Hoskins 1983; Hoskins and McIntyre 1985). There is some evidence that the early stages of such instabilities may be observable in the southern hemisphere (Randel and Stanford 1985). The physical situation is one in which upper air IPV anomalies at altitudes typical of the tropopause seem to play a comparatively minor role in the early stages (but cf. section 6(d)). Such altitudes appear to be too far above the ground, in comparison with the Rossby height  $fL/N$ , and upper air winds too strong, to permit phase-locking and sustained growth of a synoptic-scale disturbance whose amplitude is initially small.

### (c) *Lateral and vertical Rossby wave propagation*

It will prove useful to return briefly to the case of simple Rossby wave propagation on a one-signed IPV gradient, in the light of the experience gained in discussing Fig. 18.

It will have been noticed that Fig. 17 depicts a disturbance of limited extent in the  $y$  direction, its IPV anomalies being concentrated near  $y = 0$ . Such a state of things may well be only temporary if there are sufficiently strong basic IPV gradients outside the central region shown. Owing to the smoothing property of the inversion operator, the induced wind field of the IPV anomaly pattern will extend northward and southward beyond the anomaly pattern itself (unless constraining sidewalls are present, as in some

\* The sense of the internal phase tilt within the 'upper' IPV pattern is largely governed by the fact that, at the steering level itself, the northward velocity must be *exactly* in phase with the northward displacement, as can be seen from the kinematics of a growing disturbance of small amplitude viewed in the  $c = 0$  reference frame. The internal phase tilt becomes relatively larger for modes with relatively small growth rates and is important for the detailed way in which the instability balances its IPV and Eliassen-Palm fluxes (e.g. Bretherton 1966a, Eq. (4); Edmon *et al.* 1980, Eq. (4.1)). These facts can be used as the basis for an alternative way of describing Charney's instability which becomes rigorously applicable in the limit of small growth rate. Different versions of it are based on the ideas of 'critical-layer instability' (Bretherton 1966a), and 'over-reflective instability' (Gill 1965). The first version was put into quantitative form, including explicit formulae for the growth rate and a proof of the convergence of successive approximations, by McIntyre (1970, 1972), and the second has been developed very extensively in a recent series of papers by Lindzen and his collaborators (Schoeberl and Lindzen 1984, and refs.).

laboratory and theoretical models). This will in turn cause more distant IPV contours to undulate, engendering further IPV anomalies. The process can continue indefinitely if basic IPV gradients are large enough to support it out to successively greater distances in the  $y$  direction, leading to the well-known northward or southward propagation of Rossby wave activity. Vertical propagation works similarly. The quantitative meaning of having a 'large enough' basic IPV gradient depends, like the induced wind field itself, on the spatial scale of the waves. It also depends on the difference between the zonal phase speed  $c$  and the basic zonal flow  $\bar{u}(y, z)$  against which the phase has to propagate, and for given  $(\bar{u} - c)$  can be elegantly expressed in terms of the quasi-geostrophic refractive index introduced by Charney and Drazin (1961) and Matsuno (1970). This has recently found extensive use in theoretical discussions of stationary planetary wave propagation in the stratosphere.

The precise nature of the lateral and vertical propagation mechanism can be appreciated more clearly from a slight adaptation of Fig. 18, with the understanding that there is to be some judicious interpolation between the IPV patterns explicitly shown. If we imagine that the relative zonal flow  $(\bar{u} - c)$  is towards the right everywhere, and that the basic IPV gradient is positive everywhere, then we have a qualitatively correct picture of what happens near the leading edge of the disturbance as it penetrates towards positive  $y$  or  $z$ , with the top half of the figure representing the initially weak IPV anomaly pattern at the leading edge. This situation is shown in Fig. 19.

The essential point is that the IPV pattern at the leading edge is being made to grow (at a rate which can be related to the appropriate 'group velocity' component) by the induced velocity field of the lower IPV pattern, where, we suppose, the disturbance has already reached full strength. Just as with the instability, the growth depends crucially on having a phase tilt in the sense shown. But the effect of the upper pattern upon the lower pattern is now the opposite to what it was before. With the changed sign configuration in the lower pattern, as shown in Fig. 19, the velocity is now more than a quarter wavelength out of phase with the displacement so that the effect of the upper pattern on the lower pattern is to induce it to *decay*. This is how an isolated wave packet propagates northwards, or upwards as the case may be, and contrives to leave little or no disturbance behind it.

In view of the typical large-scale IPV distribution in the atmosphere (Figs. 1, 2(a)-(d)), we might expect to find some tendency for the tropopause, where IPV gradients are very strongly concentrated in the real atmosphere, to act as a Rossby waveguide. Although refractive index distributions tend to be less strongly structured, because of their dependence on  $(\bar{u} - c)$ , the expectation is to some extent borne out by objective

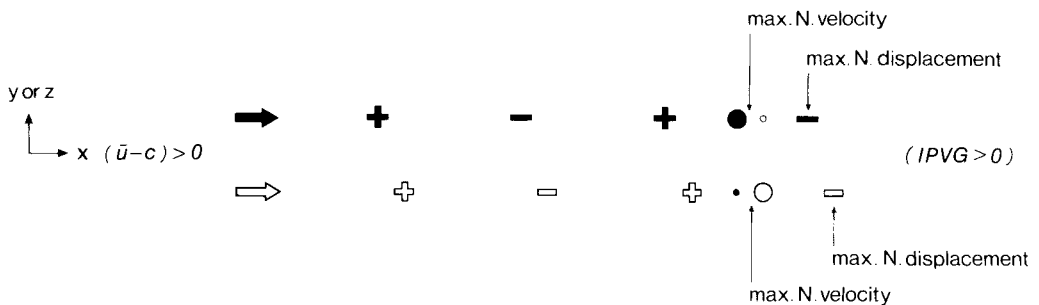


Figure 19. Pattern of IPV anomalies in a northward or upward propagating Rossby wave, represented schematically in the same way as in Fig. 18 to show the group-velocity mechanism (see text, section 6(c)). A similar picture can be used to understand the mechanism of 'critical-layer' absorption (e.g. Killworth and McIntyre 1985, section 2).

diagnostic studies of eddy statistics measuring the net flux of wave activity. This net eddy flux is often found to emerge from apparent sources in the middle and high-latitude troposphere and to split into two branches, the first going along the tropopause, mainly equatorwards, and the second going upwards into the stratosphere (e.g. Matsuno 1970; Sato 1980; Kanzawa 1984; Miles and Chapman 1984; Al-Ajmi *et al.* 1985).

(d) *The nonlinear saturation of baroclinic instabilities*

The use of IPV thinking to understand Rossby waves and related shear instabilities is by no means restricted to small wave amplitude, in the sense required by the standard linear theories of these phenomena upon which the foregoing discussion was based. IPV thinking can also give considerable qualitative insight into what happens when wave amplitudes become large for whatever reason, and, in particular, insight into the strongly nonlinear stages of a fast-growing baroclinic instability. These stages are inaccessible to analytical theory, whether linear or 'weakly nonlinear'. For the sake of brevity we merely sketch the main points here; more extensive discussions, with detailed diagnostics, may be found elsewhere (Hoskins and McIntyre 1985). Various aspects of the picture have been noted previously by, for example, Edmon *et al.* (1980), Hsu (1980), Davies (1981), Dunkerton *et al.* (1981), McIntyre (1980, 1982), Lindzen and Schoeberl (1982), Schoeberl (1982), Hoskins (1983), McIntyre and Palmer (1983, 1984) and Schoeberl and Lindzen (1984), and important precedents can be found in classical observational studies of occluding cyclones and other phenomena (e.g. Namias 1940, 1983; Berggren *et al.* 1949).

The amplitudes of lateral air-parcel displacements, and therefore of IPV anomaly strengths, are always limited in reality by constraints of an essentially kinematical nature which are neglected by linear theory. When such constraints come into play one may appropriately speak of 'nonlinear saturation'. One such constraint comes simply from the fact that there is never an infinite amount of room available for lateral air-parcel displacements to grow without bound in the way predicted, for example, by linear instability theory for a baroclinically unstable shear flow. Sooner or later the predicted displacements become comparable to the width scale of one of the regions of basic IPV gradients upon which unstable growth depends, or comparable to the width scale of the linear disturbance structure. The situation predicted by linear theory cannot then correspond, even qualitatively, to physical reality, one symptom of this being that material contours shaped initially like those in Fig. 17 begin to intersect one another. (In the case of Fig. 17 this would happen if the contour displacement amplitudes were to grow by a factor of about  $\exp(1.1)$ .) In reality, material and IPV contours which look like those of Fig. 17 in the early stages of growth are always found, in cases of practical interest, to deform irreversibly into complicated shapes rather than continuing to expand sideways. In this respect the saturation process is analogous to the breaking of waves on an ocean beach, except for the fact that here the growth in wave amplitude is due to the unstable, *in situ* interaction between the two counterpropagating Rossby waves depicted in Fig. 18, rather than to the arrival of waves propagating from somewhere else. In some ways a closer analogue is the breaking of Kelvin-Helmholtz billows.\*

The resulting constraint on the magnitudes of lateral air-parcel displacements is accompanied by a corresponding constraint on the strengths of IPV anomaly patterns in

\* In both analogies, vertical displacements of material contours (against the gravitational restoring mechanism) are considered to correspond to the sideways displacements of material contours (against the Rossby restoring mechanism, as in Fig. 17); and there are of course other differences of detail. The analogies are by no means superficial. Their basic relevance can be seen for instance from the hypotheses required to prove finite-amplitude 'nonacceleration theorems' in the general theory of wave, mean-flow interaction (Andrews and McIntyre 1978, §5; McIntyre 1980, §3; McIntyre and Palmer 1983, 1984). One of the necessary hypotheses is that the relevant material contours undulate without deforming irreversibly, i.e. that the waves do not 'break' in the sense suggested.

the region concerned. Indeed the effective strengths of the IPV anomalies may actually diminish, even in the absence of frictional and diabatic processes, when the deformation of material and IPV contours becomes severe, since the scale effect comes into play as the IPV contours wrap up. The wrapping-up process tends to produce ever smaller scales in the IPV distribution (the 'enstrophy cascade' effect), leading to destructive interference in the inversion operation as far as the original, relatively large, wave scale is concerned.

For the fastest-growing baroclinic instabilities on realistic basic jet-like flows, like the standard wave-6 case of Simmons and Hoskins (1980), it is found from numerical simulations that nonlinear saturation takes place in the manner described, and that it occurs first of all at the surface and in an adjacent layer containing the steering level. These are the places where linear instability theory predicts the largest lateral displacements. The layer is about half a density-scale-height deep. The wind, temperature and pressure fields resemble those observed in the classical occlusion process. The low-level isotherms give an indication of the shapes of the relevant material contours. Sharp surface fronts develop, in the familiar way, and these can be looked on as one manifestation of the 'cascade' to smaller scales; no such fronts are present in the initial conditions used in the simulations. By way of illustration, Fig. 20(a) shows the near-surface isotherms for day 6 of Simmons and Hoskins' standard case. Their shapes are to be contrasted with the simple, wavy shapes sketched in Fig. 17.

Low-level saturation leads on, in these cases, to a further stage of evolution describable as free Rossby wave propagation into the upper troposphere; it is an example of the *nonlinear radiation* discussed, for example, by McIntyre and Weissman (1978). Efficient upward radiation is possible because refractive index values turn out to be large

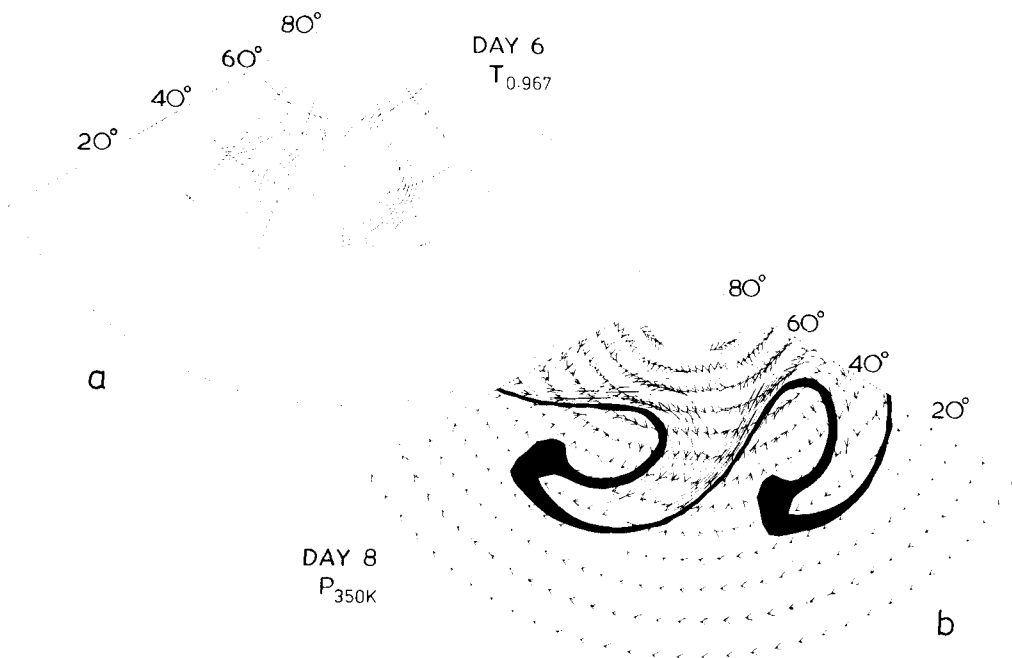


Figure 20. Some fields from the basic zonal wavenumber-six baroclinic wave life-cycle experiment of Simmons and Hoskins (1980). Shown in (a) is the temperature distribution at day 6 on the lowest 'sigma' surface, pressure = 0.9673 times surface pressure. The contour interval is 5 K. The latitudinal domain is from 0° to 90°N, and two full horizontal wavelengths are shown. In (b) the day-8 350 K IPV map is given, with contour interval 0.8 PV units. The regions with values 2.4–3.2 units have been blacked in. Also shown by arrows is the wind field on this isentropic surface in a frame of reference moving with the waves. The scale is such that the arrows nearest the equator represent a speed of  $16 \text{ ms}^{-1}$ .

enough to support free propagation of a wave-6 disturbance with matching phase speed  $c$ . Nonlinear radiation begins as soon as IPV and surface potential temperature anomalies in the saturating lower layer cease growing as fast as IPV anomalies located higher up, in the middle troposphere. Above the saturating layer, IPV contours in the main jet region have wavy shapes more like those in Fig. 17, and displacement amplitudes are still growing.

As this upper region becomes increasingly free of the influence of the lower layer, the disturbance there becomes increasingly free to propagate upward. (Some of it may also propagate downward, but if so will tend to be reflected back up.) The simulations show that the disturbance does indeed penetrate upward and that it then concentrates near the jet maximum at the tropopause, and, in most cases, appears to be guided along the tropopause mainly towards the equatorward flank of the jet (e.g. Edmon *et al.* 1980, Fig. 3). There, a second major saturation event takes place, distinctly later than the first, low-level event.

In this second saturation event, the analogy to ocean surf is closer than before and the situation is very similar indeed to that of the breaking mid-stratospheric Rossby waves discussed, for instance, by Hsu (1980), McIntyre (1980, 1982), McIntyre and Palmer (1983, 1984), Al-Ajmi *et al.* (1985), Clough *et al.* (1985) and Leovy *et al.* (1985). Here the lateral inhomogeneity of the relative zonal mean wind  $\bar{u} - c$  is a crucial factor. The saturation process is illustrated in Fig. 20(b), which presents the 350 K IPV map for day 8 of the standard case. The wind vectors on the 350 K surface are drawn relative to the wave, i.e. in the frame of reference in which  $c = 0$ . Equatorwards of  $45^\circ$ , the flow seen in this frame of reference is dominated by anticyclonic closed-streamline regions, again leading to the irreversible wrapping-up of material and IPV contours (again, contrast Fig. 17). On the eastern flanks of these gyres, high-PV air has been advected equatorwards and then westwards. The process has been studied, in idealized form, in the time-dependent theory of 'nonlinear critical layers' (e.g. Stewartson 1978; Warn and Warn 1978; Ritchie 1985; Killworth and McIntyre 1985) and, in a somewhat different type of dynamical model, by Deem and Zabusky (1978) and by Dritschel (1985) among others. It is important for the dynamical evolution whenever the closed-streamline regions grow large enough to overlap a region of significant IPV gradients, so that many IPV contours are wrapped up.

There seems little doubt that the whole sequence of events greatly influences the pattern of eddy transports, e.g. poleward eddy momentum fluxes, associated with the life cycles of realistically strong nonlinear baroclinic instabilities. It seems likely to have important implications, directly or indirectly, for our understanding of tropical-extratropical interactions and of climate and the general circulation, and we return briefly to this point in section 9.

#### (e) *Further remarks about cyclogenesis in the real atmosphere*

In section 2(c) and Figs. 5–7, we noted an example of upper-air-induced cyclogenesis in the real atmosphere in which low-level  $\theta$  gradients were weak, and appeared to play no important role in the development. In other cases surface baroclinicity does play an important role, as is well known. Many such cases have elements in common with the linear-instability situation depicted in Fig. 18 (with ordinate  $z$ ), and to some extent are describable in similar terms.

However, pre-existing upper air IPV anomalies of large amplitude are often involved, like the cyclonic anomaly seen in Fig. 5(b). Therefore the cyclogenetic situation may not depend upon the prior existence of a phase-locked, linear-instability stage, and may have a more immediate dependence on initial conditions. Theoretical idealizations of different

aspects of such situations have been proposed by Farrell (1982), building on the work of Kelvin (Thomson 1887) and Orr (1907), and by Simmons and Hoskins (1979) in the context of downstream development. In some observed cases (e.g. Uccellini *et al.* 1984, 1985; Young *et al.* 1985) the 'upper air' anomaly is one which had previously been advected down sloping isentropic surfaces to mid-tropospheric levels or even lower. In such cases 'upper air' may have to be understood as referring more to the origin of the anomaly, than to its actual altitude at the time of maximum surface development. Figures 5, 8 and 9 appear to be less extreme cases of the same thing, and other examples can be seen in Figs. 2 and 3 and in many of the case studies cited in section 1(c). The cyclonic upper air anomalies of interest evidently come in a great variety of shapes, sizes, and rates of advection, some being associated in an obvious way with prominent, large-scale upper air troughs, as in the case studies of Petterssen and Smebye (1971), and others having smaller scales which presumably go all the way down to the scales characteristic of jet streaks.

A standard cyclogenetic situation is shown schematically in Fig. 21. Suppose, in the spirit of the thought-experiment of section 4, that a cyclonic upper air IPV anomaly (which to a greater or lesser extent will be associated with a low tropopause, depending on its exact size, shape and strength) arrives over a pre-existing low-level baroclinic region, as suggested in Fig. 21(a). Thermal advection by the induced low-level circulation will tend to create a warm low-level anomaly ahead of the upper IPV anomaly (Fig. 21(b)), enhancing the effects of any low-level warm advection already present. This warm surface anomaly will induce, as in Fig. 16(a), its own cyclonic circulation. At low levels this circulation will add to the circulation induced from upper levels (Figs. 21(b), 15(a)), giving an intense low-level cyclone whose centre is a little ahead of the advancing upper-level IPV anomaly. While the low-level anomaly remains ahead of the upper-level anomaly there may be positive feedback to upper levels, temporarily resembling the

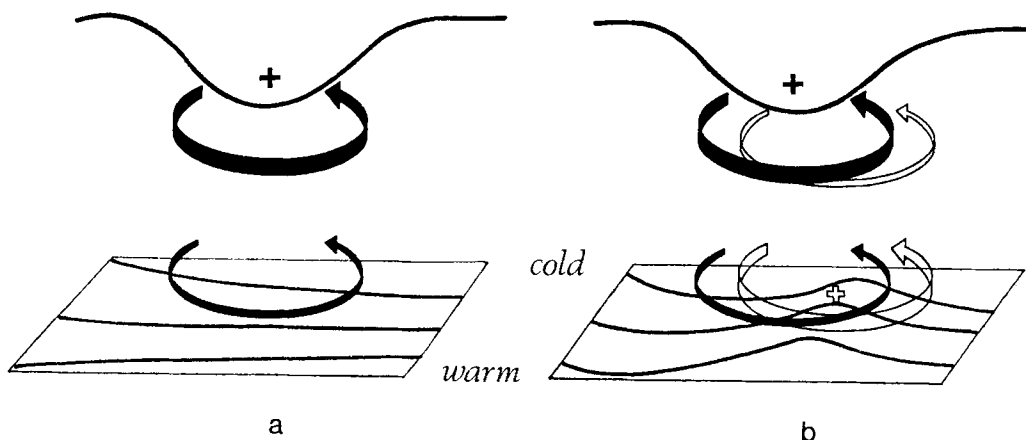


Figure 21. A schematic picture of cyclogenesis associated with the arrival of an upper air IPV anomaly over a low-level baroclinic region. In (a) the upper air cyclonic IPV anomaly, indicated by a solid plus sign and associated with the low tropopause shown, has just arrived over a region of significant low-level baroclinicity. The circulation induced by the anomaly is indicated by solid arrows, and potential temperature contours are shown on the ground. The low-level circulation is shown above the ground for clarity. The advection by this circulation leads to a warm temperature anomaly somewhat ahead of the upper IPV anomaly as indicated in (b), and marked with an open plus sign. This warm anomaly induces the cyclonic circulation indicated by the open arrows in (b). If the equatorward motion at upper levels advects high-PV polar lower-stratospheric air, and the poleward motion advects low-PV subtropical upper-tropospheric air, then the action of the upper-level circulation induced by the surface potential temperature anomaly will, in effect, reinforce the upper air IPV anomaly and slow down its eastward progression. (To this extent the situation is similar to the small-amplitude instability situation represented by Fig. 18 and described in section 6(b).)

small-amplitude instability situation in the 'helping' case, i.e. the case depicted in Fig. 18. This will tend to phase-lock the two anomalies and promote their mutual intensification. In particular, the upward extension of the circulation induced by the low-level warm anomaly will tend to intensify the upper-level IPV anomaly by advecting high-PV air equatorwards, on the left of the picture, and, because this advection is strongest just behind the upper-level IPV anomaly, will also tend, in effect, to slow down its advance.

It is well known that the combination of low-level warm advection and upper-level PVA or positive IPV advection can result in strong cyclonic development. Some idea of the possible magnitude of the effect, even in a dry atmosphere, can be gained by considering the possible strengths of the superposed wind fields induced by a cyclonic upper-level anomaly overlying a low-level warm anomaly. For example, a nearly-coaxial superposition of Figs. 15(a) and 16(a) gives surface winds as high as  $31 \text{ m s}^{-1}$ , and a very large surface pressure anomaly of  $-72 \text{ mb}$ . This of course is no more than an indication of the orders of magnitude involved, in the absence of friction, since as already explained the superposition principle holds only qualitatively for such large-amplitude anomalies.

It is of interest to note how the foregoing picture is likely to be modified by moist processes. The theory suggests what is also suggested by synoptic experience and numerical experimentation (e.g. Golding 1984), namely that moist processes can, and will on occasion, greatly enhance the surface development, even though conditions may be subcritical to moisture-driven instabilities such as CISK.

For the reasons explained in section 4, there will usually be a synoptic-scale region of rising motion within the region of reduced static stability beneath the advancing upper-level IPV anomaly (Fig. 15(a)). If condensation occurs in the rising air, as will happen if there is a sufficient supply of moisture, then the effective static stability,  $N$ , as felt by the large-scale upward motion, will be still further reduced. The effective Rossby height scale  $H$  given by the second expression in (33b) will then be increased, if the region of rising motion is sufficiently extensive horizontally—and the increase may be drastic if the rising air is sufficiently moist, as it might be, for instance, if supplied by a warm, moist, low-level airstream.

As discussed in section 3, an increased value of  $H$  implies an enhanced penetration, towards the surface, of the velocity and pressure fields induced by the upper air IPV anomaly, and a correspondingly enhanced direct contribution to the deepening of the surface cyclone. It also implies an enhanced dynamical feedback from the warm surface anomaly to upper levels. Thus one can have a situation of the sort indicated in Fig. 21(b) with tighter coupling between upper and lower levels leading to further reinforcement of the upper-level anomaly, to more vigorous low-level warm advection (increasing the moisture supply as well as the surface  $\theta$  anomaly), and hence, presumably, to a more rapid and spectacular surface development.

This qualitative picture seems consistent with the conclusions of Sanders and Gyakum (1980), Bosart (1981), Gyakum (1983), Golding (1984) and others (e.g. Palmén and Newton 1969, pp. 311–312) concerning the importance of moist processes in many cases of rapid cyclonic development outside the tropics. Equally, it is consistent with the view that upper air IPV advection may also play a key role in the development (e.g. Uccellini *et al.* 1984, 1985; Young *et al.* 1985), and that the primary effect of moisture in these cases may be to *amplify* a cyclogenetic process of the general kind depicted in Fig. 21; see also Sanders and Gyakum (*op. cit.*).

## 7. THE MAINTENANCE AND DISSIPATION OF CUTOFF CYCLONES AND BLOCKING ANTICYCLONES

We now take up the question of diabatic and frictional effects for the large-amplitude

anomalies giving rise to the cutoff cyclones and blocking anticyclones which formed the subject of sections 2–4.

Once a cyclonic PV region has cut off on an IPV map in the manner of Fig. 5, it will be surrounded by its induced cyclonic circulation and, if the surface temperature is not too low, this circulation will penetrate to the ground, giving a surface cyclone. Surface frictional processes would then begin to generate a cold, anticyclonic surface anomaly (similar to the structure illustrated in Fig. 16(b)) which, if there happens to be no low-level air motion relative to the upper air anomaly, will remain in place and ameliorate the cyclonic circulation at low levels, as suggested by a qualitative superposition of Figs. 15(a) and 16(b). However, regardless of what happens at low levels, the upper-tropospheric cyclone will persist as long as the IPV anomaly persists. The structure in Fig. 16(b) is evanescent with height and cannot cancel that in Fig. 15(a) at all levels. We note, in particular, that not all the kinetic energy of the upper air part of the circulation can be destroyed by boundary layer friction alone, since the latter cannot directly affect the upper air IPV anomaly.

The anomaly could of course, be removed by simply being advected back along isentropic surfaces into the polar stratospheric reservoir. However, synoptic experience suggests that the chances of this happening in less than a week are small. In practice, diabatic processes must be crucial to the evolution and decay of such systems, which often occurs much faster than a week, depending on the circumstances. This seems to be the basic fact behind the widely differing persistence of such features under different diabatic conditions.

In a similar manner, the anticyclonic IPV anomaly associated with a blocking anticyclone (Fig. 11(d)) induces its own anticyclonic circulation. The anomaly must persist unless the low-PV air returns to the subtropical region, as actually occurs in the example of Fig. 11, or is changed *in situ* by diabatic processes. We shall see that the latter processes tend to have a slower time scale for anticyclones. This appears to be one of the factors involved in the persistence of blocking.

In height coordinates, the PV equation in the presence of a frictional force-curl  $\mathbf{K}$  and a diabatic potential temperature source  $\dot{\theta}$  is

$$DP/Dt = (1/\rho)\zeta_a \cdot \nabla \dot{\theta} + (1/\rho)\mathbf{K} \cdot \nabla \theta. \quad (70a)$$

Multiplication of this equation by  $\rho$ , integration over a material volume  $\tau$ , with surface  $S$ , and use of the relations  $\nabla \cdot \zeta_a = \nabla \cdot \mathbf{K} = 0$ ,  $\rho P = \nabla \cdot (\zeta_a \theta)$ , etc., gives the corresponding integral statement

$$\frac{d}{dt} \iiint_{\tau} P \rho d\tau = \iint_S (\dot{\theta} \zeta_a + \theta \mathbf{K}) \cdot \mathbf{n} dS. \quad (70b)$$

It should be noted that the mass-integrated PV over  $\tau$  can therefore change only if there are non-zero values of  $\dot{\theta}$  or  $\mathbf{K}$  on its boundary  $S$ . Diabatic and frictional sources interior to the volume can only redistribute the PV; and it should be further noted that surface  $\theta$  anomalies can be included in this statement if the conventions suggested by the insets to Fig. 16 are adopted, in which case  $\dot{\theta}$  on the right-hand side of (70b) would be zero by definition.

For small-Rossby-number, large-Richardson-number flows, the vertical contributions to the dot product terms in (70a) dominate to give

$$DP/Dt \approx (1/\rho)\mathbf{k} \cdot \zeta_a (\partial \dot{\theta} / \partial z) + (1/\rho)\mathbf{k} \cdot \mathbf{K} (\partial \theta / \partial z). \quad (71)$$

In isentropic coordinates the equivalent equation is

$$DP/Dt = -\sigma^{-1}\{(f\mathbf{k} + \nabla_{\theta} \times \mathbf{v}) \cdot \nabla \dot{\theta} + K_{\theta}\} \quad (72)$$

$$\approx -\sigma^{-1}\{(f + \xi_{\theta})\partial \dot{\theta}/\partial \theta + K_{\theta}\}, \quad (73)$$

where as before  $\sigma$  stands for  $-g^{-1}\partial p/\partial \theta$ , and where  $K_{\theta}$  is the frictional isentropic force-curl analogous to the 'isentropic vorticity' defined by (9), i.e.  $K_{\theta} = \mathbf{k} \cdot \nabla_{\theta} \times \mathbf{F}$  where  $\mathbf{F}$  is the friction force per unit mass. Note that here  $D/Dt = \partial/\partial t + \mathbf{v} \cdot \nabla_{\theta} + \dot{\theta}\partial/\partial \theta$ , and that a convenient form of (73) for consideration of IPV behaviour in the presence of diabatic heating alone is

$$(\partial/\partial t + \mathbf{v} \cdot \nabla_{\theta})P \approx P^2 \partial(\dot{\theta}P^{-1})/\partial \theta \quad (74a)$$

or alternatively

$$(\partial/\partial t + \mathbf{v} \cdot \nabla_{\theta})(P^{-1}) \approx -\partial(\dot{\theta}P^{-1})/\partial \theta. \quad (74b)$$

The left-hand sides are the rates of change following an isentropic trajectory, and the simple forms of the right-hand sides facilitate computation and qualitative argument. The more elegant form (74b) which results when  $P^{-1}$  is used in place of  $P$  is reminiscent of an analytical device used by Eliassen (1983).

As discussed above, the frictional force-curl term is expected to be important within the boundary layer. In the free atmosphere, Shapiro (1976) has hypothesized that mixing of potential temperature due to clear air and other small-scale turbulence could be important in producing some of the anomalously large PV values observed in the lower stratosphere on the cyclonic side of strong jet streams. The constraint (70b) on the mass-integrated PV must of course be kept in mind here, as must the possibility of advection from upstream locations.

We now return to the role of latent heat release and radiative cooling in the dissipation and structural modification of mid-latitude cutoff cyclones and blocking anticyclones. As pointed out in section 3 (statement (iv)), one of the characteristic features of cutoff cyclones is the presence of weak static stability under the 'lowered' tropopause, e.g. under the heavy curve in Fig. 8 or in Fig. 15(a). This weak static stability is consistent with the observed tendency for deep convection to be associated with such systems if there is a sufficient moisture supply from below (e.g. Pedgley 1962, p. 159; Erickson 1971). Tropospheric convective heating, with  $P^{-1}\dot{\theta}$  diminishing upwards into the high-IPV anomaly above the 'lowered' tropopause, and changing sign as convective heating gives way to infrared cooling, will tend to reduce the strength of that anomaly locally.

For the example discussed in section 2(c) (Figs. 5–7), temperature and humidity soundings for Long Kesh (54°N 6°W) for 00z on 25 September 1982 indicate conditional instability up to 450 mb, the height of the 'lowered' tropopause for the observed 12z temperature. From the form of the right-hand sides of (74a, b) it is clear that the profile of  $\dot{\theta}P^{-1}$  is important. For relatively uniform heating in the troposphere, the decrease in  $P^{-1}$  with height implies that there is some reduction in IPV values, consistent with the upward motion of air through isentropic surfaces. However, the most dramatic effect is near the tropopause. In the lower stratosphere, the PV is so large that  $\dot{\theta}P^{-1}$  is effectively zero, irrespective of whether  $\dot{\theta}$  is dominated by infrared cooling rates or by convective heating, for any reasonable estimates. Thus for positive  $\dot{\theta}$ , IPV values in the tropopause region must be subject to large rates of diminution. Taking  $P^{-1}\dot{\theta} = 0$  at  $\theta = 305$  K,  $P = 2$  PV units at  $\theta = 300$  K, and  $P = 1$  PV unit,  $\dot{\theta} = 2.5$  K d<sup>-1</sup> at  $\theta = 295$  K gives, using centred differences in (74a), an IPV tendency at 300 K of minus 1 PV unit per day. This

is sufficient to destroy the 300 K IPV anomaly in a single day, which seems consistent with the observed behaviour of the system, Figs. 5(e), (f) in particular. By contrast, over continental interiors during wintertime the moisture supply is insufficient for much convection, and the characteristic cutoff-cyclone structure can persist much longer.

The implications of the integral constraint represented by (70b) should again be noted. Since deep convection will make  $\theta \neq 0$  only in the interior of the troposphere, away from the surface, the net effect of the convection will be to move the IPV anomaly down to lower tropospheric levels. In order to annihilate the cyclone completely, this diabatically-induced vertical redistribution of PV would have to extend all the way down to the surface, and be accompanied by the destruction of mass-integrated PV by surface friction. The need for surface friction in this hypothesized situation is clear from a consideration of the angular momentum budget of an idealized circular vortex. It can also be seen from the version of (70b) suggested by the insets to Fig. 16. If all *interior* IPV anomalies were to be destroyed by diabatic heating then in the absence of surface friction a surface  $\theta$  anomaly would still remain.

The blocking anticyclone structure as typified by Figs. 14 and 15(b) is one of large tropospheric static stability, which tends to suppress convection. It is therefore the effect of radiative cooling that must primarily be considered. Using (74) with  $P^{-1}\dot{\theta} = 0$  at  $\theta = 335$  K,  $P = 1$  PV unit at  $\theta = 330$  K, and  $P = 0.5$  PV units,  $\dot{\theta} = 1$  K d<sup>-1</sup> at  $\theta = 325$  K, gives a 330 K IPV tendency of plus 1 unit per 5 days. This suggests a time scale of a week or so for diabatic processes to modify such a blocking anticyclone.

Having previously stressed the conceptual duality between the dynamics of cutoff cyclones and blocking anticyclones, in sections 2(e) and 3, we see now that there is no such duality for their diabatic modification, which, other things being equal, tend to be much faster for cyclones than for anticyclones. The crucial difference is the tropospheric static stability induced by the IPV anomaly. In the cutoff cyclone, deep tropospheric convection is enhanced, the latent heat release leading to an efficient diabatic decay of the upper IPV anomaly on a time scale of a few days. In the blocking anticyclone, convection is suppressed, mainly by the increased static stability. Radiative cooling gives a time scale of a week or so. Of course quasi-conservative advection and re-merging into the subtropics becomes quite likely on this time scale, as did indeed occur in the examples described in section 2 and Fig. 11.

## 8. FURTHER REMARKS ABOUT CUTOFF SYSTEMS AND AIR MASSES

In stressing the distinction between 'cutoff' and 'non-cutoff' weather systems, synoptic meteorologists have traditionally defined them as systems with and without closed isobaric height contours at 500 mb, 300 mb or thereabouts. The distinction is undoubtedly important in practice, but its significance has never been entirely clear from a theoretical viewpoint since, for example, the addition of a uniform zonal flow which simply advects the whole system can easily change its classification from 'cutoff' to 'non-cutoff' if the criterion is taken literally, whereas the dynamics of the system would not be changed in any essential way.

The concurrent IPV and isobaric height maps shown in Figs. 3, 4, 5, 6, 11 and 12 suggest that the power of this synoptic idea can be accounted for theoretically by the fact that isobaric height maps to some extent provide a view, albeit a smoothed-out view, of the associated IPV distributions. The patterns seen in IPV maps suffer from no ambiguity of the kind just mentioned. In particular, the presence or absence of closed contours in IPV maps is a dynamically significant distinction, independent of incidental circumstances such as the frame of reference adopted.

This suggests that the basic idea underlying the notion of a cutoff could in principle be more precisely defined in terms of IPV distributions. As far as we can see, such a definition would be entirely consistent with the traditional synoptic view of the essential phenomenon, taking other evidence into account such as wind and temperature fields (cf. Fig. 15) together with observational case studies of the time development of the cutting-off process. For instance section 10.1 of Palmén and Newton (1969, p. 274) describes the birth of a large cutoff cyclone from the cold “polar-source region”, with which, at a certain stage of development, “it is still united by an ‘umbilical cord’ in the form of a shear line”. From the information presented it appears that the stage of development referred to is fundamentally similar to that shown in our Fig. 5 for 23 September 1982, even though the orientation, geographical location, and other details are different.

Palmén and Newton describe the polar-source region as ‘tropospheric’ (*loc. cit.*, and top of p. 284). However, it has become increasingly clear, both from examples like that of Fig. 5 and from the theoretical principles reviewed in this paper, that this concept requires modification if one is interested in questions of dynamical cause and effect. For dynamical purposes an important part of the polar-source region is Kleinschmidt’s lower-stratospheric reservoir of high-PV air. At least in cases like that of Fig. 5, the observed development appears to be largely controlled by long-range, quasi-isentropic advection of high-PV air from the lower-stratospheric reservoir. The word ‘controlled’ is used deliberately here, its use being justified by the invertibility principle. Whereas low temperature advection, for instance, may well appear important from a purely diagnostic point of view in, say, the middle troposphere ahead of the moving IPV anomaly, it can be argued that in terms of cause and effect its importance is actually secondary, in such cases, by comparison with that of IPV advection at higher altitudes. This is because much of the coldness of the free atmosphere beneath the IPV anomaly is attributable to the induced temperature field of the anomaly. As such, it *cannot be advected anywhere* unless

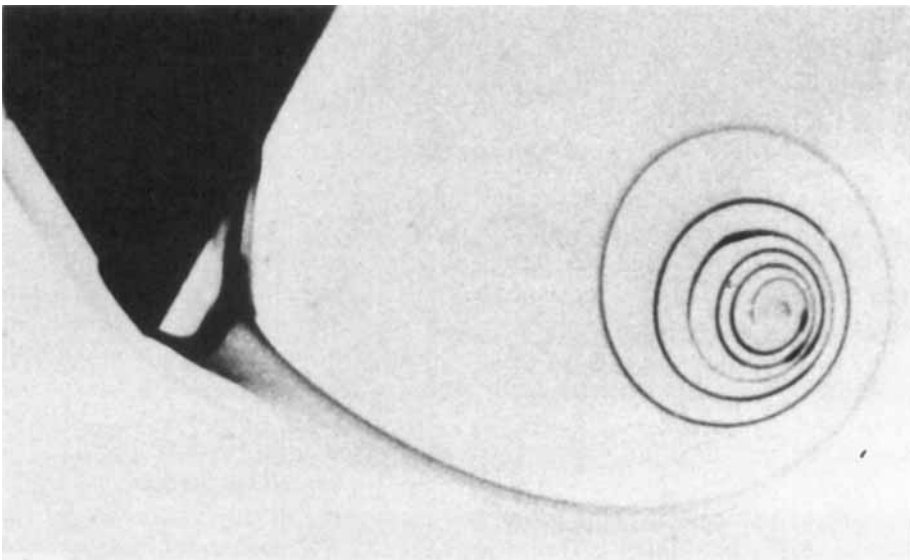


Figure 22. A standard fluid-dynamical experiment showing barotropic vortex rollup visualized by dye injection (Pullin and Perry 1980). A piston, not shown, drives water from left to right with almost constant speed normal to the axis of a wedge of  $30^\circ$  semi-vertex angle; the wedge acts as a source both of dye and of vorticity.

the anomaly is itself moving in the direction concerned. The point made in section 4 about the compensating effects of vertical motion is relevant here. Temperature advection near the ground is, of course, an entirely different matter, a fact which is related to the constraining effect of the earth's surface upon large-scale vertical motion and which has already been illustrated in several ways in section 5.

The phenomenon of cutting off exemplified in Figs. 5 and 11 appears to have counterparts in classical aerodynamics. Figure 22 shows what appears to be an aerodynamical (barotropic) counterpart to the 24 September panel in Fig. 5, as far as the cutoff cyclone and its presumed 'umbilical cord' are concerned. The figure, taken from a paper by Pullin and Perry (1980), represents a laboratory photograph using the dye method of flow visualization; the dye roughly marks high vorticity values (although the vorticity diffuses faster than the dye). The spatial resolution is, of course, far greater than that of Fig. 5, and the 'umbilical cord' shows up clearly. This type of flow is known to be accurately described by the barotropic vorticity equation, with a diffusive term included.

Features common to the aerodynamical and meteorological cases are the existence of a source of cyclonic (potential) vorticity fluid on the left, advection of cyclonic (potential) vorticity fluid from left to right, and a tendency for the furthest part of the (potential) vorticity distribution to *wind itself up* (a concept justifiable in terms of the concept of 'induced velocity field') into a compact, nearly axisymmetric vortex. Aerodynamicists use the term 'vortex rollup' to describe the phenomenon, and it has been extensively studied; see, e.g., p. 590 of the textbook by Batchelor (1967), and for more detail the review by Saffman and Baker (1979). The main difference between the two cases lies in the nature of the source region, which in the laboratory case is the boundary layer on a solid, wedge-shaped obstacle, seen at the left of the photograph, but in the meteorological case is Kleinschmidt's stratospheric reservoir of high-PV air. Also, in the atmospheric case there may well be much less spiral fine-structure in the IPV distribution than Fig. 22 might suggest, because of the different initial conditions. (And even if such structure were initially present—as was suggested in section 2(d) for another case—it would tend to be destroyed by small-scale quasi-barotropic shear instabilities.)

## 9. CONCLUDING REMARKS

Perhaps the central point we have tried to bring out in this paper is the way in which the IPV concept succinctly encapsulates all the balanced dynamics usually described in terms of advection, divergence and vertical motion. IPV thinking gives direct insight, for example, into the circumstances in which the effects of advection and vertical motion tend to cancel each other; recall again the thought-experiment described in section 4. Especially for quasi-conservative processes involving rapid advection of upper air synoptic-scale features (sections 2(c), 6(e)), IPV thinking has considerable potential for furthering our understanding of the behaviour of real weather systems. Moreover, the invertibility principle suggests that the IPV concept should remain useful even in the presence of moist or dry diabatic heating or cooling (sections 6(e), 7), along with other non-conservative effects such as friction and gravity-wave drag. As was pointed out in section 4 the crucial advantage of IPV maps over, say, isobaric absolute vorticity maps, is the conceptual separation they offer between the effects of advection on the one hand, and the effects of vertical motion on the other.

The use of coarse-grain IPV maps together with surface  $\theta$  maps should lead not only

to a clearer recognition of partial analogies with extensively studied aerodynamical phenomena (section 8), but also to a greatly sharpened ability to relate observed phenomena to theoretical concepts generally. In order to make a meaningful comparison between dynamical theory, modelling and observation, it is often necessary to know something about IPV and surface  $\theta$  gradients. For instance, such information may be necessary in order to tell whether or not a given instability mechanism could be operating, or could be about to operate, in a given synoptic situation (section 6).

The use of IPV maps could prove valuable as an aid to the quality control of numerical weather analysis and prediction, especially if appropriate image-processing and animated-graphics techniques were brought to bear. IPV maps might also be valuable in the development and assessment of numerical forecasting models, for example in problems like the embedding of fine-mesh regional models within larger-scale models. Fundamental to the success of such embedding is a sufficiently good representation, whether implicit or explicit, of the inflow of IPV features across the boundaries. This may be quite crucial, for instance, to predicting certain cases of explosive cyclogenesis (section 6(e)).

Similarly, it can be argued that the effectiveness of parametrization schemes for the physical processes governing diabatic and frictional changes in an atmospheric model (where 'frictional' refers to any sub-grid-scale momentum transfer process) should be judged, for dynamical purposes, largely by whether or not those schemes deliver the correct diabatic and frictional rates of change of IPV distributions when their output is substituted into the right-hand sides of Eqs. (70a)ff. To the extent that the invertibility principle holds, it tells us that the *only* dynamically relevant output of the 'physics package' used in the model is the net effect on the IPV distributions and on the low-level  $\theta$  distribution, assuming of course that the package does not generate spurious gravity modes. The letter 'P' is important here, as elsewhere: a consideration of the accuracy of the rates of change of PV following an air parcel is not enough for this purpose, since IPV distributions can be greatly affected, also, by diabatic motion across isentropic surfaces when vertical PV gradients are strong, as has often been pointed out. This latter effect is allowed for by Eqs. (74a, b), whose right-hand sides remind us of the importance of having estimates of moist-convective and other contributions to diabatic heating with the correct vertical as well as horizontal distribution.

Another major area in which IPV maps could prove useful is that of research into tropical, extra-tropical interactions, in which a fundamental problem is to quantify the long-range interconnections between dynamical regimes having very different scaling characteristics. There are many aspects to be considered, of which the presence of subtropical upper air cutoff cyclones, such as that illustrated in Fig. 10, is merely one indication.

The 350 K IPV map shown in Fig. 2(a) and those for subsequent days (not shown) give numerous indications of low-PV air being injected into middle and high latitudes and high-PV air moving into subtropical and tropical latitudes. This is exactly what happens in the stratospheric 'breaking Rossby waves' referred to in section 6(d). As was also noted there, very similar phenomena occur in model simulations of nonlinear baroclinic-wave life cycles. The similarity of the trailing troughs or shear lines seen in Fig. 20(b) to that in the bottom left-hand quadrant of Fig. 2(a) is striking, as is the similarity of both patterns to those seen in the winter stratosphere; see also, e.g., Fig. 2 of Elliott (1956), Figs. 2, 5c of Holopainen and Rontu (1981), and Fig. 10.4a of Palmén and Newton (1969). One point of interest is that the characteristic spatio-temporal structure of the phenomenon, when viewed as a dynamical whole, makes it a likely candidate for helping to explain the interesting lagged correlation patterns between

tropical cloudiness (cf. section 4) and mid-latitude 500 mb height field variability, recently discovered by Liebmann and Hartmann (1984).

The presence of features like  $D''$  in Fig. 2(a) suggests that some of the high-PV air in the trailing trough may wind itself up into compact vortices in the manner suggested by the aerodynamical analogy discussed in section 8. It seems very likely that this is how subtropical cutoff cyclones of the kind illustrated in Fig. 10 are formed. The same thing appears to take place on a larger scale in the middle stratosphere (Clough *et al.* 1985; McIntyre and Palmer 1984), as well as in some of the other cases mentioned. The idea seems generally consistent with synoptic as well as aerodynamical experience and it would be of interest to repeat the numerical experiment of Fig. 20 at higher resolution, and to carry out other, related simulations, to see whether such behaviour is reproduced there as well.

Upper air trailing troughs and associated phenomena are unlikely to be the only significant features in tropical IPV distributions. For instance important IPV anomalies may be expected to be generated by large-scale diabatic heating. These will be subject to the integral constraint (70b).

The induced fields of any large-scale IPV anomaly, whatever its origin, may extend into, and thus affect, middle latitudes. As a result, the tropics may appear variously as a source, an absorber, or a reflector of mid-latitude planetary-scale disturbances. Thus, for example, the Rossby wave breaking phenomenon exemplified in Figs. 2(a) and 20(b) may represent a *two-way* interaction between middle latitudes and the tropics, not only injecting disturbances into the tropics, but also changing from day to day the extent to which the tropics appears to middle latitudes as an absorber or reflector of mid-latitude planetary-wave activity. The absorbing or reflecting characteristics of the tropics depend on the phase relations between mid-latitude and tropical IPV patterns in essentially the same manner as indicated by the discussion in section 6(c) and Fig. 19. This particular two-way interaction has been studied quantitatively, in idealized form, in the theory of 'nonlinear critical layers' referred to in section 6(d). Tests of the relevance of such theoretical ideas, and of many other ideas about the dynamics of tropical, extra-tropical interactions, will ultimately rest on knowing enough, implicitly or explicitly, about real IPV distributions.

Within the tropics one has the alternative possibility of using upper air vorticity diagnoses (e.g. Sardeshmukh and Hoskins 1985, and refs.), which will be locally equivalent to IPV diagnoses if the disturbances are sufficiently deep (in comparison with the appropriate Rossby height, Eq. (33b)), and if static stability values are sufficiently near constant. It is in describing dynamical interactions between regimes on either side of the subtropical jet, with its very steep static stability change, that IPV diagnostics seem likely to have a clear advantage.

The presence of negative PV regions in Fig. 2(a), if they are real, is suggestive of dynamically significant cross-equatorial advective processes. It should be noted in this connection that if an IPV anomaly in the form of an isolated vortex having a near-circular planform were to cross the equator into the opposite hemisphere, then the vortex would still be a stable entity except perhaps to a small extent on its periphery, depending on the ambient values of the potential vorticity  $P$  and hence of the product  $f_{loc}P$  in the inequality (30). It is not true, as is sometimes assumed, that the whole vortex would become inertially unstable since, as (21) and (30) remind us, it is the sign of  $f_{loc}$  and not that of  $f$  which is dynamically relevant in relation to the sign of the PV itself.

Many other applications of the IPV concept suggest themselves. Indeed the invertibility principle implies that there are potentially as many significant applications of IPV thinking as there are balanced dynamical processes of meteorological interest, whether

linear or nonlinear, large or small scale. For instance the partial analogy with two-dimensional, barotropic aerodynamics immediately explains why we should expect to see Kármán vortex streets in the lee of mountainous islands, in the presence of stable stratification (e.g. Bugaev 1973; Thompson *et al.* 1977, and refs.), and also suggests ways of making the vortex-street concept quantitative, should this be desired, even though neither quasi-geostrophic theory nor any of its refinements, nor classical aerodynamics itself, is applicable. However, the most exciting prospects at present seem to lie in the study of synoptic and larger scales, where a significant amount of information is already available from operational analyses and forecasts, as has been illustrated here. In the present state of the art not all the features appearing in operationally-based IPV maps can be considered meaningful, of course, but it seems reasonable to hope for progressive improvement, especially if isentropic analysis methods are developed to their full potential. One incentive to progress is the fact that the quality of the best available operational IPV maps can be regarded as a sensitive measure of the quality of the analysis-forecast process itself.

In the past, practical application of the IPV concept to atmospheric data has always been rendered problematical by deficiencies in the data and by the volume of computation required. But now, in virtue of the quality already being attained in operational data analyses, and the availability of adequate computing power, coarse-grain IPV maps are beginning to look more and more like an extremely useful addition to the armoury of those interested in understanding and forecasting the behaviour of the atmosphere.

#### ACKNOWLEDGMENTS

We are grateful to the following people for their comments and assistance in the preparation of this manuscript: D. G. Andrews, R. Bleck, K. A. Browning, D. M. Burridge, M. J. P. Cullen, E. F. Danielsen, K. A. Emanuel, M. E. Farley, A. Gilchrist, J. S. A. Green, I. M. Held, A. Hollingsworth, E. O. Holopainen, M. N. Juckes, M. Kanamitsu, D. Keyser, M. Kimoto, G. A. Monk, Ts. Nitta, W. A. Norton, A. O'Neill, T. N. Palmer, R. Pierrehumbert, R. J. Reed, P. D. Sardeshmukh, M. R. Schoeberl, T. G. Shepherd, M. A. Shapiro, G. J. Shutts, A. J. Thorpe, A. F. Tuck, J. M. Wallace, L. W. Uccellini and M. V. Young. We thank especially M. A. Shapiro for supplying Fig. 9(b), A. J. Thorpe for supplying Figs. 15 and 16 and for drawing our attention to Eq. (70b), and R. Pierrehumbert for showing us a computation of IPV distributions for the fast-growing Charney mode referred to in section 6(b).

#### APPENDIX

##### *The computation of vertical motion*

Various forms of the adiabatic, frictionless omega equation are available in the literature. We first derive a new form of the equation which is consistent with the IPV approach, beginning with the frictionless, adiabatic case.

As implied by (42), (43) and (44), the quasi-geostrophic potential vorticity  $q$  may be written as

$$q = f + \nabla_h^2 \psi' + f_0^2 \frac{\partial}{\partial p} (\mathcal{N}^{-2} \partial \psi' / \partial p). \quad (\text{A.1})$$

Taking  $f_0^2 \partial^2 / \partial p \partial t$  of this equation and using the hydrostatic equation (41) and the definition of  $\mathcal{N}^2$  (45) yields

$$f_0 \frac{\partial^2 q}{\partial p \partial t} = -R \nabla_h^2 \frac{\partial \theta'}{\partial t} - f_0^2 \frac{\partial^2}{\partial p^2} \left( \frac{\partial \theta' / \partial t}{-d\theta_{\text{ref}}/dp} \right), \quad (\text{A.2})$$

where  $R = R(p)$  is defined in (20). Following Andrews and McIntyre (1976) we define a 'residual' vertical velocity

$$\tilde{\omega} = \omega + (\mathbf{v} \cdot \nabla_p \theta') / (d\theta_{\text{ref}}/dp) \simeq \omega + \nabla_p \cdot (\mathbf{v} \theta') / (d\theta_{\text{ref}}/dp). \quad (\text{A.3})$$

From the adiabatic thermodynamic equation, (A.3) may be rewritten

$$\tilde{\omega} = -(\partial \theta' / \partial t) / (d\theta_{\text{ref}}/dp). \quad (\text{A.4})$$

Using (A.4) to substitute for  $\partial \theta' / \partial t$  in (A.2) gives

$$f_0 \frac{\partial}{\partial p} \frac{\partial q}{\partial t} = -\mathcal{L}'(\tilde{\omega}), \quad (\text{A.5})$$

where the linear operator  $\mathcal{L}'$  is defined as

$$\mathcal{L}'(\omega) = N^2 \nabla_h^2 \omega + f_0^2 \partial^2 \omega / \partial p^2. \quad (\text{A.6})$$

The conservation of  $q$  moving with the geostrophic velocity enables the left-hand side of (A.5) to be written in terms of the advection of  $q$  and so the equation becomes

$$\mathcal{L}'(\tilde{\omega}) = f_0 \partial(\mathbf{v} \cdot \nabla_p q) / \partial p, \quad (\text{A.7})$$

which is of the form (49). After some manipulation it can be verified that substitution of (A.3) into (A.7) yields the usual omega equation.

(A.3) and (A.7) imply that the total vertical velocity may be written as the sum of three contributions:

$$\omega = \omega_{\text{PVA}} + \omega_{\text{BTA}} + \omega_{\text{IU}} \quad (\text{A.8})$$

where  $\omega_{\text{PVA}}$  (potential vorticity advection) is the solution of

$$\mathcal{L}'(\omega) = f_0 \partial(\mathbf{v} \cdot \nabla_p q) / \partial p \quad \text{with} \quad \omega = 0 \quad \text{on} \quad p = 0, p_0; \quad (\text{A.9})$$

$\omega_{\text{BTA}}$  (boundary temperature advection) is the solution of

$$\mathcal{L}'(\omega) = 0 \quad \text{with} \quad \omega = (\mathbf{v} \cdot \nabla_p \theta') / (d\theta_{\text{ref}}/dp) \quad \text{on} \quad p = 0, p_0; \quad (\text{A.10})$$

$\omega_{\text{IU}}$  (isentropic upgliding) is the vertical velocity given by

$$\omega = -(\mathbf{v} \cdot \nabla_p \theta') / (d\theta_{\text{ref}}/dp) \quad (\text{A.11})$$

cf. (A.3). Here the sum of  $\omega_{\text{PVA}}$  and  $\omega_{\text{BTA}}$  is equal to  $\tilde{\omega}$ , satisfying (A.7) with the boundary condition implied by (A.3).

If the boundary temperature distribution is incorporated into the interior PV distribution according to (47), then  $\omega_{\text{BTA}}$  is absorbed into  $\omega_{\text{PVA}}$ . It should be noted that in real situations there can be cancellation between  $\omega_{\text{PVA}}$ ,  $\omega_{\text{BTA}}$  and  $\omega_{\text{IU}}$ , and that this cancellation is reference-frame dependent. Of course, in a frame moving with a steady system, the situation first considered in section 4,  $\omega_{\text{PVA}}$  and  $\omega_{\text{BTA}}$  are zero and  $\omega_{\text{IU}}$  accounts for the entire vertical motion. The more general form derived here may be useful in suggesting qualitative corrections to simple isentropic relative flow analyses of vertical motion in systems which are changing with time.

For comparison we now note two other forms of the adiabatic, frictionless omega equation. In either case the boundary conditions  $\omega = 0$  at  $p = 0, p_0$  may be applied. The traditional form of the omega equation may be written

$$\mathcal{L}'(\omega) = f_0 \frac{\partial}{\partial p} \{ \mathbf{v} \cdot \nabla_p [f + \mathbf{k} \cdot (\nabla_p \times \mathbf{v})] \} + R \nabla^2 (\mathbf{v} \cdot \nabla_p \theta'). \quad (\text{A.12})$$

The two terms on the right-hand side are the vorticity advection and thermal advection terms, respectively. Following Hoskins *et al.* (1978) and Hoskins (1982), another form of the equation may be written

$$\mathcal{L}'(\omega) = 2\nabla_p \cdot \mathbf{Q} + \beta f_0 \partial v / \partial p, \quad (\text{A.13})$$

where the quasi-horizontal vector

$$\mathbf{Q} = - |R\nabla_p \theta'| \mathbf{k} \times \partial \mathbf{v} / \partial s \quad (\text{A.14})$$

and  $s$  is a quasi-eastward horizontal coordinate in the direction of the  $\theta'$  contour. It may be verified, again after some manipulation, that (A.12) and (A.13) are both mathematically equivalent to (A.8)–(A.11).

As discussed in Hoskins *et al.* (1978), the main reservation about the traditional vorticity-advection, thermal-advection form, (A.12), is the cancellation between the two forcing terms, the extent of which cancellation is frame dependent. The  $\mathbf{Q}$  vector form (A.13), after some practice at determining the forcing using (A.14), allows some insight into the vertical velocity field given by quasi-geostrophic theory. The new form (A.8)–(A.11) is attractive in providing corrections to the simple isentropic upgliding associated with IPV and boundary  $\theta$  advection relative to the system of interest and for linking the discussion with that of section 4. The sum (A.8) may on the other hand be too complicated for the simple diagnosis of other real situations.

In the presence of a frictional force-curl  $\mathbf{K}$ , an Ekman boundary layer of height-scale  $\delta$ , a diabatic potential temperature source  $\dot{\theta}$ , and topography of height  $h$ ,  $\omega$  has four additional contributions

$$\omega_{\text{FRIC}} : \mathcal{L}'(\omega) = -f_0 \partial(\mathbf{k} \cdot \mathbf{K}) / \partial p \text{ with } \omega = 0 \text{ on } p = p_0, 0; \quad (\text{A.15})$$

$$\omega_{\text{EKM}} : \mathcal{L}'(\omega) = 0 \text{ with } \omega = -\frac{1}{2} \rho g \delta \xi \text{ on } p = p_0 \text{ and } \omega = 0 \text{ on } p = 0; \quad (\text{A.16})$$

$$\omega_{\text{DIAB}} : \mathcal{L}'(\omega) = -R\nabla_h^2 \dot{\theta} \text{ with } \omega = 0 \text{ on } p = p_0, 0; \quad (\text{A.17})$$

$$\omega_{\text{TOPOG}} : \mathcal{L}'(\omega) = 0 \text{ with } \omega = -\rho_{\text{ref}} g \mathbf{v} \cdot \nabla_p h \text{ on } p = p_0 \text{ and } \omega = 0 \text{ on } p = 0. \quad (\text{A.18})$$

## REFERENCES

- |   |       |   |
|---|-------|---|
| Al-Ajmi, D. N., Harwood, R. S. and Miles, T.              | 1985  | A sudden warming in the middle atmosphere of the southern hemisphere. <i>Quart. J. R. Met. Soc.</i> , <b>111</b> , 359–389  |
| Andrews, D. G. and McIntyre, M. E.                        | 1976  | Planetary waves in horizontal and vertical shear: the generalized Eliassen–Palm relation and the mean zonal acceleration. <i>J. Atmos. Sci.</i> , <b>33</b> , 2031–2048                     |
|   | 1978  | An exact theory of nonlinear waves on a Lagrangian-mean flow. <i>J. Fluid Mech.</i> , <b>89</b> , 609–646   |
| Batchelor, G. K.  | 1967  | <i>An introduction to fluid dynamics</i> , C.U.P.   |
| Bengtsson, L., Kanamitsu, M., Källberg, P. and Uppala, S. | 1982  | FGGE research activities at ECMWF. <i>Bull. Amer. Meteor. Soc.</i> , <b>63</b> , 277–303  |
| Berggren, R., Bolin, B. and Rossby, C.-G.                 | 1949  | An aerological study of zonal motion, its perturbations and break-down. <i>Tellus</i> , <b>1</b> , 14–37  |
| Bjerknes, J.  | 1937  | Die Theorie der aussertropischen Zyklonenbildung. <i>Meteor. Zeitschr.</i> , <b>54</b> , 460–466  |
| Bjerknes, V.  | 1898a | Über die Bildung von Circulationsbewegung und Wirbeln in reibungslosen Flüssigkeiten. <i>Videnskabselskapets Skrifter. I Math. Naturv. Klasse</i> , No. 5                                   |
|   | 1898b | Über einen hydrodynamischen Fundamentalsatz und seine Anwendung besonders auf die Mechanik der Atmosphäre und des Weltmeeres. <i>Kgl. Svenska Vetenskapskad. Handl.</i> , <b>31</b> , No. 4 |
|   | 1901  | Zirkulation relativ zu der Erde. <i>Oevers. Fin. Vetensk.-Soc. Foerh.</i> , 739–775   |
|   | 1902  | Zirkulation relativ zu der Erde. <i>Met. Z.</i> , <b>19</b> , 97–108  |

- Bleck, R. 1973 Numerical forecasting experiments based on the conservation of potential vorticity on isentropic surfaces. *J. Appl. Meteor.*, **12**, 737-752
- 1974 Short range prediction in isentropic coordinates with filtered and unfiltered numerical models. *Mon. Wea. Rev.*, **102**, 813-829
- 1984 An isentropic coordinate model suitable for lee cyclogenesis simulation. *Rivista Meteor. Aeronaut.*, **43**, 189-194
- Bleck, R. and Mattocks, C. 1984 A preliminary analysis of the role of potential vorticity in Alpine lee cyclogenesis. *Beitr. Phys. Atmos.*, **57**, 357-368
- Blumen, W. 1968 On the stability of quasi-geostrophic flow. *J. Atmos. Sci.*, **25**, 929-931
- 1980 A comparison between the Hoskins-Bretherton model of frontogenesis and the analysis of an intense surface frontal zone. *ibid.*, **37**, 64-77
- 1981 The geostrophic coordinate transformation. *ibid.*, **38**, 1100-1105
- Bosart, L. F. 1981 The President's Day snowstorm of 18-19 February 1979: a subsynoptic-scale event. *Mon. Wea. Rev.*, **109**, 1542-1566
- Bretherton, F. P. 1966a Critical layer instability in baroclinic flows. *Quart. J. R. Met. Soc.*, **92**, 325-334
- 1966b Baroclinic instability and the short wavelength cutoff in terms of potential vorticity. *ibid.*, **92**, 335-345
- Bugaev, V. A. 1973 Dynamical climatology in the light of satellite information. *Bull. Amer. Meteor. Soc.*, **54**, 394-418
- Charney, J. G. and Phillips, N. A. 1953 Numerical integration of the quasi-geostrophic equations for barotropic and simple baroclinic flows. *J. Met.*, **10**, 71-99
- Charney, J. G. and Drazin, P. G. 1961 Propagation of planetary scale disturbances from the lower into the upper atmosphere. *J. Geophys. Res.*, **66**, 83-109
- Charney, J. G. and Stern, M. E. 1962 On the stability of internal baroclinic jets in a rotating atmosphere. *J. Atmos. Sci.*, **19**, 159-172 (Corrigendum in McIntyre, 1972)
- Charney, J. G. and Flierl, G. R. 1981 In *Evolution of physical oceanography* (B. A. Warren and C. Wunsch, eds.), M.I.T. Press, pp. 504-548
- Clough, S. A., Grahame, N. S. and O'Neill, A. 1985 Potential vorticity in the stratosphere derived using data from satellites. *Quart. J. R. Met. Soc.*, **111**, 335-358
- Cullen, M. J. P. and Purser, R. J. 1984 An extended Lagrangian theory of semi-geostrophic frontogenesis. *J. Atmos. Sci.*, **41**, 1477-1497
- Daley, R. 1981 Normal mode initialization. *Rev. Geophys. Space Physics*, **19**, 450-468
- Danielsen, E. F. 1959 The laminar structure of the atmosphere and its relation to the concept of a tropopause. *Arch. Met. Geophys. Bioklim.*, **A 11**, 293-332
- 1967 'Transport and diffusion of stratospheric radioactivity based on synoptic hemispheric analyses of potential vorticity'. Dept. of Met. Penn. State Univ., Report NYO-3317-3
- 1968 Stratospheric-tropospheric exchange based on radioactivity, ozone and potential vorticity. *J. Atmos. Sci.*, **25**, 502-518
- Danielsen, E. F. and Diercks, J. W. 1967 'A study of the tropopause based on numerical integration of the potential vorticity equation'. Final Report, Part I, Contract AT(30-1)-3317. U.S. Atomic Energy Commission
- Danielsen, E. F., Bleck, R., Shedlovsky, J., Wartburg, A., Haagenson, P. and Pollock, W. 1970 Observed distribution of radioactivity, ozone, and potential vorticity associated with tropopause folding. *J. Geophys. Res.*, **75**, 2353-2361
- Davies, H. C. 1981 An interpretation of sudden warmings in terms of potential vorticity. *J. Atmos. Sci.*, **38**, 427-445
- Deem, G. S. and Zabusky, N. J. 1978 Stationary V-states: interactions, recurrence and breaking. *Phys. Rev. Lett.*, **40**, 859-862
- Dritschel, D. G. 1985 The nonlinear evolution of rotating configurations of uniform vorticity. *J. Fluid Mech.*, to appear
- Dunkerton, T. J., Hsu, C.-P. F. and McIntyre, M. E. 1981 Some Eulerian and Lagrangian diagnostics for a model stratospheric warming. *J. Atmos. Sci.*, **38**, 819-843
- Edmon, H. J., Hoskins, B. J. and McIntyre, M. E. 1980 Eliassen-Palm cross-sections for the troposphere. *ibid.*, **37**, 2600-2616 (see also corrigendum, **38**, 1115, especially second last item)

- Eliassen, A. 1948 The quasi-static equations of motion. *Geofys. Publ.*, **17**, No. 3
- 1982 Vilhelm Bjerknes and his students. *Ann. Rev. Fluid Mech.*, **14**, 1–11
- 1983 The Charney–Stern theorem on barotropic–baroclinic instability. *Pure Appl. Geophys.*, **121**, 563–572
- 1984 Geostrophy. *Quart. J. R. Met. Soc.*, **110**, 1–12
- Eliassen, A. and Kleinschmidt, E. 1957 ‘Dynamic Meteorology’, in *Handbuch der Physik*, Vol. 48, 1–154, Springer-Verlag
- Eliassen, A. and Raustein, E. 1968 A numerical integration experiment with a model atmosphere based on isentropic surfaces. *Met. Ann.*, **5**, 45–63
- 1970 A numerical integration experiment with a six-level atmospheric model with isentropic information surfaces. *ibid.*, **5**, 429–449
- Elliott, R. D. 1956 Low latitude vorticity injections and the development of large scale anomalous circulation patterns. *Bull. Amer. Met. Soc.*, **37**, 270–275
- Erickson, C. O. 1971 Diagnostic study of a tropical disturbance. *Mon. Wea. Rev.*, **99**, 67–78
- Ertel, H. 1942 Ein Neuer hydrodynamischer Wirbelsatz. *Met. Z.*, **59**, 271–281
- Farrell, B. F. 1982 The initial growth of disturbances in a baroclinic flow. *J. Atmos. Sci.*, **39**, 1663–1686
- Gent, P. R. and McWilliams, J. C. 1984 Balanced models in isentropic coordinates and the shallow water equations. *Tellus*, **36A**, 166–171
- Gill, A. E. 1965 Instabilities of ‘top-hat’ jets and wakes in compressible fluids. *Phys. Fluids*, **8**, 1428–1430
- 1981 Homogeneous intrusions in a rotating stratified fluid. *J. Fluid Mech.*, **103**, 275–295
- 1982 *Atmosphere–ocean dynamics*. Academic Press
- Golding, B. 1984 A study of the structure of mid-latitude depressions in a numerical model using trajectory techniques. I: Development of ideal baroclinic waves in dry and moist atmospheres. *Quart. J. R. Met. Soc.*, **110**, 847–879
- Goldstein, S. 1938 (Editor) *Modern developments in fluid mechanics*, Vols. 1 and 2, Oxford University Press (reprinted New York, Dover, 1965)
- Green, J. S. A. 1977 The weather during July 1976: some dynamical considerations of the drought. *Weather*, **32**, 120–128
- Gyakum, J. R. 1983 On the evolution of the QE II storm: Parts I and II. *Mon. Wea. Rev.*, **111**, 1137–1155 and 1156–1173
- Haynes, P. H. 1985 Nonlinear instability of a Rossby-wave critical layer. *J. Fluid Mech.*, **161**, 493–511
- Hide, R. and Mason, P. J. 1975 Sloping convection in a rotating fluid. *Adv. Phys.*, **24**, 47–100
- Holland, W. R., Keffer, T. and Rhines, P. B. 1984 Dynamics of the oceanic general circulation: the potential vorticity field. *Nature*, **308**, 698–705
- Holopainen, E. O. and Rontu, L. 1981 On shear lines in the upper troposphere over Europe. *Tellus*, **33**, 351–359
- Holton, J. R. 1975 *The dynamic meteorology of the stratosphere and mesosphere*. Am. Met. Soc., Boston (Met. Monogr. 15)
- Hoskins, B. J. 1974 The role of potential vorticity in symmetric stability and instability. *Quart. J. R. Met. Soc.*, **100**, 480–482
- 1975 The geostrophic momentum approximation and the semi-geostrophic equations. *J. Atmos. Sci.*, **32**, 233–242
- 1982 The mathematical theory of frontogenesis. *Ann. Rev. Fluid Mech.*, **14**, 131–151
- 1983 ‘Modelling of the transient eddies and their feedback on the mean flow’, in ‘Large-scale dynamical processes in the atmosphere’ (B. J. Hoskins and R. P. Pearce, eds.), Academic Press, 169–199
- Hoskins, B. J. and Bretherton, F. P. 1972 Atmospheric frontogenesis models: mathematical formulation and solution. *J. Atmos. Sci.*, **29**, 11–37
- Hoskins, B. J. and Draghici, I. 1977 The forcing of ageostrophic motion according to the semi-geostrophic equations and in an isentropic coordinate model. *ibid.*, **34**, 1859–1867
- Hoskins, B. J., Draghici, I. and Davies, H. C. 1978: A new look at the  $\omega$ -equation. *Quart. J. R. Met. Soc.*, **104**, 31–38

- Hoskins, B. J. and West, N. V. 1979 Baroclinic waves and frontogenesis. Part II: Uniform potential vorticity jet flows—cold and warm fronts. *J. Atmos. Sci.*, **36**, 1663–1680
- Hoskins, B. J., James, I. N. and White, G. H. 1983 The shape, propagation and mean-flow interaction of large-scale weather systems. *ibid.*, **40**, 1595–1612
- Hoskins, B. J. and McIntyre, M. E. 1985 On the role of nonlinear radiation, wave propagation and wave breaking in the life cycles of nonlinear baroclinic instabilities. To be published; preprints available from DAMTP, Cambridge
- Hsu, C.-P. F. 1980 Air parcel motions during a numerically simulated sudden stratospheric warming. *ibid.*, **37**, 2768–2792
- Illari, L. 1984 A diagnostic study of the potential vorticity in a warm blocking anticyclone. *ibid.*, **41**, 3518–3526
- Illari, L. and Marshall, J. 1983 On the interpretation of eddy fluxes during a blocking episode. *ibid.*, **40**, 2232–2242
- Kanzawa, H. 1984 'Four observed sudden warmings diagnosed by the Eliassen-Palm flux and refractive index', in *'Dynamics of the Middle Atmosphere'* (eds J. R. Holton and T. Matsuno), Dordrecht, Reidel; Tokyo, Terra Scientific Publishing Co., pp 307–331
- Kato, S. 1966 Diurnal atmospheric oscillation. 1: Eigenvalues and Hough functions. *J. Geophys. Res.*, **71**, 3201–3209
- Kelley, W. E. and Mock, D. R. 1982 A diagnostic study of upper tropospheric cold lows over the western North Pacific. *Mon. Wea. Rev.*, **110**, 471–480
- Kennelly, M. A., Evans, R. H. and Joyce, T. M. 1985 Small-scale cyclones on the periphery of a Gulf Stream warm-core ring. *J. Geophys. Res.*, **90**, 8845–8857
- Keyser, D. and Shapiro, M. A. 1985 A review of the structure and dynamics of upper-level frontal zones. *Mon. Wea. Rev.*, (to appear)
- Killworth, P. D. and McIntyre, M. E. 1985 Do Rossby-wave critical layers absorb, reflect, or over-reflect? *J. Fluid Mech.*, **161**, 449–491
- Kleinschmidt, E., 1950a Über Aufbau und Entstehung von Zyklonen (1. Teil) *Met. Runds.*, **3**, 1–6
- 1950b Über Aufbau und Entstehung von Zyklonen (2. Teil) *Met. Runds.*, **3**, 54–61
- 1951 Über Aufbau und Entstehung von Zyklonen (3. Teil) *Met. Runds.*, **4**, 89–96
- 1955 Die Entstehung einer Höhenzyklone über Nordamerika, *Tellus*, **7**, 96–110
- 1957 In 'Dynamic meteorology' by Eliassen, A. and Kleinschmidt, E., *Handbuch der Physik*, **48**, 112–129
- Krishnamurti, T. N. 1975 'Lectures in tropical meteorology'. Florida State Univ., Report No. 75–8
- Leith, C. E. 1980 Nonlinear normal mode initialization and quasi-geostrophic theory. *J. Atmos. Sci.*, **37**, 958–968
- Leovy, C. B., Sun, C.-R., Hitchman, M. H., Remsberg, E. E., Russell, J. M., Gordley, L. L., Gille, J. C. and Lyjak, L. V. 1985 Transport of ozone in the middle stratosphere: evidence for planetary wave breaking. *ibid.*, **42**, 230–244
- Ley, B. E. and Peltier, W. R. 1978 Wave generation and frontal collapse. *ibid.*, **35**, 3–17 (also **35**, 2379–2380)
- Liebmann, B. and Hartmann, D. L. 1984 An observational study of tropical–midlatitude interaction on intraseasonal time scales during winter. *ibid.*, **41**, 3333–3350
- Lighthill, M. J. 1963 'Boundary-layer theory', in *Laminar boundary layers* (L. Rosenhead, ed.) Oxford University Press (see pp. 55, 93)
- Lindzen, R. S. 1966 On the theory of the diurnal tide. *Mon. Wea. Rev.*, **94**, 295–301
- Lindzen, R. S. and Schoeberl, M. R. 1982 A note on the limits of Rossby wave amplitudes. *J. Atmos. Sci.*, **39**, 1171–1174
- McDowell, S., Rhines, P. and Keffer, T. 1982 North Atlantic potential vorticity and its relation to the general circulation. *J. Phys. Ocean.*, **12**, 1417–1436
- McIntyre, M. E. 1970 On the nonseparable baroclinic parallel-flow instability problem. *J. Fluid Mech.*, **40**, 273–306
- 1972 Baroclinic instability of an idealized model of the polar night jet. *Quart. J. R. Met. Soc.*, **98**, 165–174
- 1980 Towards a Lagrangian-mean description of stratospheric circulations and chemical transports. *Phil. Trans. R. Soc.*, **A296**, 129–148

- 1982 How well do we understand the dynamics of stratospheric warmings? *J. Met. Soc. Japan*, **60**, 37–65
- McIntyre, M. E. and Weissman, M. A. 1978 On radiating instabilities and resonant overreflection. *J. Atmos. Sci.*, **35**, 1190–1196
- McIntyre, M. E. and Palmer, T. N. 1983 Breaking planetary waves in the stratosphere. *Nature*, **305**, 593–600
- 1984 The 'surf zone' in the stratosphere. *J. Atm. Terr. Phys.*, **46**, 825–849
- Mahlman, J. D. 1965 Relation of stratospheric-tropospheric mass exchange mechanisms to surface radioactivity peaks. *Arch. Met. Geophys. Bioklim.*, **A15:1**, 1–25
- 1979 Structure and interpretation of blocking anticyclones as simulated in a GFDL general circulation model. In 'Proceedings of the Thirteenth Stanstead Seminar' (T. Warn, ed.) McGill Univ., *Publ. in Met.*, **123**, 70–76
- Matsuno, T. 1970 Vertical propagation of stationary planetary waves in the winter northern hemisphere. *J. Atmos. Sci.*, **27**, 871–883
- Miles, J. 1964 Baroclinic instability of the zonal wind. *Revs. Geophys.*, **2**, 155–176
- Miles, T. and Chapman, W. A. 1984 Intercomparison of planetary-scale diagnostics derived from separate satellite and radiosonde time-mean temperature fields. *Quart. J. R. Met. Soc.*, **110**, 1003–1021
- Namias, J. 1940 *An introduction to the study of air-mass and isentropic analysis*, 5th Edition. Boston, Amer. Met. Soc. (see pp. 136–161)
- 1983 The history of polar front and air mass concepts in the United States—an eyewitness account. *Bull. Amer. Met. Soc.*, **64**, 734–755
- Obukhov, A. M. 1964 Adiabatic invariants of atmospheric processes. *Meteorologiya i gidrologiya*, **2**, 3–9
- 1984 'On potential vorticity'. In *N. E. Kochin and the development of mechanics*, (in Russian). (A. Yu. Ishlinskii, editor). Moscow, Nauka, pp. 84–93
- Ogura, Y. and Portis, D. 1982 Structure of the cold front observed in SESAME-AVE III and its comparison with the Hoskins–Bretherton frontogenesis model. *J. Atmos. Sci.*, **39**, 2773–2792
- Orr, W. M'F. 1907 The stability or instability of the steady motions of a perfect liquid and of a viscous liquid. Parts I and II. *Proc. Roy. Irish Acad.*, **A27**, 9–68 and 69–138
- Palmén, E. and Newton, C. 1948 A study of the mean wind and temperature distribution in the vicinity of the polar front in winter. *J. Met.*, **5**, 220–226
- 1969 *Atmospheric circulation systems*. Academic Press
- Pedgley, D. E. 1962 *A course in elementary meteorology*. H.M.S.O. London
- Pedlosky, J. 1964 The stability of currents in the atmosphere and the oceans. Part 1. *J. Atmos. Sci.*, **21**, 201–219
- Peltonen, T. 1963 A case study of an intense upper cyclone over eastern and northern Europe in November 1959. *Geophysica (Helsinki)*, **8**, 225–251
- Petterssen, S. and Smebye, S. J. 1971 On the development of extratropical cyclones. *Quart. J. R. Met. Soc.*, **97**, 457–482
- Platzman, G. 1949 The motion of barotropic disturbances in the upper troposphere. *Tellus*, **1(3)**, 53–64
- Prandtl, L. and Tietjens, O. G. 1931 *Hydro- und Aeromechanik*, Vol. 2. Springer-Verlag, Berlin
- Pullin, D. I. and Perry, A. E. 1980 Some flow visualization experiments on the starting vortex. *J. Fluid Mech.*, **97**, 239–256
- Randel, W. J. and Stanford, J. L. 1985 An observational study of medium-scale wave dynamics in the southern hemisphere summer. Part I: Wave structure and energetics. *J. Atmos. Sci.*, **42**, 1172–1188
- Reed, R. J. 1955 A study of a characteristic type of upper-level frontogenesis. *J. Met.*, **12**, 226–237
- Reed, R. J. and Sanders, F. 1953 An investigation of the development of a mid-tropospheric frontal zone and its associated vorticity field. *ibid.*, **10**, 338–349
- Reed, R. J. and Danielsen, E. F. 1959 Fronts in the vicinity of the tropopause. *Arch. Met. Geophys. Biokl.*, **A11**, 1–17
- Reiter, E. R. and Mahlman, J. D. 1965 Heavy radioactive fallout over the southern United States, November 1962. *J. Geophys. Res.*, **70**, 4501–4520

- Rhines, P. B. 1970 Edge-, bottom-, and Rossby waves in a rotating, stratified fluid. *Geophys. Fluid Dyn.*, **1**, 273–302
- 1979 Geostrophic turbulence. *Ann. Rev. Fluid Mech.*, **11**, 401–441
- Ritchie, H. 1985 Rossby wave resonance in the presence of a nonlinear critical layer. *Geophys. Astrophys. Fluid Dynamics*, **31**, 49–92
- Robertson, A. W. 1984 'Ertel potential vorticity as a tropospheric variable'. Ph.D. thesis, University of Reading
- Robinson, A. R. 1983 (Editor). *Eddies in Marine Science*. New York, Springer
- Rossby, C. G. 1937a Aerological evidence of large-scale mixing in the atmosphere. *Trans. Am. Geophys. Union*, **18**, 130–136
- 1937b Isentropic analysis. *Bull. Am. Met. Soc.*, **18**, 201–209
- 1938 On temperature changes in the stratosphere resulting from shrinking and stretching. *Beitr. Phys. Freien Atmos.*, **24**, 53–59
- 1939 Relation between variations in the intensity of the zonal circulation of the atmosphere and the displacements of the semi-permanent centers of action. *J. Marine Res.*, **2**(1), 38–55
- 1940 Planetary flow patterns in the atmosphere. *Quart. J. R. Met. Soc.*, **66**, Suppl., 68–87
- Saffman, P. G. 1981 Dynamics of vorticity. *J. Fluid Mech.*, **106**, 49–58
- Saffman, P. G. and Baker, G. R. 1979 Vortex interactions. *Ann. Rev. Fluid Mech.*, **11**, 95–122
- Salmon, R. 1983 Practical use of Hamilton's principle. *J. Fluid Mech.*, **132**, 431–444
- 1985 New equations for nearly geostrophic flow. *ibid.*, **153**, 461–477
- Sanders, F. and Gyakum, J. R. 1980 Synoptic–dynamic climatology of the 'bomb'. *Mon. Wea. Rev.*, **108**, 1589–1606
- Sardeshmukh, P. D. and Hoskins, B. J. 1985 Vorticity balances in the tropics during the 1982–83 El Niño–Southern Oscillation event. *Quart. J. R. Met. Soc.*, **111**, 261–278
- Sarmiento, J. L., Rooth, C. G. and Roether, W. 1982 The North Atlantic tritium distribution in 1972. *J. Geophys. Res.*, **87C**, 8047–8056
- Sato, Y. 1980 Observational estimates of Eliassen and Palm flux due to quasi-stationary planetary waves. *J. Met. Soc. Japan*, **58**, 430–435
- Schoeberl, M. 1982 Vacillation, sudden warmings and potential enstrophy balance in the stratosphere. *J. Atmos. Sci.*, **39**, 1862–1872
- Schoeberl, M. R. and Lindzen, R. S. 1984 A numerical simulation of barotropic instability. Part I: Wave-mean flow interaction. *J. Atmos. Sci.*, **41**, 1368–1379
- Shapiro, M. A. 1974 A multiple-structured frontal zone jet stream system as revealed by meteorologically instrumented aircraft. *Mon. Wea. Rev.*, **102**, 244–253
- 1976 The role of turbulent heat flux in the generation of potential vorticity in the vicinity of upper-level jet stream systems. *ibid.*, **104**, 892–906
- 1978 Further evidence of the mesoscale and turbulent structure of upper level jet stream frontal zone systems. *ibid.*, **106**, 1100–1111
- 1980 Turbulent mixing within tropopause folds as a mechanism for the exchange of chemical constituents between the stratosphere and troposphere. *J. Atmos. Sci.*, **37**, 994–1004
- Shaw, Sir Napier 1930 *Manual of Meteorology. Vol. III: The Physical Processes of Weather*. Cambridge University Press
- Shimamura, M. 1981 The upper-tropospheric cold lows in the northwestern Pacific as revealed in the GMS satellite data. *Geophys. J. (Tokyo)*, **39**, 119–156
- Shutts, G. J. 1983 The propagation of eddies in diffluent jetstreams: eddy vorticity forcing of 'blocking' flow fields. *Quart. J. R. Met. Soc.*, **109**, 737–761
- 1985 A case study of eddy forcing during an Atlantic blocking episode. *Adv. Geophys.* (to appear)
- Shutts, G. and Thorpe, A. J. 1978 Some aspects of vortices in rotating, stratified fluids. *Pure Appl. Geophys.*, **116**, 993–1006
- Simmons, A. J. and Hoskins, B. J. 1979 The downstream and upstream development of unstable baroclinic waves. *J. Atmos. Sci.*, **36**, 1239–1254

- 1980 Barotropic influences on the growth and decay of nonlinear baroclinic waves. *ibid.*, **37**, 1679–1684
- Spar, J. 1943 The correlation between specific humidity and potential vorticity in the atmosphere. *Bull. Amer. Met. Soc.*, **24**, 196–200
- Staley, D. O. 1960 Evaluation of potential-vorticity changes near the tropopause and the related vertical motions, vertical advection of vorticity, and transfer of radioactive debris from stratosphere to troposphere. *J. Met.*, **17**, 591–620
- Starr, V. P. and Neiburger, M. 1940 Potential vorticity as a conservative property. *J. Marine Res.*, **3**, 202–210
- Stewartson, K. 1978 The evolution of the critical layer of a Rossby wave. *Geophys. Astrophys. Fluid Dyn.*, **9**, 185–200
- Sugi, M. and Kanamitsu, M. 1982 A study of a subtropical upper level cyclone using JMA operational forecast model. *J. Met. Soc. Japan*, **60**, 932–945
- Thomson, R. E., Gower, J. F. R. and Bowker, N. W. 1977 Vortex streets in the wake of the Aleutian Islands. *Mon. Wea. Rev.*, **105**, 873–884
- Thomson, W. (Lord Kelvin) 1887 Stability of fluid motion—rectilinear motion of viscous fluid between two parallel planes. *Phil. Mag.*, **24**, 188–196
- Thorpe, A. J. 1985 Diagnosis of balanced vortex structure using potential vorticity. *J. Atmos. Sci.*, **42**, 397–406
- Tribbia, J. 1979 Nonlinear initialization on an equatorial beta-plane. *Mon. Wea. Rev.*, **107**, 704–713
- Uccellini, L. W., Johnson, D. R. and Schlesinger, R. E. 1979 An isentropic and sigma coordinate hybrid numerical model: model development and some initial tests. *J. Atmos. Sci.*, **36**, 390–414
- Uccellini, L. W., Kocin, P. J., Petersen, R. A., Wash, C. H. and Brill, K. F. 1984 The President's Day cyclone of 18–19 February 1979: synoptic overview and analysis of the subtropical jet streak influencing the precyclogenetic period. *Mon. Wea. Rev.*, **112**, 31–55
- Uccellini, L. W., Keyser, D., Brill, K. F. and Wash, C. H. 1985 The President's Day cyclone of 18–19 February 1979: Influence of upstream trough amplification and associated tropopause folding on rapid cyclogenesis. *ibid.*, **113**, 962–988
- Vaughan, G. and Tuck, A. F. 1985 'Aircraft measurements near jet streams' in 'Atmospheric Ozone' (Proc. Quadrennial ozone symposium IAMAP-WMO) (C. S. Zerefos and A. Ghazi, eds.) Dordrecht, Reidel. 572–579
- Warn, T. and Warn, H. 1978 The evolution of a nonlinear critical level. *Studies in Appl. Math.*, **59**, 37–71
- Williams, G. P. and Yamagata, T. 1984 Geostrophic regimes, intermediate solitary vortices and Jovian eddies. *J. Atmos. Sci.*, **41**, 453–478
- Woods, J. D., Leach, H. and Fischer, J. 1985 Mapping the components of isopycnic potential vorticity in the seasonal thermocline. To be published; preprint available from Institut für Meereskunde, U. of Kiel, F.R.G.
- Young, M. V., Monk, G. A. and Browning, K. A. 1985 Interaction of a baroclinic leaf cloud and dry intrusion in a developing cyclone. To be published; preprint available from the Meteorological Office, Bracknell